INVESTIGATION OF THE EFFECTS OF CLOUD COVER ON Ku-BAND SATELLITE LINK AND EARTH'S POTENTIAL GRADIENT

by

Ashneel Avishek Prasad

This thesis is submitted to the University of the South Pacific in the partial fulfillment of the requirements for the Degree of Master of Science

Division of Physics
School of Engineering and Physics
Faculty of Science, Technology and Environment
University of the South Pacific
Suva
Fiji Islands

December 2009

Declaration

Statement by Author

I, Ashneel Avishek Prasad, hereby declare that this submission is my own and that, to the best of knowledge and belief, it contains no material previously published or written by another person nor material which to a substantial extent has been accepted for an award of any other degree or diploma of a university or other institute of higher learning, except where due acknowledgement is made in the text.

The research was completed without collaboration with any other person and all sources of information have been acknowledged.

Signature..... Date.....04/12/09.....

Name.....ASHNEEL AVISHEK PRASAD.....

Student ID No:.....S0200928O.....

Statement by Supervisor

The research in this thesis was performed under my supervision and to my knowledge is the sole work of Mr. Ashneel Avishek Prasad.

Signature..... Date..4/12/09.....

Name..V. RAMACHANDRAN.....

Designation..SENIOR LECTURER IN PHYSICS.....

Acknowledgements

I wish to acknowledge the University Research Committee of USP for funding this project. My sincere gratitude and deep appreciation also goes to my supervisor, Dr. Visagaperuman Ramachandran for his assistance, patience, and guidance throughout this project. The electric field data provided by Mr. Vickal Kumar is also appreciated.

My sincere thanks also goes out to the Senior Technician of Division of Physics, Mr. Viti Buadromo for his generous contribution. In particular, his involvement in programming the datalogger to record the PBS signal strength and Earth's PG, along with providing me with data for solar radiation, windspeed, humidity, and rainfall.

I would also like to thank Dr. Ajal Kumar, Dr Sushil Kumar, and Mr. Ravin Deo in providing valuable information and criticism on different aspects of the study.

Special thanks to the colleagues of the Physics Division for helping in building the Fieldmill calibration structure. In particular, I appreciate the support of Mr. Shivneel Prasad, Mr. Neil Singh, Mr. Jope Cawanibuka, Mr. Radesh Lal, Mr. Duke Singh, Mr. Avinesh Rohit, Mr. Amit Deo, and Mr. Sunil Chand.

Thanks are also due to Mr. Sheik Ahmed of Pacific Broadcasting Services for providing valuable information.

I would also like to thank my friends who have provided me with the necessary motivation and help through the research. To name a few Mr. Lalin Shandil, Mr. Imran Jannif, Mr. Rajeev Lal, and Mr. Roniel Latchman.

Finally I would like to thank my parents and my brother whose sacrifices, encouragement and motivation helped me in completing this project.

Abstract

This thesis investigates the effect of cloud cover on one of the universally present atmospheric parameter, namely the Earth's vertical electric field or the Potential Gradient (PG), close to the surface of the Earth and the effect of cloud cover on satellite down link. The measurement site was The University of the South Pacific (18.13°S, 178.47°E). As cloud cover directly affects the solar insolation, it was used as one of the parameters to distinguish between fair-weather and cloudy days. Continuous record of the PG for the period 1st June 2005 to 30th June 2006 and simultaneous records of solar insolation during this period were analyzed. Days with peak insolation > 800 W/m^2 and having the expected bell shaped variation of solar insolation were considered as fair-weather days, and on this basis, 31 days were classified as fair-weather days. In analyzing the PG values, records which fell in the range 0 – 1000 V/m were considered. The average diurnal variation of PG showed a bimodal oscillation with a dominant peak in the morning, close to 7 am LT. The evening peak coincided with the *Carnegie peak* and the daily average PG was ~ 125 V/m. The relatively low value of this average value indicates that the measurement site is relatively "clean" during fair-weather days with little effect from atmospheric aerosols. For the period of study, another 31 days showed the bell shaped variation in solar insolation but with decreased peak values and were classified as cloudy days. Assuming the same criteria used for the selection of PG data on fair-weather days, the daily averages of PG for all these days were found to be significantly less than 125 V/m. As the solar insolation and the PG varies with time of the day, their magnitudes compared to the average fair-weather day values are further analyzed to find the correlation between cloud cover and the surface PG. Observations clearly show that the percentage reduction in PG is nearly proportional to the intensity of the cloud cover. A possible reason for this dependence of PG on cloud cover is discussed.

To study the effect of cloud cover on satellite down links, the Ku-band signal centered at 12.648 GHz from *Intelsat* 701 was monitored. Simultaneous measurements of *RF* signal strength and solar insolation were made for 3 months (29th August to 26th October 2007) continuously. During this period, 11 days were classified as fair weather days. Contrary to the expectation that the *RF* signal strength should remain constant, it exhibited variation (~ 61 dBm – ~ 68 dBm) in addition to

the scintillations. The signal remained relatively high in the nighttime hours compared to the daytime hours. During the period of study, 37 days were classified as cloudy days, records on these days again showed a diurnal variation with a mean strength of ~ 50 dBm. Further analysis of the cloudy day records showed a nearly linear dependence of the percentage reduction in *RF* signal strength to the intensity of the cloud cover. This reduction is attributed to the increased scattering loss by cloud droplets.

Abbreviations

a	radius of scattering object
A	Amperes
A/m	Amperes per meter
ac	alternating current
A_e	effective aperture of the antenna
am	ante meridiem
A_p	physical aperture of the antenna
B	Magnetic induction
coax	coaxial cable
C	Coulombs
C_A	atmospheric capacitance
cm^3	cubic centimeters
CO_4^-	carbon tetraoxide anion
CRT	Cathode Ray Tube
CS110	Campbell Scientific 110
C_{sca}	total energy scattered
D	Electric displacement
D	directivity
dB	Decibel
dB/km	Decibels per kilometer
dB/mm	Decibels per millimeter
dBm	ratio of decibels referenced to one milliwatt
dBW	Decibel Watt
dc	direct current
E	Electric Field
e	electronic charge
E	electric field vector
E_0	initial uniform electric field in free space
EFS1000	Electric Field Mill Sensor 1000 series
EM	Electromagnetic
E_m	Electric field intensity in the medium
EUV	Extreme Ultraviolet

E_Z	Earth's vertical electric field
F	propagation factor
F	force
F	Farads
F/m	Farads per meter
G	gain
GaAsFET	Gallium Arsenide Field Effect Transistor
GEC	Global Electric Circuit
GHz	Gigahertz
GMT	Greenwich Mean Time
G_r	receiving antenna gain
G_t	transmitting antenna gain
H	Magnetic field vector
h	altitude
H^+	hydrogen ion
H_2O	water molecule
H_3O^+	hydronium ion
He^+	helium ion
HI	High
hrs	hours
i.e.	that is
I	intensity of the scattered wave at a distance
I_0	incident intensity of the wave
IF	intermediate frequency
ITU-R	International Telecommunication Union – Recommendation
J	current density
JCI1131	John Chubb Instruments 131
$\mathbf{J}_S$	surface current density
k	propagation constant
k_-	mobility factor of negative ions
k_+	mobility factor of positive ions
km	kilometer
km^3	cubic kilometers
kV	kilovolts

Ku band	Kurtz-under band
LabVIEW	Laboratory Virtual Instrument Engineering Workbench
LED	Light Emitting Diode
LNA	Low Noise Amplifier
LNB	Low Noise Block
LO	Low
LO	Local Oscillator
LSB	Least Significant Bit
LT	Local Time
m	complex relative refractive index
m/s	meters per second
MCS	Mesoscale Convective System
MHz	Megahertz
mm/hr	millimeters per hour
ms	milliseconds
MSB	Most Significant Bit
MV	Megavolts
n	real relative refractive index
n_1	refractive index of the surrounding medium
n_2	refractive index of the spherical particle
nm	nanometers
NO^+	nitrogen oxide cation
O^+	oxygen cation
O_2	oxygen molecule
O_2^-	superoxide anion
O_2^+	superoxide cation
PBS	Pacific Broadcasting Services
PCI	Personal Computer Interface
pF	picofarads
PG	Potential Gradient
pm	post meridiem
P_{OUT}	output power
P_r	received power
P_t	transmitted power

PVC	Poly Vinyl Chloride
r	distance between source point and center of the sphere
$\mathbf{r}_1$	unit vector pointing from the source point to the observation point
R^2	correlation coefficient
R_A	atmospheric resistance
RF	Radio Frequency
S	scintillation index
s'	surface enclosing the surrounding dielectric
S/m	Siemens per meter
SAP	stratospheric aerosol particles
SR	solar radiation
SR'	solar radiation prime
T	transmission
T_A	noise temperature of the antenna
T_S	sky temperature
TV	television
U	wind speed
UHF	Ultra High Frequency
USP	University of the South Pacific
V	Volts
v	phase velocity
V/m	Volts per meter
VCO	Voltage Controlled Oscillator
VHF	Very High Frequency
W	Watts
W/m^2	Watts per square meter
α	attenuation constant
β	phase constant
δ	scattering parameter
ε	permittivity
ε	efficiency
ε_0	permittivity of free space
ε_r	dielectric constant of the medium
ε_r'	apparent dielectric constant

λ	wavelength
μ	permeability
μ_0	permeability of free space
μH	microhenry
μm	micrometer
μ_r	permeability of the medium
ρ	charge density
ρ_b	bound volume charge density
ρ_f	free volume charge density
ρ_S	surface charge density
σ	conductivity
σ_b	bound surface charge density
σ_E	conductivity at Earth's surface
σ_f	free surface charge density
τ'	volume enclosing all the charges
τ_A	atmospheric time constant
ω	angular frequency
Ω	ohms
Π	ionization production rate

Table of Contents

List of Figures

List of Tables

Chapter 1

Introduction

1.0 Introduction – Effects of aerosols on physical parameters

The propagation medium in the Earth's troposphere includes water vapor, cloud, fog, ice, dust, smoke etc, which can be collectively characterized as *aerosols*. Such aerosol particles suspended in the gaseous atmosphere affect many atmospheric parameters. Some of these effects are changes in the conductivity of the atmosphere, production of condensation nuclei, production of scattering nuclei for scattering in remote sensing or communication and contribution to back scattering of radiation. In the study of the Global Electric Circuit (GEC) researchers have concentrated on relating it to the Earth's vertical electric field (or potential gradient PG) during fair weather. Researchers [Siingh *et al*., 2007; Israel, 1973; Jayaratne and Verma, 2003] have reported that the suspended particles in the atmosphere modify the Earth's vertical electric field (PG). The impairment mechanisms for electromagnetic waves propagating through the troposphere include absorption, scattering, refraction, diffraction, multipath, scintillation, depolarization etc. In addition, the characteristics of the ionosphere play an important role when considering propagation from outer space. The dependence of attenuation of solar radiation in the spectral region of 270 – 2800 nm by three different aerosol sizes showed that increasing aerosol concentration reduced the photo-synthetically active radiation in the direct solar beam [Unsworth and McCartney, 1973]. Attenuation studies by low temperature cloud (<20 ºC) on *RF* signals at high frequency (>50 GHz) has been reported [Allen, 1983]. Ippolito [1986, pp 50-59] has presented a comparative account of the cloud attenuation and light rainfall. This study deals with the investigation of the effect of cloud cover on the Earth's electric field and the effect on satellite communication downlink.

The water-vapor content of the air varies considerably, depending on the temperature and relative humidity. The water particles in the atmosphere contribute to the formation of cloud structures such as strato-nimbus and cumulo-nimbus. These in turn affect the PG rendering them as non-fair-weather days. The electric field on these types of days is termed as 'non-fair-weather' day electric field. Dickinson [1975] proposed that variations in cosmic ray flux could provide a mechanism whereby solar activity would produce a direct impact on cloud cover by modulating atmospheric ionization, resulting in the electrification of aerosol and increasing its

effectiveness to act as condensation nuclei. The processes involved are complex but if they do take place then there is scope for considerable amendment to the value for solar radiative forcing of climate based on incident irradiance alone.

Other processes, such as changes in the Earth's electric field that might modify cloud cover have also been proposed [Tinsley, 2000]. The effect of rain rate on radio wave propagation has been studied by many researchers [Allnut and Haidara, 2001; Pan *et al.*, 2000; Pan *et al.*, 2001; Pan and Allnut, 2001; Ramachandran and Kumar, 2004]. The International Telecommunication Union has produced a recommendation for computing the attenuation of Ku band signals by rain (P61-8 ITU-R Recommendation, 2003). Based on measurements done in the tropical regions Ramachandran and Kumar [2005] proposed a model which modifies the ITU-R recommendation for Ku-band satellite communication.

Attenuation of radio wave signals by clouds is similar to the attenuation by very light rainfall. Cloud attenuation depends on cloud characteristics such as type, thickness and coverage [Ippolito, 1986, pp 56-58]. The presence of clouds affects radio wave propagation by effectively absorbing and scattering the wave: a process described by Rayleigh scattering. The cloud characteristics may also influence the non-fair-weather day PG. These factors also influence the insolation during daytime. Solar radiation is assumed to be a measure of cloud coverage. The signal strength of satellite links and the PG can be monitored over the 24 hour period of a day. However the solar radiation can be monitored only during the day time. It will be scientifically challenging to investigate the dependence of solar radiation on PG and satellite signal attenuation. Therefore detailed analysis should be carried out with data taken during the day time. Assuming similar cloud coverage from 6.00 pm to 6.00 am LT the analysis could be extended for the night.

1.1 Research Objectives

The objectives of the proposed work are:

a) To study the diurnal variation of the Earth’s fair-weather electric field and correlate it with solar radiation other atmospheric parameters such as;
   - wind speed,

- aerosol content,
- level of ionization.

b) To measure the absolute value of Earth's vertical electric field and correlate it with the cloud cover and lightning discharge.

c) To study the diurnal variation of a television signal (Pacific Broadcasting Services) and correlate it with cloud cover.

1.2 Thesis Organization

The thesis is presented in 5 chapters. Chapter 2 deals with the fundamental theory of radio wave propagation in the troposphere and space communication and the effect of atmospheric particulates on signal attenuation. This is followed by theoretical and experimental foundations of the Earth's electric field or potential gradient (PG) in Chapter 3. In Chapter 4, the methodology adopted during this research work has been described. This is presented in two sections. The first part describes the methodology adopted for the measurement of the Earth's PG. This is followed by the procedures adopted for the measurement of the signal strength of the PBS satellite signal. Chapter 5 presents the result of the findings of this research work and discusses them. Chapter 6 finally summarizes the important findings of this work.

Chapter 2

Physics of Radiowave Propagation

2.0 Radiowave Propagation

This chapter begins by looking at the propagation of electromagnetic waves together with characteristics such as polarization, dispersion, attenuation and scattering. The different modes of wave propagation are also discussed. Since the propagation of electromagnetic waves is strongly dependent on the property of the medium, this chapter is concluded with the sources of ionization and the electrical conductivity of the lower atmosphere.

2.1 Physics of Radiowave propagation

An electromagnetic wave is made up of both an electric field (**E**) and a magnetic field (**H**) vectors. Both **E** and **H** are perpendicular to each other, and are perpendicular to the direction in which the wave propagates. Figure 2.1 shows the directions of electric and magnetic fields and the direction of propagation for the simple case of uniform plane wave.

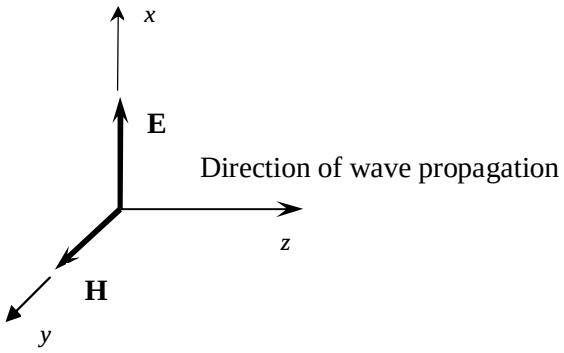

Figure 2.1: Propagation of electromagnetic waves.

The electric and magnetic fields are governed by a set of four equations, known as *Maxwell's equations*, which are known to form the basis for the entire electromagnetic field theory. In the differential form, the equations are stated as:

$$\nabla \times \mathbf{E} = -\frac{\partial \mathbf{B}}{\partial t} \tag{2.1}$$

$$\nabla \times \mathbf{H} = \mathbf{J} + \frac{\partial \mathbf{D}}{\partial t} \tag{2.2}$$

$$\nabla \bullet \mathbf{D} = r \tag{2.3}$$

$$\nabla \bullet \mathbf{B} = 0 \tag{2.4}$$

where **D** and **B** are the electric displacement and the magnetic induction respectively. **J** and ρ represent the current and charge densities. Solutions to these equations are obtained by employing boundary conditions. The boundary conditions state that across the boundary between two media, the tangential components of **E** and the normal components of **B** are continuous, and the tangential components of **H** and the normal components of **D** are discontinuous by the amount $\mathbf{J}_S$ (surface current density) and ρ_S (surface charge density) respectively.

2.1.1 Polarization

The orientation of the electric and magnetic fields with respect to the Earth is termed as *polarization*. If an electric field is parallel to the Earth, the electromagnetic wave is said to be *horizontally polarized,* and if it is perpendicular to the Earth, the wave is *vertically polarized* [Frenzel, 1998, p 635].

2.1.2 Dispersion

If we consider the general case of a lossy medium that is charge free (ρ = 0), the Maxwell's equations can be used to derive Helmholtz' wave equations for the electric and magnetic field. An equation for the electric field for an electromagnetic (EM) wave propagating in a lossy medium can then be obtained by solving the wave equation for the electric field. The Helmholtz wave equation for electric field is [Bansal, 2006, p 165]

$$\nabla^2 \mathrm{E} - k^2 \mathrm{E} = 0 \tag{2.5}$$

where k is the propagation constant for a wave of angular frequency ω, and is given by:

$$k = \sqrt{\left(-w^2 m_0 m_r e_0 e_r + j m_0 m_r s w\right)} = a + jb \tag{2.6}$$

where σ is the conductivity of the medium, α is the attenuation constant, β is the phase constant, $\mu = \mu_0 \mu_r$ is the permeability of the medium, and ε is the permittivity which is given by $\varepsilon = \varepsilon_0 \varepsilon_r$. The permeability ($\mu_0$) and the permittivity ($\varepsilon_0$) of free space are $4\pi \times 10^{-7}$ A/m and 8.854×10^{-12} F/m respectively, and μ_r and ε_r are permeability and dielectric constant of the medium respectively. [Bansal, 2006, p 166].

If the medium is a perfect dielectric (σ = 0) then k will be an imaginary quantity, showing that the wave will propagate without any attenuation and dispersion. In general the relation

$$k = j\frac{w}{v} \tag{2.7}$$

is called the dispersion relation. Dispersion is the frequency dependence of the phase velocity of the electromagnetic wave.

For imperfect dielectrics, k will have both real and imaginary components, implying that the wave will propagate with attenuation. Then α and β are given by [Bansal, 2006, p 165]:

$$a = w\sqrt{\frac{me}{2}\left[\sqrt{1+\left(\frac{s}{we}\right)^2}-1\right]} \tag{2.8}$$

$$b = w\sqrt{\frac{me}{2}\left[\sqrt{1+\left(\frac{s}{we}\right)^2}+1\right]} \tag{2.9}$$

Using (2.3) and utilizing the fact that $\mathbf{B}=\mu\mathbf{H}$, $\mathbf{D}=\varepsilon\mathbf{E}$, and $\mathbf{J}=\sigma\mathbf{E}$, it can be shown that the apparent dielectric constant ε_r' is given by:

$$e_r' = e_r - j\frac{s}{we_0}. \tag{2.10}$$

2.1.3 Attenuation by absorption

Assuming the wave propagates in the *z*-direction and is polarized in the *x*-direction, solving the wave equation (2.5) for the electric field yields [Bansal, 2006, p 165]:

$$E_x = E_0 e^{-az}\cos(wt - bz) \tag{2.11}$$

From (2.6) it can be inferred that as the EM wave propagates in the medium, its amplitude is reduced by e^{-az} . The reduction in the amplitude or intensity of electromagnetic wave carrying information is called attenuation. For gaseous media attenuation is measured in units of decibels per unit length of medium. Rain attenuation is measured in dB/mm of rainfall.

Between frequencies of 50 - 60 GHz the attenuation of EM waves by the atmosphere increases from 0.5 dB/km to almost 20 dB/km, and is due to water vapor (H_2O) and molecular oxygen (O_2) [Fleagle and Businger, 1963, p 21]. According to Stephens

[1994, p 116], the peak absorptions of microwaves by water vapor occurs at 22.235 GHz and 183 GHz.

Attenuation of radiowaves can be characterised into two forms; scintillation and fade. Scintillation is the rapid fluctuation of the amplitude, phase, angle of arrival, and polarization. A measure of scintillation is the scintillation index (S), defined as

$$S = \frac{s_x}{m_x} \tag{2.12}$$

where s_x is the standard deviation of the received power and m_x is the mean power. Fade is described as signal reduction over a longer duration.

2.1.4 Attenuation by scattering

EM waves undergo attenuation by scattering. Scattering is a process whereby some radiation is forced to deviate from the original trajectory by one or more localized non-uniformities in the medium through which it passes [Frenzel, 1998, pp 667 - 668]. Some of the non-uniformities in the Earth-ionosphere waveguide that effectively scatter the EM wave include aerosol particles, water droplets, and clouds [Bansal, 2006, p 175].

The most important gas in the atmosphere, from the point of view of its interaction with EM waves, is water vapor [Stephens, 1994, p 14]. Water vapor is especially important in the troposphere because of its role in cloud formation and precipitation. It is also one of the most variable components of the atmosphere. In the tropics, water vapor may account for up to 4% (by volume) of the atmosphere, while in polar regions or in dry desert air, it may be only a fraction of a per cent [Fleagle and Businger, 1963, p 22]. These water droplets contribute to scattering of the EM wave. Apart from water vapor in the troposphere, the average relative humidity is close to 50 % [Stephens, 1994, p 120].

If the cloud drops and rain water drops are spherical in shape, the type of scattering is determined by the scattering parameter δ [Ippolito, 1986, p 59],

$$d = \frac{2p\,r}{l} \tag{2.13}$$

where λ is the wavelength of the wave and r is the radius of the scattering object. Depending on the magnitude of δ, scattering can be classified into two types: *Rayleigh scattering* and *Mie scattering*.

If $\delta < 0.1$, the scattering process is defined by Rayleigh scattering. Rayleigh scattering happens when it is drizzling and in cloud and fog. If $0.1 < \delta < 50$, the scattering process is defined by Mie scattering. Mie scattering is dominant during moderate to heavy rain [Ippolito, 1986, p 57].

2.2 Cloud Physics

It is believed that thunderstorms are the major generators of Global Electric Circuit (GEC) [Siingh *et al.*, 2007]. In a developing isolated thunderstorm cell, the motion of cloud particles are primarily upward as moist air from the sub cloud boundary layer rises above the condensation level where it becomes buoyant. This updraft causes a cloud of several km thickness. The water drops formed during this updraft can be divided into two types: small drops with typical radii of 10 to 100 μm which remain suspended in the air and are carried upward by the updraft (cloud drops) and rain drops large enough to have fall velocities equal to or greater than that of the updraft ($5 - 10$ ms^{-1}). These drops (rain water) reach typical radii of 0.1 to 1 mm and have water content of typically 0.1 to 1 gram per kilogram of air [Volland, 1984, p 23].

Scattering in clouds is classified as Rayleigh scattering, since for the water particles in the cloud $\delta < 0.1$. This process is demonstrated theoretically with the aid of an isolated sphere. The isolated sphere is illuminated by a parallel beam of linearly polarized radiation. The water drop becomes polarized by the electromagnetic field due to the displacement of the electrons with respect to the nuclei and also due to the partial orientation of the permanent dipoles that are already present. Provided the particle is small compared to the wavelength, the instantaneous field which it experiences due to the electromagnetic wave is uniform and parallel to the external field [Kerker, 1969, p 32], as shown in Figure 2.2.

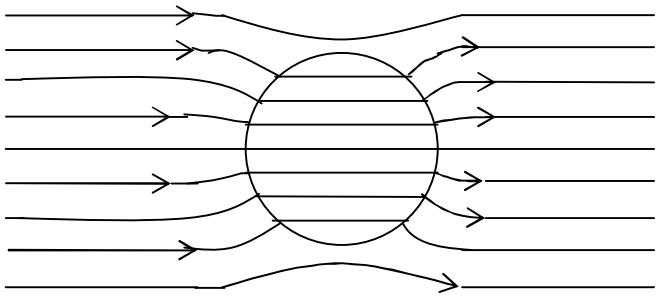

Figure 2.2: Scattering of a uniform electric field by a homogeneous sphere. The field within the sphere is uniform.

The electric field intensity within the sphere is given by [Kerker, 1969, p 32]:

$$\mathbf{E}_{\text{int}} = \left[\frac{3e_2}{e_1 + 2e_2}\right]\mathbf{E}_0 \tag{2.14}$$

where ε_1 and ε_2 are the permittivity of the sphere and the external medium, respectively. Outside the sphere the field is composed of two parts; the initial uniform field, E_0, that would have existed in the absence of the particle, and superimposed upon this is an induced field identical with that which would be given by a simple dipole oriented parallel to the incident field with dipole moment

$$p = 4pe_2a^3\left[\frac{e_1 - e_2}{e_1 + 2e_2}\right]E_0 \tag{2.15}$$

where a is the radius. If the incident field oscillates harmonically, then to a close approximation the induced dipole will follow synchronously so that

$$pe^{iwt} = 4pe_2a^3\left[\frac{e_1 - e_2}{e_1 + 2e_2}\right]E_0e^{iwt} \tag{2.16}$$

where the exponential factor describes the time dependence. Thus, the spherical particle acts as an oscillating electric dipole which now radiates waves in all directions [Kerker, 1969, p 33].

The field E_0 radiated by the dipole is given by [Lorrain and Corson, 1970, p 98]

$$E_0 = \frac{1}{4pe_0}\int_{t'}\frac{(r_f + r_b)\mathbf{r}_1}{r^2}\,dt' + \frac{1}{4pe_0}\int_{s'}\frac{(s_f + s_b)\mathbf{r}_1}{r^2}\,da' \tag{2.17}$$

where r_f and r_b are free and bound volume charge densities respectively, σ_f and σ_b are the free and bound surface charge densities, r is the distance between the source point and the centre of the sphere, $\mathbf{r}_1$ is a unit vector pointing from the source point to

the observation point, t' is any volume enclosing all the charges, and s' is the surface enclosing the surrounding dielectric [Lorrain and Corson, 1970, p 98].

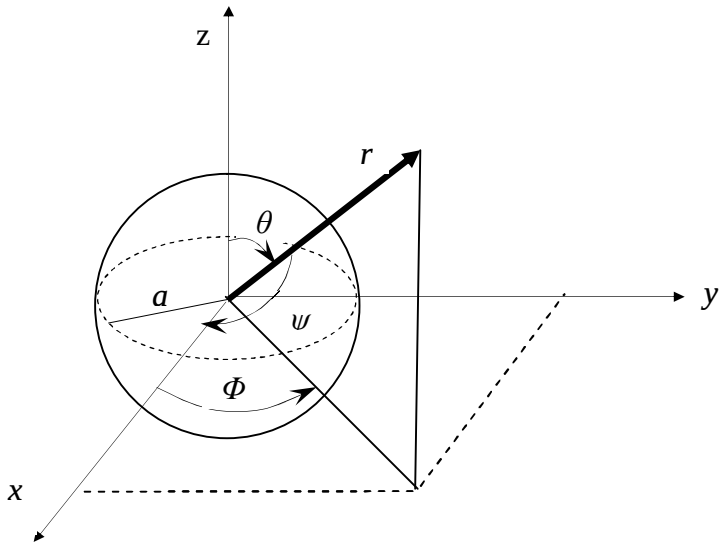

Figure 2.3: Geometry for Rayleigh scattering. Incident wave travels along positive *z*-axis with electric vector polarized along *x*-axis. Particle with radius *a* has its center at the origin. Direction of scattered wave is defined by polar angles θ and Φ.

In Figure 2.3 above, the linearly polarized incident wave is propagating along the positive *z*-axis with its electric vector parallel to the *x*-axis. The induced dipole is at the origin and is also oriented along the *x*-axis. The scattering direction is taken from the origin to the point defined by the polar coordinates (r,θ,Φ).

$$x = r\sin q\cos f;\quad y = r\sin q\sin f;\quad z = r\cos q$$

The angle measured from the scattering direction to the dipole is ψ. The angle of observation, θ, is measured from the forward to the scattered directions and defines the scattering plane or the plane of observation. For an incident wave of unit intensity, the intensity of the scattered wave at a distance r from the particle is given by [Kerker, 1969, p 33]

$$I = \frac{16p^4a^6}{r^2l^4}\left|\frac{n^2-1}{n^2+2}\right|^2\sin^2 y \qquad (2.18)$$

where n is the relative refractive index, i.e., the ratio n_1/n_2, where n_1 and n_2 are the refractive indices of the surrounding medium and the spherical particle respectively, and λ is the wavelength in the medium.

If the scattering particle causes attenuation by both absorption and scattering, n will be characterized by a complex relative refractive index, m. When the imaginary part is small compared to the real part ($m = n$), the intensity of the scattered wave is given by equation 2.18.

When the scattering is in the yz-plane and ψ = 90°, the incident beam is perpendicularly polarized with respect to the scattering plane. The scattered radiation, also perpendicularly polarized, has intensity

$$I_1 = \frac{16p^4a^6}{r^2l^4}\left(\frac{n^2-1}{n^2+2}\right)^2 \tag{2.19}$$

When the scattering is in the xz-plane, the polarization is parallel to the scattering plane and ψ, which may now take on all values, is related to θ by

$$y = (p/2) - q \tag{2.20}$$

so that

$$I_2 = \frac{16p^4a^6}{r^2l^4}\left(\frac{n^2-1}{n^2+2}\right)^2 \cos^2 q \tag{2.21}$$

The ratio of the intensity of the horizontal to the vertical component of the scattered light is defined as the polarization ratio, and is given by

$$r_u(q) = I_2 / I_1 = \cos^2 q \tag{2.22}$$

The main features of Rayleigh scattering are:

(1) The dependence of scattering upon the inverse fourth power of the wavelength, and

(2) Complete polarization at 90° (when ψ = 90°).

The total energy scattered by a particle in all directions is given by Kerker [1969, p 34]:

$$C_{sca} = \int_0^p \int_0^{2p} Ir^2 \sin y \, dy \, df \tag{2.23}$$

Upon integration, with the aid of (2.18), C_{sca} is given by:

$$C_{sca} = \frac{128p^5a^6}{3l^4}\left(\frac{n^2-1}{n^2+2}\right)^2 \tag{2.24}$$

The efficiency factor for scattering is found by dividing total energy scattered by the cross-sectional area (πa^2). Then the efficiency factor for scattering, Q_{sca}, is given as

$$Q_{sca} = \frac{8}{3} a^4 \left(\frac{n^2 - 1}{n^2 + 2} \right)^2 \tag{2.25}$$

where $a = 2p\,a / l$ is a dimensionless size parameter. The efficiency factor represents the fraction of energy geometrically incident upon the particle which is scattered in all directions. The upper limit of particle radius for which the above equation is valid is generally set at $a/\lambda \leq 0.05$ [Kerker, 1969, p 37].

For N particles per unit volume, the attenuation due to scattering is

$$-dI / dx = NC_{sca} I \tag{2.26}$$

And the transmission is given as:

$$T = I_l / I_0 = \exp\left(-NC_{sca} l\right) \tag{2.27}$$

where I_0 is the incident intensity and I_l is the intensity of the beam emerging at a distance l travelled in the scattering medium [Kerker, 1969, p 38].

2.3 Modes of EM wave propagation

EM wave propagation deals with the transfer of energy or information from one point (a transmitter) to another (a receiver) through the media such as material space, transmission line or waveguide. Wave propagation over the Earth's surface may assume one of the following three principal modes [Bansal, 2006, p 175]:

1) Surface (ground) wave propagation along the Earth's surface,
2) Space wave propagation through the lower atmosphere, and
3) Sky wave propagation by reflection from the upper atmosphere.

Figure 2.4 shows the 3 modes of wave propagation that occur over the surface of the Earth. Also shown in the figure is the satellite communication link.

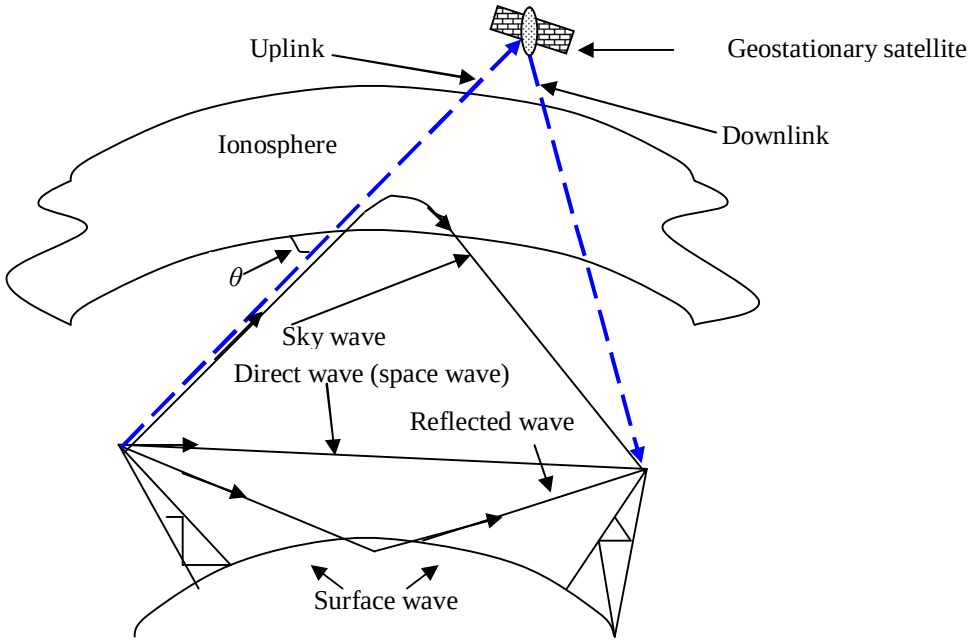

Figure 2.4: Modes of wave propagation

2.3.1 Surface Wave

The surface (or ground) wave takes effect at the low-frequency end of the spectrum (~ 2 - 5 MHz) and is directed along the surface over which the wave is propagated [Bansal, 2006, p 175]. The conductivity of the Earth determines how well ground waves are propagated. Waves can travel a greater distance with less attenuation if the medium has better conductivity [Bansal, 2006, p 175]. The best propagation of ground waves occurs over salt water because water is an excellent conductor at these frequencies. The conductivity of sea water is ~ 4 S/m [Volland, 1984, p 7]. Conductivity of the Earth is usually lowest in low-moisture areas such as deserts [Volland, 1984, p 23]. At frequencies above 5 MHz, the Earth begins to attenuate radio signals [Frenzel, 1998, p 670].

2.3.2 Space Wave

The space wave consists of the direct wave and the reflected wave. The direct wave travels from the transmitter to the receiver in nearly a straight path while the reflected wave is due to ground reflection [Bansal, 2006, p 175]. Direct-wave radio signalling is often referred to as *line-of-sight communications*. Line of sight communications is characteristic of most radio signals with a frequency of above approximately 30 MHz, particularly Very High Frequency (VHF), Ultra High Frequency (UHF), and microwave signals [Frenzel, 1998, p 673].

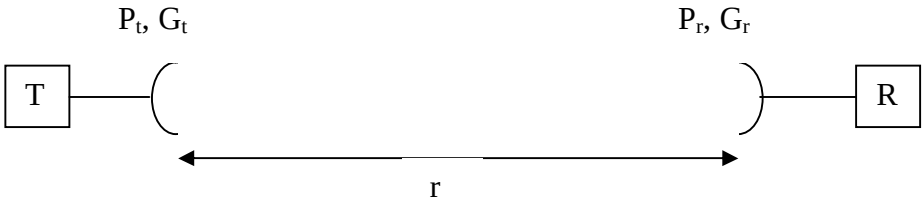

Figure 2.5: Basic wireless system (reproduced from Bansal [2006]).

If the receiver and transmitter have a clear line-of-sight path between them as in Figure 2.5, and are separated by a distance *r*, the power received P_r by the receiving antenna is given by the Friis equation [Bansal, 2006, p 176]:

$$P_r = G_r G_t \left(\frac{l}{4p\,r} \right)^2 P_t \tag{2.28}$$

where P_t is the transmitted power, G_r and G_t are the receiving and the transmitting antenna gains respectively, and λ is the wavelength of the transmitted signal. It can be seen from equation (2.28) that the received power falls off as the square of the separation distance *r* (*free space path loss*).

In case the propagation path is in a lossy medium, a correction factor *F* is included in the Friis equation to account for the effect of the medium, commonly known as the *propagation factor* [Bansal, 2006, p 176].

$$F = \frac{E_m}{E_0} < 1 \tag{2.29}$$

where E_m and E_0 are the electric field intensities in the medium and free space respectively. Then the Friis equation for a lossy medium is given as [Bansal, 2006, p 176]:

$$P_r = G_r G_t \left(\frac{l}{4p\,r} \right)^2 P_t \left| F \right|^2 \tag{2.30}$$

2.3.3 Sky Wave

Under certain conditions, EM waves in a limited frequency range (below 30 MHz) directed towards the sky are bent back towards the Earth by the ionosphere. This process is highly dependent on the condition of the ionosphere (its level of ionization) and the signal frequency [Bansal, 2006, p 175].

The ionosphere is generally considered to be divided into three layers, these being the D, E and the F layers; the F layer is subdivided into F_1 and F_2 layers. The D and E layers, the farthest from the sun, are weakly ionized. They exist only during daylight hours, during which they tend to absorb radio signals in the medium frequency range from 300 kHz to 3 MHz. The F_1 and F_2 layers, closest to the sun, are the most highly ionized and have the most effect on radio signals. The F layers exist during both day and night. The primary effect of the F layer is to cause refraction of radio signals when they cross the boundaries between layers of the ionosphere with different layers of ionization. The refraction is governed by Snell's Law [Frenzel, 1998, p 671].

2.3.4 Satellite Communication

For long range communication, satellites are used. The transmission frequencies are above 30 MHz (generally 1 - 30 GHz). Some types of communication employ a satellite placed at a height of approximately 35 803 km above the equator that orbits the globe at the same speed with which the Earth rotates. Thus, the satellite remains stationary with respect to any point on the Earth's surface. This type of satellite is called a ***geostationary*** satellite. The signals are sent to the satellite via an ***uplink*** wave and then re-transmitted via a ***downlink*** wave [Stephenson, 1994, p 10].

To avoid interference with the downlink signals, the uplink station sends the signals at a different frequency. The angle of transmission (θ) from the uplink station varies from 3° to 90°. The uplink station controls the internal functions of the satellite, and the transmitted microwave power beam is extremely narrow, in order not to interfere with adjacent satellites in the geo-path [Stephenson, 1994, p 11].

The satellites employ transponders for receiving and transmitting the signal. A transponder receives the uplink signal, amplifies, downconverts, and re-transmits as downlink signal to the receiving stations. Separate transponders are used for each channel and are powered by solar panels with backup batteries for eclipse protection. In the Pacific, the downlink frequency band ranges from 11.70 - 12.75 GHz [Stephenson, 1994, p 12].

The uplink and downlink signals are much higher in frequency than the normal TV signals which are in the VHF and UHF bands. The received power from the satellite is extremely weak when it reaches the Earth. As the radiated signal of a transponder travels towards the Earth it looses power by spreading over an increasingly wide area thus diluting the signal strength - the *free space path loss* (equation 2.28). The downlink signal, being *microwave electromagnetic radiation*, suffers severe attenuation by water vapour or any obstruction in the line-of-sight of the antenna [Stephenson, 1994, pp 12 - 19]. Moderate rainfall can reduce the signals by 3 dB which is enough to give a noisy reception. Severe rainstorms can reduce the signals by as much as 10 dB [Stephenson, 1994, p 21].

The downlink signal is received using an antenna, a *low noise block* (LNB), a coaxial cable, and a spectrum analyzer. In microwave satellite communication systems, the antenna usually consists of a parabolic reflector (dish) and a feedhorn. In a receiving system, such as used in this research, the reflector focuses radio waves onto the feedhorn for detection and conversion into electrical signals. In a transmitting system the reflector concentrates the radio waves emitted by the feedhorn into a narrow beam aimed towards the satellite [Stephenson, 1994, p 24].

The dish antennas are of two types: *Prime-Focus* Parabola and *Offset* antenna. The main distinction between the two types of antennas is that the Prime-Focus Parabola reflects the incoming signals to the focal point which is along the principal axis of the dish whereas the Offset antenna, made from part of the Prime-Focus Parabola, focuses the incoming signal to the focal point which is off-center. Figure 2.6 below shows the two types of dish antennas.

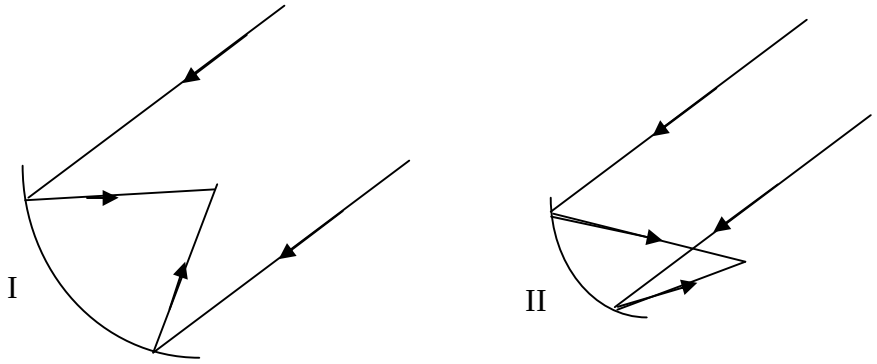

Figure 2.6: Prime Focus Parabolic Dish antenna (I) and Offset Dish antenna (II)

Antennas are usually classified by their efficiency, illumination, aperture, directivity, gain, and noise-temperature.

Antenna efficiency (ε) is the ratio of the signal strength transmitted towards or received from a particular direction in space by a real antenna to the signal strength that would be obtained with a theoretically perfect antenna of the same physical size. Antenna efficiency depends on the effective aperture, the physical aperture, how accurate the surface is, how it replicates the desired shape, and on the reflectivity of the surface [Balanis, 2005, p 65].

Antenna illumination is the radiation of EM energy from the feedhorn to the surface of the parabolic reflector of a transmitting antenna, or the focusing of EM energy captured by the reflector of a receiving antenna towards the feedhorn. With perfect illumination, no signal energy is lost to the surroundings, but in practice there is always some loss [Balanis, 2005, p 44].

Antenna aperture is the total reflective area of a parabolic antenna (dish) over which radio waves are captured or radiated. The effective aperture is smaller than the physical aperture and is related to it by the antenna efficiency, given by [Balanis, 2005, p 69]:

$$e = \frac{A_e}{A_p} \tag{2.31}$$

where ε is the efficiency, A_e is the effective aperture, and A_p is the physical aperture.

The directivity D of an antenna is given by the ratio of the maximum power density in a given direction to the average power over a sphere, and is a dimensionless ratio ≥ 1. For a parabolic dish antenna the directivity is given as [Balanis, 2005, p 45]:

$$D = 4p\,\frac{A_e}{l^2} \tag{2.32}$$

where A_e is the effective area of the dish and λ is the wavelength.

If the antenna is lossless its *gain G* is equal to its directivity. However, if the antenna is not 100 percent efficient, the gain is less than the directivity, given as [Balanis, 2005, p 45]:

$$G = eD \tag{2.33}$$

where e is the efficiency of the antenna ($0 \leq e \leq 1$).

The noise temperature is a measure of how much noise an antenna detects from the surrounding environment and outer space. The noise temperature T_A of the antenna (assumed *lossless*) is equal to the sky temperature T_S, and *not* the physical temperature of the antenna [Balanis, 2005, p 105].

2.4 Atmospheric Physics

The presence of the ionosphere and atmospheric precipitates such as cloud, fog, raindrops, hail, snow, and aerosols significantly affects EM microwave propagation [Bansal, 2006, p 175]. Aerosol is composed of sea salt, smoke, dust, and haze particles [Stephens, 1994, p 20]. The different categories of aerosol particles based on their size as given by Junge [1955] are:

- *Aitken particles* with dry radii < 0.1 μm
- *Large particles* with dry radii $0.1 \leq r \leq 1.0$ μm
- *Giant particles* with dry radii in excess of 1.0 μm

The concentration of aerosol varies with time and location, and decreases with increasing horizontal distance from the seashore towards open ocean [Stephens, 1994, p 20].

Atmospheric aerosol is believed to originate in 4 main ways; (1) by condensation and sublimation of vapors during the formation of smokes and heat by combustion, (2) by chemical reactions between trace gases produced either from natural sources or by combustion, (3) by the mechanical disintegration and dispersal of matter at the Earth's surface, either as droplets of sea-water over the oceans, or as soil and mineral-dust particles over the continents, and (4) by coagulation of nuclei leading to the formation of larger particles of mixed constitution [Fleagle and Businger, 1963, p 114].

The major regions of the Earth's atmosphere that are of importance in radio wave propagation are the troposphere and the ionosphere. At frequencies approximately 100 MHz to 300 GHz, the troposphere is by far the most important factor contributing to propagation characteristics of EM waves. Troposphere is the lower atmosphere consisting of a non-ionized region extending from the Earth's surface up to about 15 km. The ionosphere is the Earth's upper atmosphere in the altitude region from 60 km to one earth radius (6370 km). Sufficient ionization exists in this region to influence wave propagation [Bansal, 2006, p 174].

2.4.1 Sources of ionization

The Earth's crust contains radioactive material, mainly Uranium, Thorium, and their decay products. Beta and gamma rays emitted from the ground can ionize the molecules of the air in the first few meters above ground. Radon, a decay product of Uranium 238, is a major ionization source in the first few 100 m above ground over the continents. The ionization production rate Π on the ground is of the order of $4 - 5 \times 10^7$ $m^{-3}s^{-1}$. The second major source of ionization is galactic cosmic rays. The ionization production rate due to cosmic rays has a maximum of about $\Pi = 10^7$ $m^{-3}s^{-1}$ at mid-latitudes near 15 km height, decreasing to about $\Pi = 10^6$ $m^{-3}s^{-1}$ at sea level. These rates decrease by a factor of about two at the equator [Volland, 1984, pp 4 - 5].

Solar X-ray and extreme ultraviolet (EUV) radiation are the principle sources of ionization above 70 km altitude. Their ionization rates depend on latitude, time of day, and season. Other sources of ionization in this height region are irregularly occurring highly energetic electrons and protons of magnetospheric origin [Fleagle and Businger, 1963, p 118].

The ionization sources separate the molecules of the neutral air into ions and electrons. The electrons get attached to neutral molecules forming negative ions. Positive and negative ions form molecular clusters via a hydration process. Examples of such clusters, called small ions, are $H_3O^+ (H_2O)_n$, $H^+ (H_2O)_n$, $O_2^- (H_2O)_n$, and $CO_4^- (H_2O)_n$, with $n \approx 4 - 8$, depending on the water vapour content of the air. The small ions disappear either by recombination with each other or by attachment to aerosol particles forming relatively immobile, large ions.

At heights above 70 km water vapour becomes of minor importance. The ion clusters are replaced mainly by singly charged positive ions like O^+, NO^+, O_2^+, and in greater heights H^+, and by the electrons [Stephens, 1994, p 23]. The solar EUV radiation ($\lambda < 0.12\ \mu$m) is responsible for the formation of various ionospheric layers with a maximum electron density of the order of $10^{12}\ m^{-3}$ within the ionospheric F2 layer near 250 km altitude. The principle ions at that height range are H^+, He^+, and O^+ [Volland, 1984, pp 5 - 6].

2.4.2 Electric Conductivity of Lower and Middle Atmosphere

The electric conductivity of the atmosphere below 60 km is nearly isotropic and varies with height. It depends on the product of the ion density and the mobility factor [Volland, 1984, p 6]:

$$s = s_+ + s_- = en(k_+ + k_-) \tag{2.34}$$

where $e = 1.6 \times 10^{-19}$ C is the electronic charge and n is the number density. The mobility factor, k, describes the ability of positive and negative ions to move. During their motion, the positive and negative ions collide with the neutral particles. At ground level, the mobility factor of the positive small ions is about $k_+ \approx 1.4 \times 10^{-4}\ m^2/(V\ s)$ and somewhat larger for the negative small ions. The mobility of the large ions is several orders of magnitude smaller. Therefore, the large ions do not contribute significantly to charge transport. The average electric conductivity of air at the Earth's surface is about $\sigma_E \approx 10^{-3}$ S/m [Volland, 1984, p 6].

Chapter 3

Earth’s Electric Field

3.0 Atmospheric Electricity

Benjamin Franklin's famous experiment in 1752 "drawing lightning from the cloud" by a kite is generally considered as the beginning of the science of Atmospheric Electricity. The term "Atmospheric Electricity" reflects the earlier efforts to study mainly the electrostatic component of the geo-electromagnetic field. This subject now includes thunderstorm electrification, the global electric circuit, along with lightning and related phenomena, and the propagation of lightning pulses in the atmosphere.

This atmospheric electricity, and consequently the Earth's electric field, is part of the Global (atmospheric) Electrical Circuit (GEC) for which several models have been proposed. The GEC arises from a balance between charge generation in disturbed weather regions and a globally distributed current of small ions flowing in fair-weather regions [Harrison, 2005]. The GEC extends throughout the atmosphere from the planetary surface to the lower layers of the ionosphere.

3.1 Fair-Weather Electricity and Potential Gradient (PG)

The atmospheric conditions are regarded as fair-weather ones if "no processes of charge separation are taking place in the atmosphere" and for these atmospheric conditions "the electrical phenomenon are reasonably steady, so that the principal of the quasi-static state can be used" [Anisimov, 2003]. For analysis a 'Fair-Weather Day' is considered as a day with less than 3 octa (3/8) cloud cover, wind speed less than 4 m/s and no precipitation [Latha, 2003].

A popular model for understanding the global electrical environment assumes two spherical equipotential regions, the Earth's surface (negatively charged) and a highly conducting positively charged electrosphere – *equalizing layer* assumed to be coinciding with the lower layer of the ionosphere, connected together by weakly conducting lower and middle atmosphere [Wilson, 1920]. The potential difference between the electrosphere and the Earth's surface gives rise to a vertical electric field or *potential gradient* (PG) within the Earth's atmosphere.

It is now worthwhile to define 'electric field'. In electrostatics, the electric field **E** at a point is defined as force **F** acting on a unit charge. For moving a positive charge

against the field work is done. The work per unit charge is the *electric potential difference*. Thus, the Electric Field or the PG is the rate of variation of potential with distance. In this study the electric field or the PG refers to the Earth's vertical electric field. The mean fair-weather PG at the Earth's surface is directed downwards and has been found to vary in the range of 100 - 130 V/m [Harrison, 2005; Markson, 1978; Volland, 1984].

According to Wilson's hypothesis the electric potential difference (3×10^4 V) between the Earth's surface and lower ionosphere is supported by thunderstorms activity. The general feature of the GEC is the vertical electric current (2×10^{-12} A/m^2), which flows downward from the lower electrosphere to the negatively charged Earth's surface. Volland [1984, p 7] reports that the average potential difference between ground and electrosphere, called the atmospheric electric potential, is approximately 240 kV. According to Muhleisen [1977] this potential varies between 180 - 400 kV.

Wilson [1920] hypothesized that the potential of equalization layer as measured on Earth under fair weather region is the summative effect of the global disturbed weather feedback. Williams and Heckman [1993] considered lightning, point discharge, conduction and precipitation currents as the feedback charge transfer pathways in analyzing foul weather. They concluded that conduction current other than lightning is the dominant charger for the Earth's surface.

Electric field measured at the Earth's surface is considered as one of the major sources of information in studies of atmospheric electricity, be it global, regional or local [Latha, 2003]. The quasi-static electric field on the Earth's surface is always orthogonal to the ground thus indicating that Earth's surface behaves like an electric equipotential layer for quasi-continuous electric fields [Volland, 1984, p 17].

3.2 The diurnal variation of PG – *Carnegie Curve*

The globally accepted 24-hr electric field variation curve, or more conveniently termed as the *Carnegie* curve, originated through long term electric field measurements over the ocean. The *Carnegie* curve has a maximum at 18 - 21 hrs GMT and a minimum at 3 - 4 hrs GMT, in phase with global thunderstorm curve

[Harrison, 2005]. Electric field or the PG variation follows the same pattern over cleaner stations such as Antarctica or mountaintops [Latha, 2003].

The Carnegie curve originated during the early twentieth century, named after the wooden geomagnetic survey vessel, *Carnegie*, operated by the Carnegie Institute of Washington [Harrison, 2005]. Many standardized atmospheric electricity measurements were made in this vessel around the world's oceans. The reason being, oceanic air is particularly suitable for fair weather measurements as it is usually remote from continental sources of aerosol pollution. In fair weather and air unpolluted by aerosol particles, diurnal variations in PG is due to changes in the total electrical output of global thunderstorms and shower clouds [Siingh *et al.*, 2007].

Whipple [1929] discovered a positive correlation between the *Carnegie curve* and diurnal variation in thunderstorm activity in three areas where they are mainly concentrated; Central Africa, East Asia and America (*mainly in northern hemisphere*). Lightning discharges are also believed to affect PG [Davydenko *et al.*, 2004]. For a thunderstorm of 50 km^3 volume, 10^3 coulombs could be generated in 20 minutes, and this rate of charging is consistent with the discharge rate observed in lightning [Fleagle and Businger, 1963, pp 86]. Similar to thunderstorm activity, lightning activity is prevalent in the northern hemisphere than in the southern hemisphere and mostly occurs over the land [Siingh *et al.*, 2007]. According to Christian [2003], 78% of all lightning occurs between 30°S and 30°N, with Africa the greatest source of lightning region and that there is a global mean land to ocean lightning flash ratio of 10:1.

According to Brown's hypothesis [1935], the double oscillation in local diurnal variation curve of PG over land surface would be the resultant of a single 24-hour fluctuation superimposed by a depression around noon (due to convection). Israel [1948] attributes the variation of local electric field to the resistivity of lower atmospheric layer. As small ions practically determine the local conductivity, it will depend upon the rate of production of small ions and recombination with ions of opposite sign or attachment with bigger particles. Considering the vertical atmospheric mass exchange over land, Franke [1949] mathematically proved that the diurnal variation of the electric field shows a curve with double oscillations.

Delgado *et al.,* [2003] states that it is not only that the electric field is controlled by pollution dependent conductivity but also the dipole moment of the pollutants rearrange themselves as per the prevalent electric field. It is well established that atmospheric ions and charged nuclei and their interaction in the presence of various meteorological parameters give rise to the variation in the local component of the electric field in the atmosphere.

3.3 Surface PG measurement techniques

Early PG measurements mostly used a potential probe, also known as a collector. The potential was measured at the height of the collector. Many different collectors have been employed in the past, viz a burning fuse, a water dropper, a radioactive source and a long wire antenna. In the long wire antenna the effective resistance between the air and the probe was reduced by increasing the area of the collector. In the burning fuse, water dropper and radioactive source, the effective resistance between the air and the probe was reduced by introducing additional ions into the region of air adjacent to the collector [Harrison, 2005].

Early in the nineteenth century Sir Francis Ronalds measured the PG at Kew Observatory, near London, using a lantern-probe-and-straw-electrometer. Later in the mid-nineteenth century Lord Kelvin made major improvements in the instrumentation named later as Kelvin apparatus. This apparatus was being used at Kew Observatories from 1898 to 1981. Later in the nineteenth century, C.T.R. Wilson developed an instrument named later as Wilson's apparatus that measured the air-earth-current and PG. The apparatus consisted of a portable gold leaf electrometer, connected to a horizontal, circular collecting plate, a battery, a variable capacitor, surrounded by an earthed guard ring and a brass cover for the collecting plate. The mean air-earth current density and mean PG were found by timing the change in potential from a sequence of covering and uncovering the plate [Harrison, 2005].

Late in the nineteenth century and in the beginning of twentieth century the vertical profiles of atmospheric electrical parameters were found using balloon ascents. The general feature observed was a decrease in the vertical electric field's magnitude with height [Harrison, 2005].

Nowadays PG measurements are made using mechanical field machines, more commonly known as field mills. These field mills generally offer a more rapid time response and dynamic range [Harrison, 2005].

3.4 Generators and Sources of the Global Electric Circuit (GEC)

For many purposes air acts as a good insulator but when careful measurements are made, air turns out to have characteristic conductivity which varies with time, location, and height. C.T.R Wilson, and Elster and Geitel have attributed the conductivity of air to the movement of positive and negative ions of molecular size through the air in the presence of an electrical field [Fleagle and Businger, 1963, pp 114]. Since the air is electrically conducting, an electric field in the atmosphere cannot be maintained indefinitely, but must be generated by non-electric forces [Volland, 1984, p 1]. To have the vertical electric field, the potential difference must be maintained. Listed below are 6 common sources which contribute to the potential difference.

3.4.1 Thunderstorms

Traditionally the thunderstorm is accepted as the primary aeroelectrical generators driving the GEC [Anisimov, 2003]. From the lower layer of a cloud, net negative charges are transferred to the Earth and from the top layers positive charges are transferred to the conducting upper electrosphere making it a positive potential. This potential difference is believed to cause the PG in the atmosphere. Charge separation inside the thunderstorms leads to the development of huge electric potentials [Milikh and Valdivia, 1999]. In a volume of approximately 50 km^3 there may be stored electrical charge amounting to more than 10^3 coulombs [Fleagle and Businger, 1963, pp 85]. This leads to thunderstorms.

Thunderstorms are more pronounced in the northern hemisphere than in the southern hemisphere. If an active thunderstorm is considered, an upward current flows from thunderstorm to ionosphere, which is known as *Wilson current*. This current consists of field dependent current, convection current, lightning current, precipitation current and displacement current [Siingh *et al.*, 2007]. It spreads around the globe through the ionosphere/magnetosphere along the geomagnetic field lines to the opposite hemisphere, in which the current returns to the Earth as the fair-weather air-Earth

current. Here, the ionosphere and magnetosphere are treated as passive elements. Any disturbance in the atmospheric environment causes a variation in electrical conductivity and electric field system of the atmosphere [Anisimov, 2003].

The accepted thunderstorm hypothesis of aeroelectricity generation was based on the assumption about electrosphere as an equipotential high-conductivity surface. Modern routine research of ionosphere has displayed an electrical potential difference in the lower ionosphere at all latitudes [Anisimov, 2003]. According to Volland [1984, p 26], the dusk-to-dawn potential difference on the polar cap ranges from 20 kV - 100 kV. At high latitudes, with horizontal scales approximately 500 km, the vertical electric field varies by 20 % [Bering, 1998]. Anisimov [2003] in his study showed that the electrical potential difference at mid-latitudes to be more than 4 kV.

Measurements have never shown a complete absence of fair-weather electric field for any length of time, thereby suggesting continuous operation of thunderstorm and other generators in maintaining the current flowing in the global circuit [Siingh *et al.*, 2007].

3.4.2 Ionospheric Dynamo

The regular tidal wind system drives ionospheric plasma at dynamo layer heights thus affecting the ions and electrons. The massive ions move with the neutrals and the electrons are controlled by the geomagnetic field. The differential motion of ions and electrons is responsible for horizontally flowing electric currents. This in turn develops an electric polarization field termed as the *dynamo electric field*. This field tends to converge in some regions of space causing an accumulation of positive charges and diverges in other regions causing negative charges to accumulate. An electric field is produced by the separation of these charges and a current starts to flow. When this current drains the charges at the same rate at which it is being accumulated a net current is produced. Currents and electric fields produced by the ionospheric wind dynamo are relatively weak in comparison with those of solar wind/magnetospheric dynamo at high latitudes [Siingh *et al.*, 2007].

At the ground the electric fields of ionospheric dynamo is about 5% of the main global electric field [Anisimov, 2003]. The ionospheric dynamo is affected by the absorption of ozone at the low latitudes and presence of stronger winds at the higher latitudes [Siingh *et al.,* 2007].

3.4.3 Magnetospheric Dynamo

The solar wind exerts stress to the outer atmosphere which in turn is applied to the terrestrial ionosphere and upper atmosphere. Due to the high thermal energy of the plasma, the drift motion causes charge separation setting up a polarization electric field. The current generated due to this field flows along the geomagnetic field lines down into the ionosphere on the dawn side and up from the ionosphere on the dusk side, both footprints being electrically connected by the dynamo region [Siingh *et al.,* 2007]. The dusk-to-dawn difference (20 – 100 kV) onto the polar cap is generated by the magnetospheric dynamo action, including the solar wind and the Earth's magnetic field. The dusk-dawn electric fields are large sources of quasi-DC field of GEC [Anisimov, 2003]. At lower latitudes the work done by the currents in the ionosphere overcomes the drag on the flow over the polar cap away from the sun and on the flow back towards the sun. The plasma moves anti-sunward across the polar cap due to the force applied by the solar wind, predominantly by reconnection with the magneto-sheath magnetic field [Russell and Fleishman, 2002]. Based on azimuthal flow of magnetospheric plasma, the generator of the atmospheric electric field can influence the distribution of electric field and current [Anisimov, 2003].

3.4.4 Schumann Resonance

Schumann resonance is due to lightning effects, which can be linked to thunderstorms. According to Siingh *et al.,* [2007], lightning discharges between thunderclouds and the ground radiate powerful radio noise bursts over a wide frequency spectrum, ranging from a few Hz to higher than several hundreds of MHz. These noises propagate over long distances through the Earth-ionosphere waveguide. Radio noise below 50 Hz can propagate globally with very little attenuation [Jones, 1999] and constructive interference of these waves result in resonance (*Schumann resonance*) in the Earth-ionosphere cavity, with a fundamental frequency of 8 Hz [Sentman and Fraser, 1999].

Variation in Schumann resonance modes is determined by temporal and spatial distribution of global lightning. Variations in solar activity and nuclear explosions produce disturbances in the ionosphere thereby affecting Schumann resonance. Variation in frequency, bandwidth of the resonance mode and amplitude of the Schumann resonance mode are caused by solar proton events. According to Sentman and Fraser [1999], Schumann resonance intensity depends upon the height of the ionosphere and solar cycle, and responds to solar flares, magnetic storms and solar proton events. Williams [1992] has linked our weather and climate to Schumann resonance and global electric circuit.

The essence of Schumann resonance is that the GEC is modulated by a small current.

3.4.5 Optical emission above the thunderstorm

During intense thunderstorms, the return stroke current does not end always in the cloud; but continues to move upwards, terminating in the lower atmosphere causing optical emissions above the cloud and creating a transient electric field. These emissions can be categorized as sprites, elves, blue jets and blue starters [Siingh *et al.*, 2007]. The following paragraph gives a brief description of the 4 categories of optical emissions.

Sprites appear as luminous pinkish red columns of duration around 50 ms and extend from 30 -90 km in altitude and approximately 1 km in width [Lyons, 1996]. Sprites may occur over any area as long as energetic thunderstorms are present, producing detectable ELF and VLF transients and a vertical electric field perturbation of 0.73 V/m in the stratosphere. According to Siingh *et al.,* [2007], sprites also provide a link between tropospheric processes in thunderstorms and mesospheric processes in the upper atmosphere. Elves are lightning induced flashes that can spread over 90 km in altitude and 300 km laterally in the ionosphere. Blue jets can be classified as slow moving fountains of blue light from the top of the cloud [Siingh *et al.*, 2007]. These 4 categories of optical emissions have minimal effect on surface PG measurements

3.4.6 Mesoscale Convective System

It is *estimated* that Mesoscale Convective System (MCS) also affects the GEC. MCS is the huge electrical active region with stratiform precipitation in horizontal layers,

extending to more than 150 km, whose charge is much larger than a typical thunderstorm. Direct measurements of the electric field have shown that extensive stratiform cloud regions play significant role in the GEC formation [Marshal, 2001].

According to Anisimov [2003] previous GEC models have not estimated the contribution of MCS stratiform clouds into the current budget of GEC and the influence of MCS on the altitude profile of PG and on the ionosphere potential. From Wilson's hypothesis one of the fundamental problems of GEC is the problem of the current budget i.e. thunderstorm currents and the return currents of fair-weather regions have to be in the balance. The modern model of GEC includes contribution by multi-layer structure of the MCS. The model determines the electric field and current inside and in the vicinity of MCS. It has been concluded by Anisimov (2003) that MCS's can serve as an effective generator of GEC formation.

Factors such as solar wind, solar flares, galactic cosmic rays, ionospheric-magnetospheric dynamo, thundercloud, geomagnetic disturbances, solar magnetic sector boundary crossings, solar cycle variations and auroral activity also affect the components of GEC [Siingh *et al.*, 2007].

3.5 Effect of Thunderstorms on PG and the GEC model

A few models of the global electric circuit have appeared over the years.

Hays and Roble [1979] presented a quasi-static model that couples many of the elements operating in the global circuit. They considered thunderstorms as positive and negative point charge pairs constituting current sources that can be randomly distributed in various thunderstorm regions around the Earth, including the effects of the Earth's orography and electrical coupling along geomagnetic field lines in the ionosphere and magnetosphere. However, they did not consider latitudinal, longitudinal and height variations of the atmospheric conductivity. Makino and Ogawa [1984] considered a numerical model including the conductivity details, but neglected the distribution of aerosol particle concentration near the Earth-surface and its subsequent effect on the global resistance. Sapkota and Varshneya [1990] studied the effects of pollution due to aerosol particle ionization caused by corona discharges, solar activity, and of stratospheric aerosol particles (SAP) on the GEC. They have

shown that an increase in SAP increases the global resistance, while decreasing both global current and ionospheric potential. Ogawa [1985] proposed a simple equivalent circuit for the atmosphere, an equipotential surface for the ionosphere and treats the thundercloud as a constant current generator with a positive charge at the top and a negative charge at the bottom.

Markson [1978] proposed a popular GEC model, shown below in Figure 3.1.

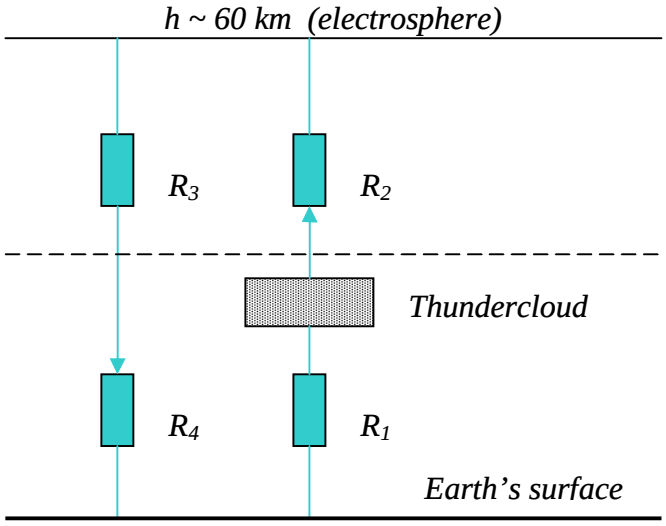

Figure 3.1: The Global Electric Circuit model as proposed by Markson [1978].

In this model it is assumed that the Earth has a negative electric charge about 6×10^5 C, the resistance R_1 under thunderstorm cloud when lightnings are observed is of the order $10^4 – 10^5$ Ω; R_2 above thunderstorm cloud is of the order $10^5 – 10^6$ Ω; the load resistors R_3 and R_4 are equal to 15 Ω and 150 Ω respectively, giving a total load resistance of 165 Ω.

According to Volland [1984, p 17] the load resistance equals to 230 Ω. Ruhnke [1969] proposed the fair weather load resistance to be 300 Ω. In the atmosphere, at each moment, there are ~ 1500 lightnings with total current ~ 1500 A charging the Earth by negative electricity. This current keeps the constant electrospheric potential at approximately +250 kV relative to the Earth's surface. Simultaneously the total discharged current ~ 1500 A flows in the atmosphere (through the resistors R_3 and R_4) over the fair-weather portions of the globe. In a region far way from the thunderstorm activity the value of the average current densities, at an altitude

$h \approx 55$ - 80 km, flowing between equalizing layer and the Earth's surface is $J \approx 10^{-12}$ A/m^2 [Chalmers, 1967]. Volland [1984, p 13] included the capacitive effect of 2.9 F between the Earth and the ionosphere, giving a time constant of $\tau_A = R_A C_A \approx$ 11 minutes, hence concluding the system would discharge within a few tens of minutes if the charge generators were to cease operation.

Other features of the GEC include the electrical conductivity and the columnar resistance of the atmosphere. The electrical conductivity depends upon the distribution of ions, electrons and the presence of a magnetic field in the atmosphere [Siingh *et al.*, 2007]. Close to the ground, ionization is produced as a result of emission of radioactive gases from the soil. From the ground to an altitude of 60 km, galactic cosmic rays are regarded as the principle source of ionization. Above 60 km ultraviolet radiation can be thought to be the major source of ionization. Small ions occur in number concentrations of 500 - 600 cm^{-3} near sea level, decreasing to about 300 cm^{-3} at an altitude of 0.74 km [Reiter, 1992]. Large ions have a lower electrical mobility in air and, thus decrease the electrical conductivity of the atmosphere [Reiter, 1984].

The electrical conductivity generally increases with altitude due to the increase in cosmic ray's energy spectrum and charged particles precipitating from the magnetosphere. When measured from the Earth's surface to an altitude of 80 km, electrical conductivity increases from 10^{-13} to 10^{-7} S/m [Cho and Rycroft, 1998]. The increase in conductivity with altitude leads to the columnar resistance of the atmosphere being concentrated near the Earth's surface. According to Markson [1981], cosmic rays ionize the atmospheric gas constituents and modify the atmosphere's columnar resistance. The fair-weather current flow is closely linked to the vertical variations of aerosol and ion concentration in the atmosphere. Both these parameters determine the total resistance of the atmosphere. Volland [1984, p 26] finds the columnar resistance between sea level and ionosphere to be 1.18×10^{17} Ωm^2 and claims it to be smaller over mountains. In highly polluted areas, the columnar resistance increases significantly and lowers the air-earth current [Siingh *et al.*, 2007].

Solar activity also tends to influence the conductivity. Increase in solar activity leads to a decrease in galactic cosmic ray flux in mid latitudes which in turn leads to a decrease in the conductivity. At the same time, solar protons may be 'funneled' by the Earth's magnetic field to the polar regions resulting in an increased conductivity [Siingh *et al.,* 2007].

The electrical conductivity in clean atmosphere is inversely proportional to aerosol particle content in the air [Siingh *et al.,* 2007]. Aerosol particles are mainly composed of sea salt, wind-blown dust and smoke and occur in concentration of a few hundred cm^{-3} in polar and oceanic region to over tens of thousands cm^{-3} in industrial areas [Israel, 1970]. According to Cobb and Wells [1970], the electrical conductivity is considered as an index of atmospheric aerosol loading over the open ocean and has been used to estimate global changes in the background air pollution level. According to Jayaratne and Verma [2003], the electric field at continental stations is affected by local sources of pollution as well as by convective up-currents due to strong ground heating and exhibits a bimodal pattern. One of the modes coincides with the maximum global thunderstorm activity occurring at 19 hrs GMT (19 hrs LT), while the other occurs in the early morning around 7 hrs LT. The magnitude of this second mode is determined by the temporal variations in atmospheric pollutant dispersion characteristics. Dispersion increases with convection, which increases with surface temperature and is generally a maximum during the afternoon hours [Oke, 1987].

Pollutants in the form of atmospheric particulate matter have a significant effect on small ions in that they tend to attach to each other. This process of attachment creates large ions at the expense of small ions [Jayaratne and Verma, 2003]. Turco *et al*., [1998] and Marsh and Svensmark [2000] suggested that galactic cosmic rays could generate aerosol particles that can act as cloud condensation nuclei and affect the formation and thickness of cloud, particularly over the ocean. They also found a strong association between cosmic ray flux and low clouds, at around 3 km altitude. Svensmark and Friss-Christensen [1997] have shown a correlation between cosmic rays and cloud cover. Thus, it is likely that cosmic rays influence the GEC as well as weather and climate. However, Adlerman and Williams [1996] suggested that

electric field measurements over land aimed at monitoring the global circuit had little value, as they were covered by local pollution.

Williams [2005] has suggested using the GEC as a tool for studying the Earth's climate and climate changes, because of its direct connection with lightning activity. The global electric circuit has been found to response to global temperature changes on time scales ranging from diurnal, through seasonal to El Nino-Southern Oscillation scales [Siingh *et al.,* 2007]. The measurement of Earth's vertical potential gradient therefore helps in the objective of linking the GEC to our climate and weather.

3.6 Effect of Wind on Earth's PG

A simple model for predicting the vertical wind speed profile is the 'Power Law Profile'. Its basic form is:

$$\frac{U(z)}{U(z_r)} = \left(\frac{z}{z_r} \right)^a \tag{3.1}$$

where $U(z)$ is the wind speed measured at height z, $U(z_r)$ is the wind speed at a height z_r, and α is the power law coefficient, given by:

$$a = 0.096 \log_{10} z_0 + 0.016 (\log_{10} z_0)^2 + 0.24 \tag{3.2}$$

where z_0 is the surface roughness length, which characterizes the roughness of the ground terrain [Manwell *et al.,* 2002, pp 43 - 44]. Latha [2003] relates the PG pattern observed during the daytime to wind speed. In the presence of wind, the sand and dust particles are believed to be blown up to considerable heights. The wind speed at any height can then be calculated using a known value for wind speed at any other height, and further links to the PG with wind speed can be established.

Chapter 4

Methodology

4.1 Methodology – Part I

In this project, two physical quantities namely Earth's potential gradient and a satellite signal strength are investigated in detail to find any correlation with cloud cover. To describe the procedures adopted, this chapter is divided into two parts. Part 1 of this chapter describes the instruments used and procedure adopted in collecting the Earth's electric field data. The main instrument used in data collection is the Electrostatic Fieldmeter (JCI 131) which is described in detail in section 4.1.2.1. The main feature of this fieldmeter is that it can detect the field continuously in adverse weather conditions with great sensitivity. The connecting cable and datalogger are also discussed in the same section. The experimental set-up and procedure are described in section 4.1.3.

4.1.1 Earth's Potential Gradient

There exist three components of the Earth's electric field; lateral, longitudinal, and height dependent vertical component. In *Cartesian* coordinate system these components can be termed as the *x*, *y*, and *z* components. To measure all the three components of the electric field simultaneously, Kamra [1983] developed a *dc* spherical field meter that can be used to measure inclined electric field in situations such as in the vicinity of trees, mountains, buildings, below electrified clouds, in dust and snow storms, or even in some non fair-weather conditions where space charges may produce large horizontal field components.

In this research, however, the prime focus is the measurement of the vertical component of the Earth's electric field, E_z, which is generally referred to as the potential gradient (PG). There are several types of field mills available nowadays that offer robust operation in adverse weather conditions and yet provide sensitive measurements of the Earth's PG to an accuracy of ± 1 %.

Figure 4.1 shows the behaviour of Earth's electric field lines in the presence of any obstacle. It also shows the corresponding variation in the potential at various heights. The equipotential lines and electric field lines shown in Figure 4.1 are that of a Fair-weather day. In the case of foul weather (*presence of atmospheric aerosols and clouds*), the electric field is believed to get altered at the ground surface. The equipotential lines are also expected to correspondingly change.

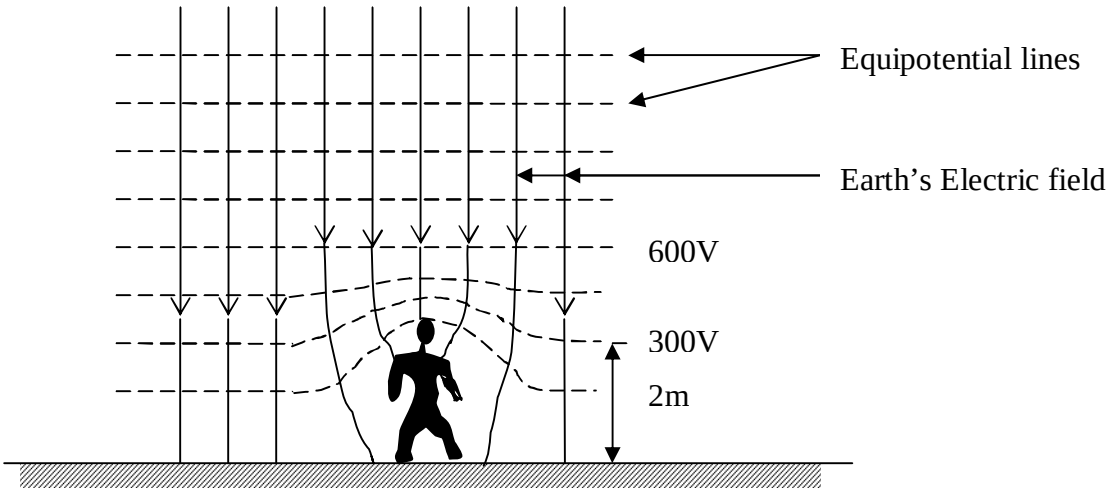

Figure 4.1: Variation in E and V in the presence of an obstacle.

A summary of the different methods used earlier for the measurement of Earth's PG is given in section 3.3. Nowadays the electric field is measured using modern field mills. The JCI131 Electrostatic Fieldmeter, the EFS 1000 Series Electric Field Mill, and the CS110 Electric Field Meter are few of the most readily available electric field mills that have applications in areas such as blasting operations, aerospace, atmospheric research, construction sites, golf courses and swimming pools, and in hazardous materials management. The specifications of these fieldmills are tabulated below:

Table 4.1: Showing the specifications of 3 most commercially available electrostatic fieldmeters

Field Mill Type	Power requirements	Accuracy	Max Range	Operating Conditions
EFS 1000	100-240 V ac, 50/60 Hz	± 1 %	20 kV/m	(-30) - 60°C
CS 110	11-16 V dc @ 750 mA	± 1 %	212 kV/m	(-25) - 50°C
JCI 131	18-36 V dc @ 400 mA	± 1 %	2000 kV/m	0 - 40°C

The JCI131 field mill was used here because it can be operated continuously over a long period. The experimental arrangement used to measure the Earth's electric field is shown in the block diagram in Figure 4.2.

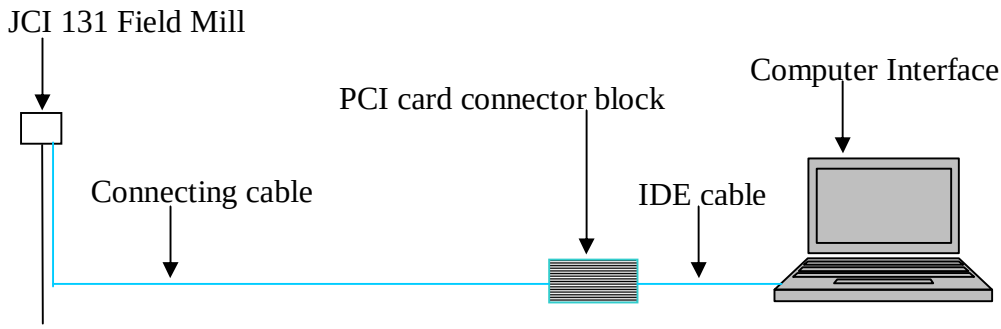

Figure 4.2: Block Diagram showing the components employed in measuring the Earth's electric field.

The JCI131 Field Mill was interfaced to a computer via a PCI card connector block. A manufacturer specified cable was used to connect the JCI131 Field Mill to the PCI card connector block. The connecting cable contains nineteen connecting wires. Out of these only 9 were of primary importance in this study. Each connecting wire is designated by an alphabet labeled on the connector sockets on each ends of the cable. The pins corresponding to these 9 wires were:

B − Earth (0V)

C − connected to positive terminal of the power supply

D − connected to negative terminal of the power supply

E − fieldmeter zero

F − fieldmeter signal output

G − range bit 0 (Most significant bit - *MSB*)

H − range bit 1 (Least significant bit - *LSB*)

P − field health drive

T − field health signal

Description of the pins used

Pin B is used to ground the outer case. Pins C & D were connected to positive and negative terminals of the power supply respectively. The supply voltage was set to 20 V at 400 mA. Pin E is used to ground the field mill. Pin F gives the field signal output.

The field meter automatically responds to the variations in the electric field by selecting either of 4 sensitivity ranges; 1, 2, 3, and 4. These ranges are displayed

using binary notation with 00 corresponding to range 1, 01 corresponding to range 2, 10 corresponding to range 3, and 11 corresponding to range 4. The MSB of these ranges are indicated by pin G and the LSB by pin H.

Pin P employs 2 logic levels to indicate the transition states; logic '0' indicates the smooth running of the chopper by lighting a virtual green LED and logic '1' indicates the presence of foreign objects or insects that obstruct the chopper from turning smoothly by lighting a virtual red LED.

Pin T employs 2 logic levels to indicate the health status of the signal; logic '0' indicates an unhealthy incoming signal and logic '1' indicates the signal contains valid information.

4.1.2 Instrumentation

This section describes the fieldmeter used in this research along with the recommended connecting cable and the datalogger (computer interface).

4.1.2.1 The JCI131 Electrostatic Fieldmeter

The JCI131 Electrostatic Fieldmeter, product of John Chubb Instruments, is a fieldmill designed for precise, high resolution continuous measurement of electric fields in adverse environmental conditions. The design is such that there is no need to ground the rotating chopper thereby making it suitable for long term continuous monitoring of fair-weather atmospheric electric fields and in adverse conditions – such as those associated with thunderstorm and volcano activity.

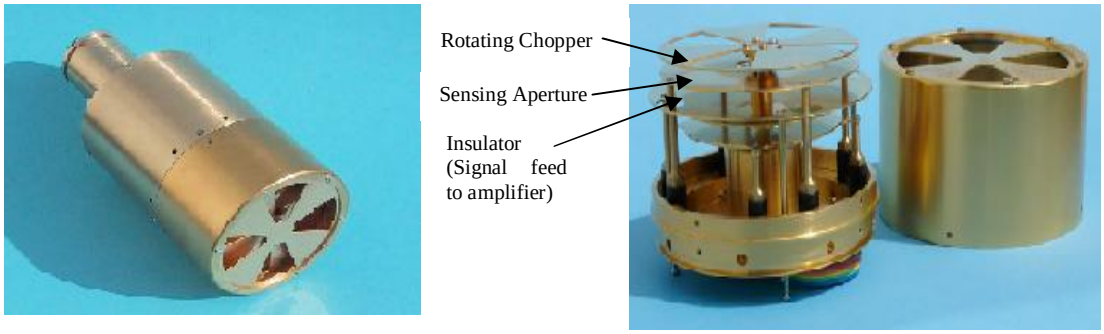

Figure 4.3: Showing the design of the JCI131 Electrostatic Fieldmill.

The top surface of the casing is divided into eight sectors with four alternate sectors removed. The field lines enter the field mill through these open sectors. A similar circular plate, with four alternate sectors removed, is mounted above a circular sensing unit. This plate (rotating chopper) is rotated at a constant speed, so that the sensing unit is exposed to the field lines when the openings in the sectors coincided. The sensing unit (sensing aperture) is mounted using an insulated PVC tubing, isolating the aperture. Within the insulator is the signal feedline to the amplifier and other signal conditioning units. The conditioned signal is accessible at the output which is located at the bottom of the field mill.

Immunity to adverse environmental conditions is achieved using large gaps between the sensing surface to other nearby structures of the fieldmill, long insulation surface tracking paths and a sealed region for the signal processing circuit board. Low noise, good reading, and zero stability are achieved by gold plating all the rotating chopper assembly and sensing surfaces and all surfaces of the sensing region. The diameter of the sensing surface is kept large to provide good signal modulation and achieve good signal to noise ratio at low signal levels. Gold plating helps to avoid electrochemical potential differences between surfaces and ensures that when surfaces are cleaned they return to well defined surface conditions. The large gaps between the rotating chopper and sensing surfaces also minimize the influence of any surface contamination during operation.

The basic chopping frequency is set close to 275 Hz by the manufacturer. This frequency is chosen to be well away from harmonics of possible 50 or 60 Hz mains power supply signals.

To operate the fieldmill, the head unit requires a regulated power supply of 18 - 36 V at 400 mA. The sensing head unit includes two circuit boards; one for providing regulated power supplies and the other for running the fieldmill. The fieldmill provides an analogue full scale output signal of 2 V proportional to the electric field at the sensing aperture as 2 V for 2, 20, 200, or 2000 kV. The maximum output of 2 V for these four field ranges are indicated by the two ‘automatic-changing’ range bits; G (*MSB*) and H (*LSB*). The range bits G (MSB) and H (LSB) indicate the output voltages (bits 00→2 kV, 01→20 kV, 10→200 kV, 11→2000 kV). These sensitivity

ranges are provided with high resolution, low noise and a stable zero. The range selection of the device is automatic however it can be overridden by holding range indicating signal lines HI (+5 V) or LO (earth).

Weighing at about 3kg it is appropriate to mount the fieldmeter sensing head at the top of a pole, facing upwards. On the other hand the EFS 1000 Series Electric Field Mill and the CS110 Electric Field Meter face downward when mounted. This arrangement in the later instrument reduces the effects of atmospheric pollutants and precipitation. For the JCI131 meter, the sensing unit is enclosed by a case, called *Health Shield*, which contains 4 holes at the base to avoid collecting atmospheric pollutants and precipitate.

4.1.2.2 Connecting Cable

The fieldmeter was connected to the computer interface using a PVC insulated cable. This is the manufacturers' recommended cable; DEF Stan 61-12 PVC insulated, overall braid screened. The cable length is 100 m. The fieldmeter contains a sealed 19w Mil socket connector at the back (Pattern 105. Socket: AB05 210014-19SN00). '19w' indicates the enclosed cable contains 19 connecting wires, each isolated from each other.

4.1.2.3 LabVIEW

The software used in this research project to record the data was the commercially available Laboratory Virtual Instrument Engineering Workbench (LabVIEW) software. To record data with LabVIEW the necessary components required to interface are the *PCI card connector block* and an *IDE cable*. The PCI card connector block contains 50 terminals that can be interfaced to the computer at any single time. This interface is made complete with an IDE cable containing 50 connecting wires.

LabVIEW is a programming software but unlike writing codes this software is icon-based. It contains two windows; the front panel that is usually called the display and the block diagram where the programming is done. The block diagram consists of icons logically wired together. These icons are called sub VI's which are pre-programmed and ready to be used in any program the user wants to design. The front

panel displays the primary motive of the program. In this research a simple datalogger was designed that was recording the raw data to a spreadsheet file. The front panel displays the actual signal strength, the sensitivity range of the field mill, the field health drive, the time delay, and the field health signal.

4.1.3 Experimental Procedure

This section outlines the procedure involved in data collection

To check for the calibration of the JCI131 field mill a calibration structure was built. Two sets of 5 m × 5 m wire mesh frames were made using aluminium corner rods, binding wires, 1 inch × 1inch wire mesh, and plastic-strappings. These frames were hung using nylon ropes at a height of 4.5 m and 5 m above the ground. Four pine posts, 6 inches × 2 inches, and 6 meters in length, located at the corners of the wire-mesh were used as the support posts. A third 5 m × 5 m wire mesh frame was laid over the ground below the two suspended frames. The frame at 5 m height was connected to ground. The purpose of this connection was to prevent the Earth's electric field lines inducing a potential on the mesh at 4.5 m. The mesh at 4.5 m was connected to a 5 kV *dc* supply. The potential generated across this frame and the ground was varied.

The JCI131 field mill was mounted on top of a support pole 2 m high, placed at the center of 5 m × 5 m wire mesh frame placed on the ground. The pole was made by welding a galvanized pipe, 2 inch in diameter, to a pipe having a diameter of 1.5 inches. The 1.5 inch end of the pipe was mounted in the ground and the field mill was mounted on the 2 inch end. A hole was cut in the 2 inch pipe to allow for the connecting cable.

The field mill was then linked to the PCI card using the connecting cable. A PCI card was used to interface the fieldmeter signal(s) to LabVIEW. This card is connected to a data acquisition card via an IDE cable. This is the recommended cable since it contains the appropriate pin connections (50 pins).

A program was designed previously by Mr. Vickal Kumar to register the electric field data in units of *V/m.* A few refinements were made to the program while the

equipment was tested. The calibration data observed on the front panel of the program did not compare well with that expected from those produced by the applied *dc* voltage. The instrument was cleaned according to the manufacturers' guidelines and tested again but to no avail. The JCI131 field mill was sent back to United Kingdom for repairs and was received back after 3weeks.

Electric field data for 2 weeks was recorded. The data was then averaged and graphed to see the diurnal pattern. To be effective, the data acquired from the field mill was expected to be close to the readily available literature values. But the pattern observed showed fluctuations; from negative values to a high of 1 MV. The recording was done on fair-weather days which implied the readings of 1 MV were not the true response of the fieldmeter. This fieldmeter was later declared faulty and could not be used further in this research.

A similar research to analyze the fair-weather electric field of the Earth was previously carried out at the University of the South Pacific by Mr. Vickal Kumar. Raw electric field data for the first 7 months of 2006 was made available by Mr. Kumar. This data was used as the investigation data for this part of the project where the effect of cloud cover on Earth's PG is studied in detail.

4.2 Methodology – Part II

The second part of this research is the study of the effect of some atmospheric parameters on a popular television signal – PBS. The PBS signal is transmitted from Sydney and received in Fiji through INTELSAT 701. Most communication satellites operate in the microwave frequency spectrum. The microwave frequency spectrum is divided up into frequency bands. The most widely used frequency bands are the *C*-band and *Ku*-band [Frenzel, 1998, p 631]. According to the IEEE standard, the C-band ranges from 4 to 8 GHz and Ku-band ranges from 12 to 18 GHz. The most widely used satellite communications band during the late 1990's was the C-band [Frenzel, 1994, p 294]. Nowadays, Ku, K, and Ka bands are mostly used for satellite communications.

4.2.1 Pacific Broadcasting Services (PBS)

PBS and Sky Pacific are two leading television service providers in Fiji that offer the luxury of selecting from a multiple number of channels. PBS, utilizing the Ku-band of the EM spectrum, offers 13 channels while Sky Pacific, employing the C-band, offers 16 channels. While Ku-band is cheaper to operate than C-band, and provides for a more protected service, it has one drawback. Ku-band signals weaken when they pass through rain, a condition called rain fade.

This has been studied by many researchers [Allnut and Haidara, 2001; Pan *et al.*, 2000; Ramachandran and Kumar, 2004]. It is widely believed that at times, even when the rain rates are small or nil, the PBS signal experiences attenuation. This attenuation may be due to the cloud cover. The effect of cloud cover on PBS signal strength then becomes an interesting investigation area of EM wave propagation.

4.2.2 Instrumentation

A receiver site, such as used in this research to receive the PBS signal, consists of an antenna designed to collect and concentrate the signal to its focal point where the *feedhorn* is located. This channel the microwaves to an electronic circuit called a *low noise block* (LNB) which amplifies and downconverts the signal to a lower intermediate frequency (IF) which is later transmitted by a coaxial cable (coax) [Stephenson, 1994, p 13].

The experimental arrangement used to receive the PBS signal is shown as a block diagram in Figure 4.4.

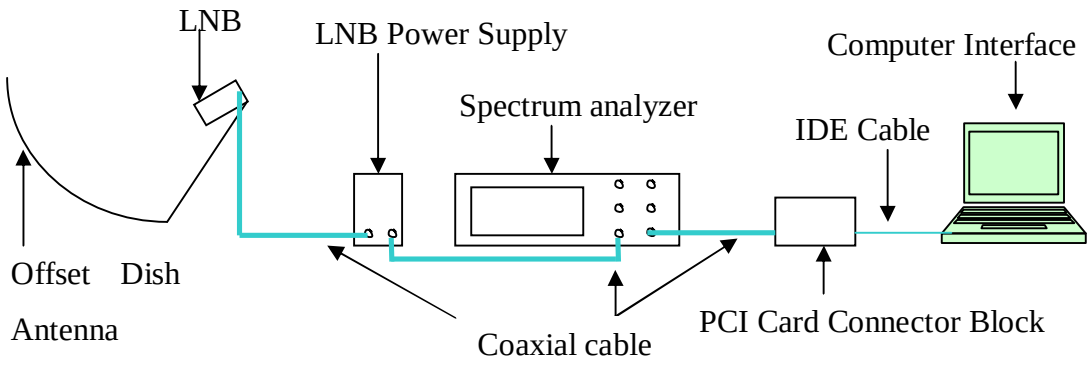

Figure 4.4: Block diagram showing the components required to receive the PBS signal

The frequency of PBS signal transmission is 12.648 GHz. The different components used to receive the signal are described below.

4.2.2.1 Antenna

An offset dish antenna, with an offset angle of 30°, was used in this research. The diameter of the dish antenna was 1.2 m. The advantage of using an Offset dish antenna is that the receiving device (feedhorn) does not cast its shadow on the dish.

4.2.2.2 Feedhorn and Low Noise Block (LNB)

In a receiving system, the feedhorn collects and focuses radio waves that are incident on its aperture. The feedhorn is mounted at the focus of the parabolic reflector. A Low Noise Block (LNB) is a device that processes weak satellite signals directed by an antenna reflector into a feedhorn, whilst introducing as little electrical noise as possible in the process [Gibson, 1997, p 58]. Figure 4.5 shows the mechanical block diagram of a LNB.

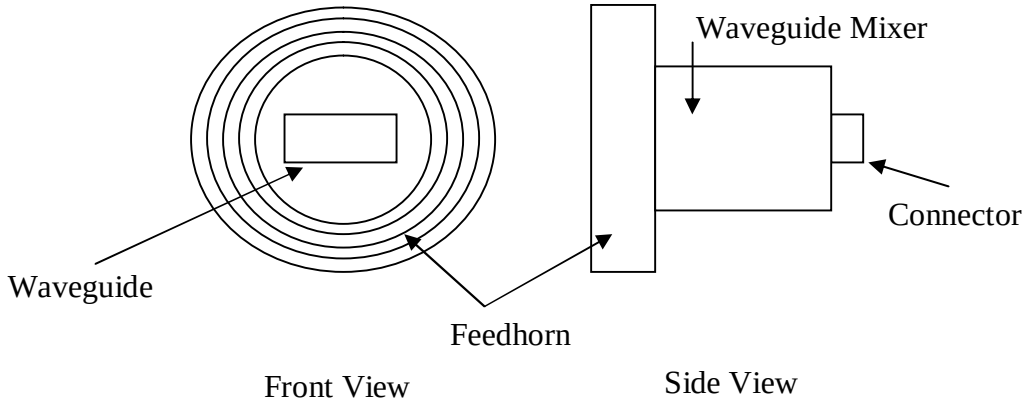

Figure 4.5: Diagram showing the mechanical block diagram of LNB.

A LNB consists of a bandpass filter, followed by a high gain, low noise microwave amplifier and a frequency converter, which downconverts the RF signal to a lower intermediate frequency [Frenzel, 1998, p 608].

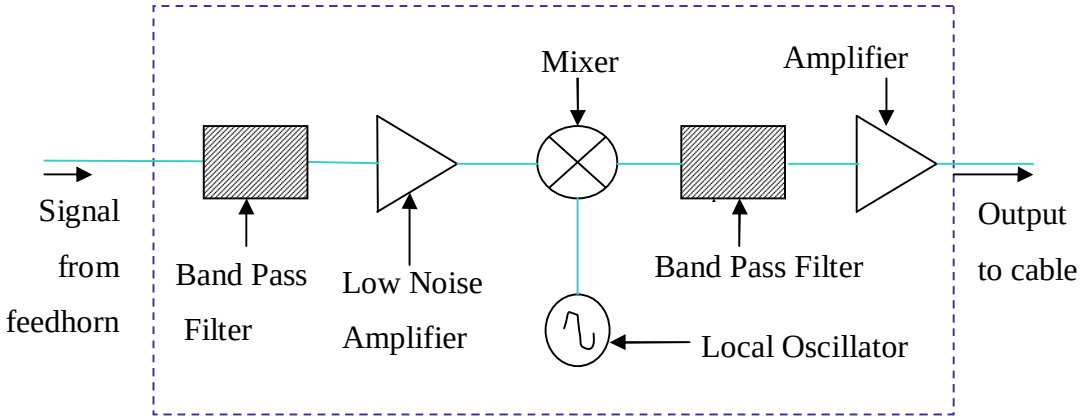

Figure 4.6: Electronic Block Diagram of the waveguide mixer.

The signal first goes through a bandpass filter which only allows the intended band of microwave frequencies to pass through. The signal is very weak at this point even though it has been multiplied by the gain of the receiving antenna. The desired signal is then amplified by a Low Noise Amplifier (LNA), usually a GaAsFET circuit. Amplifiers with low noise temperature are used to increase the level of the signal. Once the signal has been amplified, it is translated in frequency. This is done in a mixer circuit. The output signals are the sum and difference of the incoming signal and the local oscillator (*LO*) frequency [Frenzel, 1994, p 297]. For example, in this case the sum and difference of the incoming PBS signal (12.648 GHz) and *LO*

(11.3 GHz) are 23.948 GHz and 1.348 GHz respectively. The mixer output is then fed to a bandpass filter. In this project, the filter was a low pass filter which allows the 1.348 GHz signal to pass through and reject the 23.948 GHz signal.

4.2.2.3 Connecting Cable

Special coaxial transmission cable (Model # RG 57) provided the simplest method of transmission of IF signal to the spectrum analyzer. The principal use of coax is as a transmission line for radio frequency signals with low loss. It is practical to have a connecting cable with the lowest possible losses and immunity to stray radio frequency.

4.2.2.4 LNB Power Supply Set-up

The LNB, being an active device, was powered using a dc power supply set at 17 volts, which allows the local oscillator to operate at 11.3 GHz. The arrangement is shown in Figure 4.7.

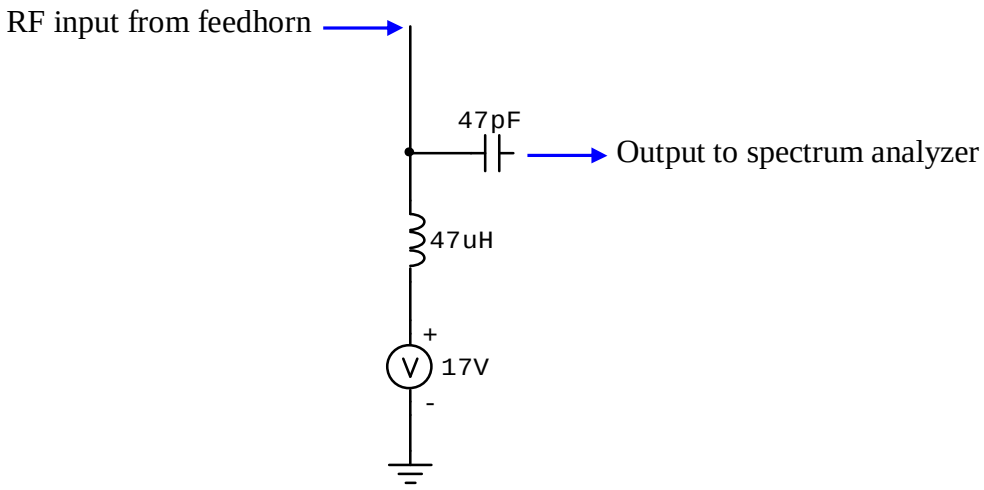

Figure 4.7: LNB Power Supply set-up.

The purpose of the series 47 μH inductor was to prevent the *ac* signal coming out of the LNB to enter the power supply. The purpose of the shunt 47 pF capacitor was to block the 17 V *dc* signal entering the spectrum analyzer, thereby only allowing the *ac* signal to the input of the analyzer.

4.2.2.5 Spectrum Analyzer

There are two general ways of looking at signals: the time domain and the frequency domain. The time domain of the signal can be observed on an oscilloscope. For frequency domain observation of signals *Spectrum Analyzers* are used [Blake, 2002, p 30]. Figure 4.8 below shows the basic block diagram of a spectrum analyzer.

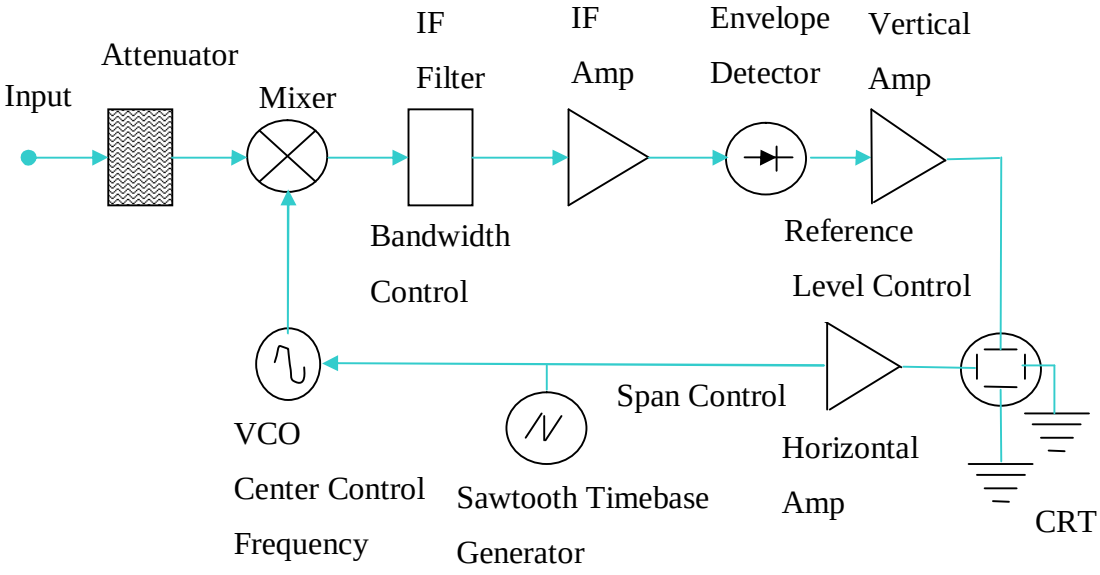

Figure 4.8: Block diagram of a Spectrum Analyzer.

The incoming signal is applied to a mixer, along with a swept-frequency signal generated by a local oscillator in the analyzer. The mixer produces outputs at the sum and difference of the two frequencies that are applied to its input [Blake, 2002, p 30].

The filter can be arranged to be either at the sum or the difference of the frequencies. As the oscillator frequency varies, the part of the spectrum that passes through the filter changes. The oscillator is a voltage-controlled oscillator (VCO) whose frequency is controlled by a sawtooth wave generator that also provides the horizontal sweep signal for the cathode ray tube (CRT) [Blake, 2002, p 31].

The filter output is an ac signal that must be rectified and amplified before it is applied to the vertical deflection plates of the CRT. If the amplification is linear, the vertical position of the trace will be proportional to the signal voltage amplitude at a given frequency [Blake, 2002, p 32].

4.2.2.6 Datalogger (*Computer Interface*)

The strength of the PBS signal, centered at 1.348 GHz, was measured in volts from the vertical output terminal of the spectrum analyzer. The signal from this terminal was interfaced to the computer (datalogging program designed in LabVIEW). The procedure for interfacing was similar to that described in Section 4.1.2.3.

4.2.3 Experimental Set-up and Procedure

The INTELSAT 701 is located at 180°E. It broadcasts PBS TV signals from Sydney to Fiji at a frequency of 12.648 GHz. This signal was studied as part of the project. The measurement site was University of the South Pacific (USP), Suva, Fiji, located at 18.13°S and 178.47°E.

A dish antenna with an offset angle of 30°, together with a LNB located at the focal point of the antenna, was used to receive the signal. The local oscillator frequency of the LNB was 11.3 GHz. LNB down-converted the received Ku band signal to 1.348 GHz. The output from the LNB was connected to the spectrum analyzer (Model # 8555A) by a coaxial cable. The vertical output port of the spectrum analyzer indicates the signal strength in Volts. This output is proportional to the total area under the signal trace viewed on the screen. This signal was recorded in the computer described in Section 4.2.2.6.

A program was designed in LabVIEW to sample the signal at every 10 seconds and output the average of 6 data points as 1-minute data. The 1-minute data was recorded to a spreadsheet file.

Rainfall data was recorded in the datalogger (Model # CR23X). The datalogger, programmed using '*logger-net*', was used to record the rainfall rate corresponding to the tipping bucket rain-gauge arrangement. The specification of the tipping bucket is given below

Diameter	:	200 mm [Model RDG-0]
One tilt of bucket	:	0.2 mm of rainfall

The rainfall rate was measured and recorded every second. The total amount of rainfall over the hour and over the day was recorded.

4.3 Solar radiation

Solar radiation data was measured using a solarimeter (Model # CM 21). This solarimeter detects the direct radiation and the diffused radiation coming from all the directions. The total radiation falls on the sensing surface, commonly known as a plastic dome, which is hemispherical in shape. The CM 21 solarimeter can measure incoming solar radiation, in the range of 305 – 2800 nm, up to a maximum of 4000 W/m^2. The high optical quality of the domes employed in the solarimeter reduces the error to less than 10 W/m^2. The response of the solarimeter is governed by Lambert's Cosine Law. Few special features of the solarimeter include high sensitivity, low impedance, low temperature response, and low non-linearity.

The output from the solarimeter was connected to the datalogger (CR23X). This datalogger was programmed to sample the solar radiation every 10 minutes and then average and record it over the hour. Hourly average values are therefore used in this research.

Chapter 5

Results and Discussion

5.0 Chapter Overview

This research deals with the effect of cloud cover on Earth's vertical electric field or PG and on Ku band signal strength. Following the format of the presentation of the methodology in Chapter 4, the results are also presented in two sections. Section 5.1 presents the findings on the variation of PG while Section 5.2 presents the results of the study of the PBS signal strength.

5.1 Earth's Electric Field

The Earth's electric field data, measured at Suva, Fiji (18.08°S, 178.45°E), was grouped into three "types of days": Fair-weather days, Cloudy days and Rainy days. The following sub-sections describe the classification of days into the three types of days, followed by grouping the electric field data for the corresponding types of days. The electric field (PG) data for the different types was averaged and plotted against local time to examine the effect of cloud cover on the variation of PG.

5.1.1 Classification of Days

Alexander [1999] described a cloudless day with insolation level reaching up to 879 W/m^2 as a fair-weather day. From a study in England (52°N, 0°W), Monteith and Unsworth [1990] have presented insolation level around noontime is more than 800 W/m^2 for a cloudless day in summer. Since solar radiation intercepted at the Earth's surface is dependent on the latitude of the measurement site, this value is expected to vary around 800 W/m^2. Ramachandran *et al.,* [2007] considered a fair-weather day as having peak solar radiation value of greater than 800 W/m^2. For this study a 'Fair-weather day' is considered as having insolation levels of 800 W/m^2 or more whereas a cloudy day is taken with values below 800 W/m^2. Figure 5.1 shows the sample solar radiation patterns observed at the measurement site for two different day types; Fair-weather day and Cloudy day.

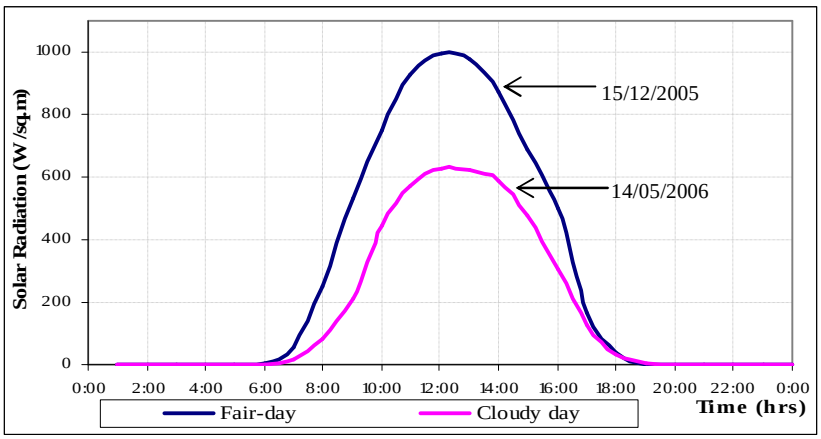

Figure 5.1: Solar radiation pattern for a fair-weather day and a cloudy day

The solar radiation data in Figure 5.1 are averaged values of solar radiation over 1-hour interval. A solar radiation curve is expected to peak when the sun is overhead. In Fiji, the maximum insolation is observed at 12 noon with very little variation between 11 am and 1 pm local time (LT). Another feature of the insolation curve is its 'bell-shape'; increasing from a low of zero in the early morning hours to a maximum, and then decreases to a low of zero in the late evening hours.

A rainy day is determined by looking at the rainfall data. The solar radiation curve for an arbitrary rainy day depends on the intensity of cloud cover and the duration of rainfall. A larger mass of cloud will take longer to discharge than a smaller mass of cloud given they both discharge at the same rate through a considerably similar area. As the smaller mass of cloud clears out, more insolation is received at the Earth than that received when a larger mass of cloud clears. Hence, the solar radiation curve for a rainy day can differ from other rainy days.

After classifying the days as fair, cloudy, and rainy, the electric field data was sorted out into the three groups. Solar radiation data was also grouped along with the electric field data into the three groups. PG data recorded from December 2005 to July 2006 is used in this study. From 131 days, 75 days were found as fair-weather days and 56 days as cloudy days. The effect of rain on Earth's electric field is not investigated here since it had already been studied by Kumar [2003] (See section 5.1.6).

5.1.2 Electric Field on Fair-weather days

The classification of days described in the previous section is a generalized one. For example, there are some days with no negative PG recorded and some days with negative PG. There are also days when the PG values are higher than 1000 V/m. The maximum PG recorded was 5273 V/m, on 27th July 2006. Ramachandran ***et al.,*** [2007] attribute this high potential to foreign particles (pieces of grass, leaves etc.) coming in contact with the sensing aperture of the fieldmill. For this reason the days were further grouped using the number and letter system for classification of potential gradient (adapted from Harrison, 2005) as shown in Table 5.1.

Table 5.1: Number and letter system for classification of potential gradient [*Adapted from Harrison, 2003*]

First character	Requirement
0	No negative PG measured midnight to midnight
1	One or more negative measured, but with a total duration less than 3 hours
2	Negative PG measured, with total duration longer than 3 hours
Second character	**Requirement**
A	PG always less than 1000 V/m in all 48 30 min periods
B	PG greater than 1000 V/m for less than 6 individual hours
C	PG greater than 1000 V/m for more than 6 individual hours

The 75 fair-weather days were further grouped according to the classification given in Table 5.1. Electric field data corresponding to group '0a' is analysed and presented here. This group contains 31 days during the period beginning 1st June 2005 to 30th June 2006 for which this analysis is carried out.

The electric field data was recorded using two execution intervals: 10-seconds and 1-minute. The electric field data for 31 days was averaged to represent one set of '24-hr Fair-days average electric field data'. Figure 5.2 shows the averaged diurnal electric field variation for the 10-second recording interval.

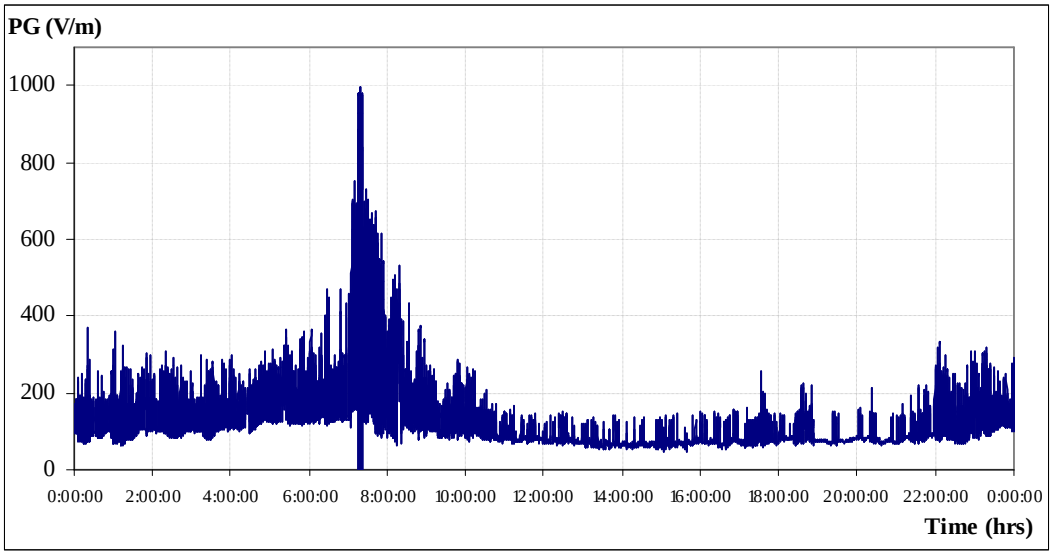

Figure 5.2: Average diurnal variation in PG with 10-second recording interval.

It can be seen in Figure 5.2 that the maximum PG, when averaged over 10-second intervals, is close to 1000 V/m and is observed around 7 am LT.

The averaged diurnal variation for the 1-minute recording interval is presented in Figure 5.3 below.

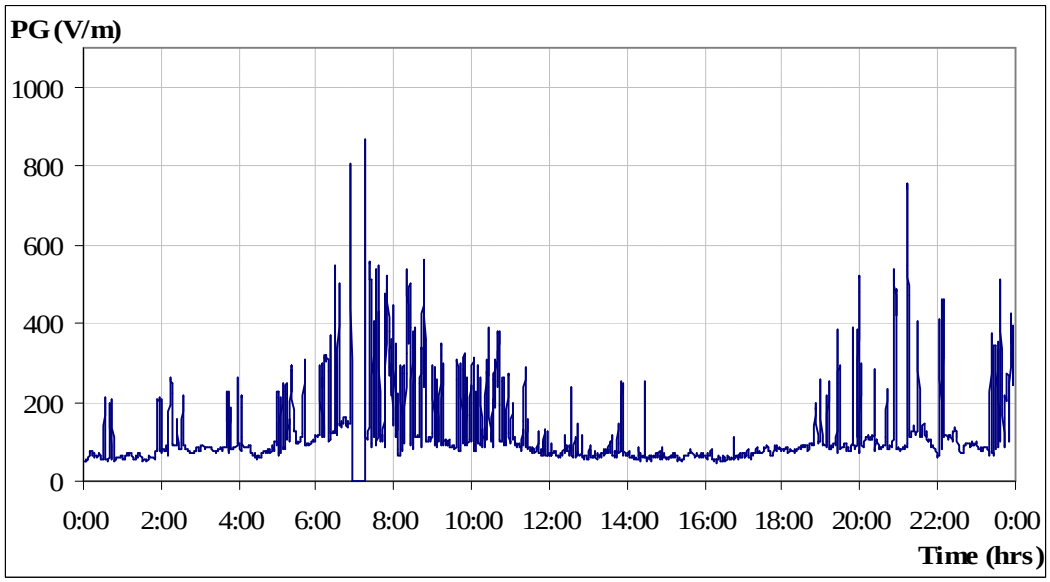

Figure 5.3: Diurnal variation in PG using 1-minute averaged values.

It can be seen from the above figure that the electric field attains very high values around 7 am and 9 pm LT. The maximum PG, when averaged over 1-minute intervals, is close to 850 V/m. The 10-second averaged diurnal pattern and the 1-

minute averaged diurnal pattern was further averaged over 30-minute intervals. The resulting pattern is presented in Figure 5.4. When Figure 5.4 is compared with Figure 5.2 and Figure 5.3 it is seen that the averaging effect over longer time intervals reduces the very minute fluctuations and peak values of PG. However the trend of the times of occurrence of maxima and minima was unaltered.

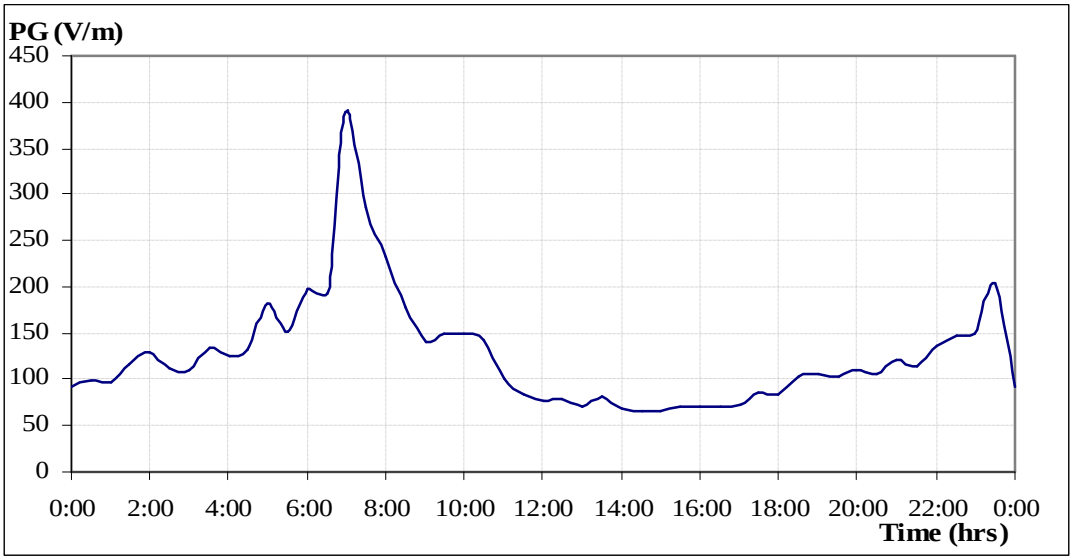

Figure 5.4: Diurnal variation in PG using 30 minutes averaged values.

The pioneering analysis of diurnal variation of PG was based on hourly measurement [Harrison and Aplin, 2002]. The solar radiation used in this work was averaged over one hour. Further Panneerselvam *et al.*, [2003] have suggested that to identify possible signatures of the GEC on PG, the hourly averaging procedure is most suitable. For this reason, the PG variation was analysed using one hour averages so that any possible correspondence could be drawn.

Figure 5.5 shows the variation of 'fair-weather days' electric field when averaged over hourly intervals. Also shown is the average solar radiation pattern for the corresponding 31 fair-weather days.

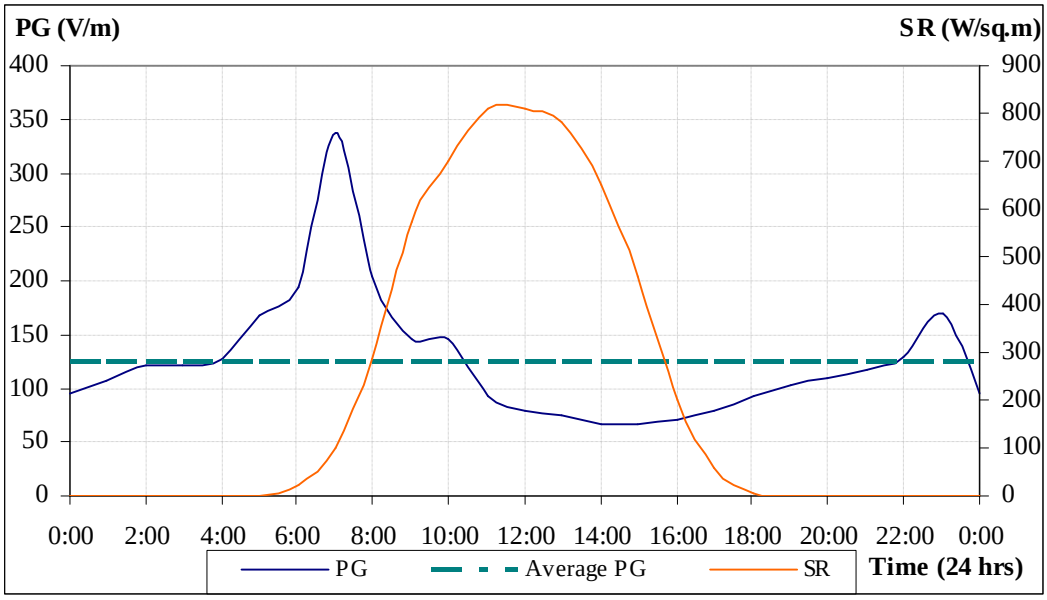

Figure 5.5: Diurnal variation in PG and solar radiation using 1 hour averaged values.

Few reasonings behind the diurnal variation of PG are described in Section 3.2. Latha [2003] suggested that the variation of resistivity of the lower layer of the atmosphere is due to various factors such as 1) changes in vertical convection, 2) ions of various size ranges, 3) aerosol content variation affecting them, and 4) space charge formation. Electrical conductivity is inversely proportional to aerosol concentration and a reduction in conductivity tends to increase the PG in order to maintain constant current.

The diurnal variation of the electric field presented in Figure 5.5 is explained in the following paragraphs. The explanation begins with the variation of PG from early morning hours and continues along the diurnal variation profile till the late night hours. Contributions by factors such as aerosol content, ionization, and wind, which are believed to affect PG, are discussed. The effect of regional thunderstorm activity is also considered in this discussion.

The mean fair-weather PG at this station is 125.70 V/m. This value is in close agreement with the value of 120 V/m reported by Harrison [2005]. Ramachandran *et al.*, [2007] carried out a similar analysis for 63 fair-weather days at the same measurement site and for the same period and found the average surface PG to be 143 V/m. The difference in the values can be attributed to the fair-weather days

considered in the two analyses. The selection criterion for the fair weather days in the study carried out by Ramachandran *et al.*, [2007], differed slightly from that adopted here, therefore could have included days with higher average PG values which eventually increased the average PG for the period of study.

The morning maximum, 'Sunrise peak', observed at this station occurs around 7 am LT. The potential gradient at this hour is 336.49 V/m. The rapid increase to the morning maximum could be due to the sudden solar influx [Saha and Anathakrishnan, 1976]. Marshall *et al.,* [1999] suggested that nearness to water bodies may enhance sunrise effect. In their study, Marshall *et al.,* [1999] further showed that enhanced positive electrode layers accumulate very close to the surface before sunrise since radioactivity in the soil and air is relatively little. They attributed the vertical mixing of the electrode layer charge leads to an increased electric field. The measurement site is located approximately 500 meters from the sea. The reason for the very high morning peak might then be due to the station being close to the sea.

Dhanorkar and Kamra [1994] observed an increase in total aerosol concentration close to ground early in the morning. The possible reason for increase in aerosol concentration could be the morning rush hour of traffic. Garimella and Deo [2007] found the concentration of total suspended particles in Suva's air to be in the range of 9 - 43 $\mu g/m^3$. These particles are mainly composed of sodium, iron, and zinc. They have attributed the source of these particles is mainly limited to crustal material, industrial dust, sea spray and vehicular emissions.

Chalmers [1967] suggested the increase in PG during the sunrise hour(s) is due to the beginning of vertical convection. Law [1963] studied fair weather ionization close to ground and concluded that PG follows the increase in positive charge density.

The PG decreases gradually after 10 am LT from 145.37 V/m to a minimum of 67.15 V/m, the lowest observed in the 24-hour cycle (3 pm LT). Latha [2003] proposed that the atmosphere is well-mixed and the winds are relatively high during this period, which follows directly from Kamra's [1968] explanation that high winds significantly reduce the PG and at times reverses PG. From a study in Casper, USA, Manwell *et al.*, [2002] showed that the wind speed is highest around 2 pm.

The effect of wind on surface PG is also investigated here. Wind speed was recorded at a height of 2 m using a '3-cup' anemometer arrangement. The datalogger was programmed to sample the wind speed every second and record the average value over the hour. To relate wind speed with PG, wind speed at a height of 1 m was calculated using the 'Power Law Profile' (Section 3.6). The presence of nearby buildings and trees significantly affect the extent of wind that is believed to effect the PG. Figure 5.6 below shows the horizontal wind profile on a fair day (3rd February, 2006). This horizontal wind profile closely follows that reported by Manwell *et al.*, [2002].

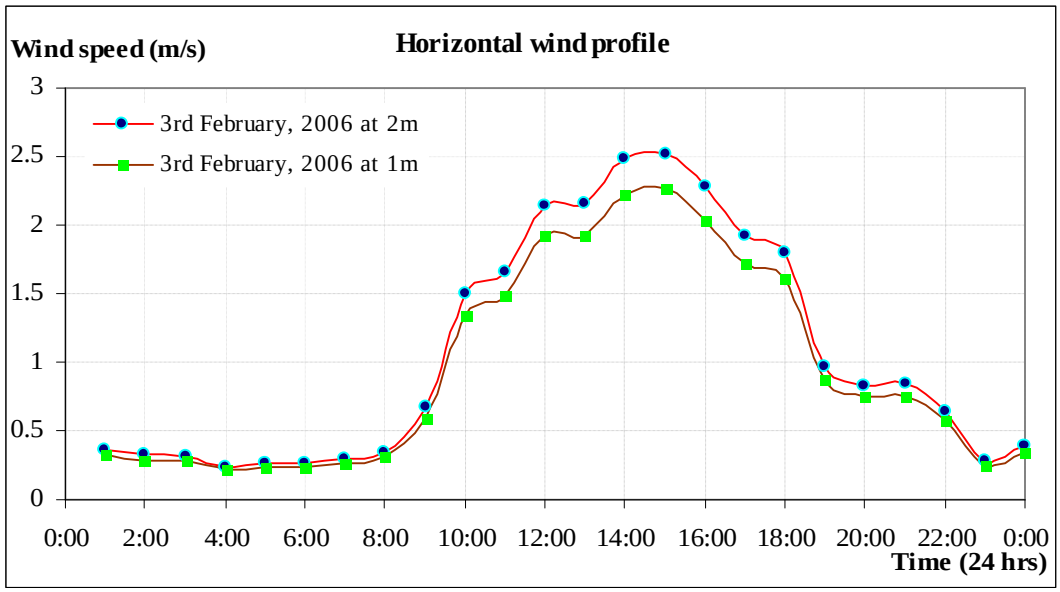

Figure 5.6: Horizontal wind profile at a height of 1 m and 2 m for a fair day.

The figure above shows that wind speed is highest between 2 pm and 3 pm LT. The measurement site is classified as a terrain having few trees. Manwell *et al.*, [2002] stated the corresponding surface roughness length (characteristic describing the roughness of the ground terrain) for a terrain with few trees is 0.1 m. Using equation 2.32, α is 0.895. The wind speed at a height of 1 m ($U(z)$) was found using equation 2.31. After 3 pm LT the wind speed starts to decrease and the electric field starts to increase.

The evening peak in PG of 170.26 V/m is observed around 11 pm LT. At this hour, on 3rd February 2006, the wind speed is 0.22 m/s, which coincidently is the evening minimum.

The evening peak, as explained by Latha *et al.*, [2003], is due to the lowering of exchange layer heights that has its maximum in the afternoon. Around this time the wind speed and convection reduces significantly which allows the aerosol to settle to the lower layers resulting in an intense layer above ground level. This leads to reduced conductivity, which in turn increases the PG [Raj *et al.*, 1997].

Israel [1970] and Jayaratne and Verma [2003] noted that the evening peak in PG diurnal variation coincides with the maximum global thunderstorm activity around 19 hrs UT. Ramachandran *et al.*, [2007] showed that the peak thunderstorm activity for the region was observed around 21 hrs LT and it coincided well with the time of the secondary maxima in PG.

5.1.3 Electric Field on Cloudy days

The cloudy days were classified as having solar radiation values of less than 800 W/m^2. If the cloud cover remained constant the solar radiation curve is expected to have a 'bell-shaped' response (as seen in Figure 5.1). In the case of varying cloud cover on a certain day, the solar radiation pattern changes accordingly. Such days are neglected from this analysis. Similar to the selection criterion adopted for fair-weather days, electric field data corresponding to group '0a' (Table 5.1) are analysed and presented here. This group contains 26 days. As cloud cover increased the general tendency has been a decrease in PG. Figure 5.7 shows the average 'cloudy days' electric field pattern averaged over hourly intervals. Also shown is the average solar radiation pattern for the corresponding 26 cloudy days.

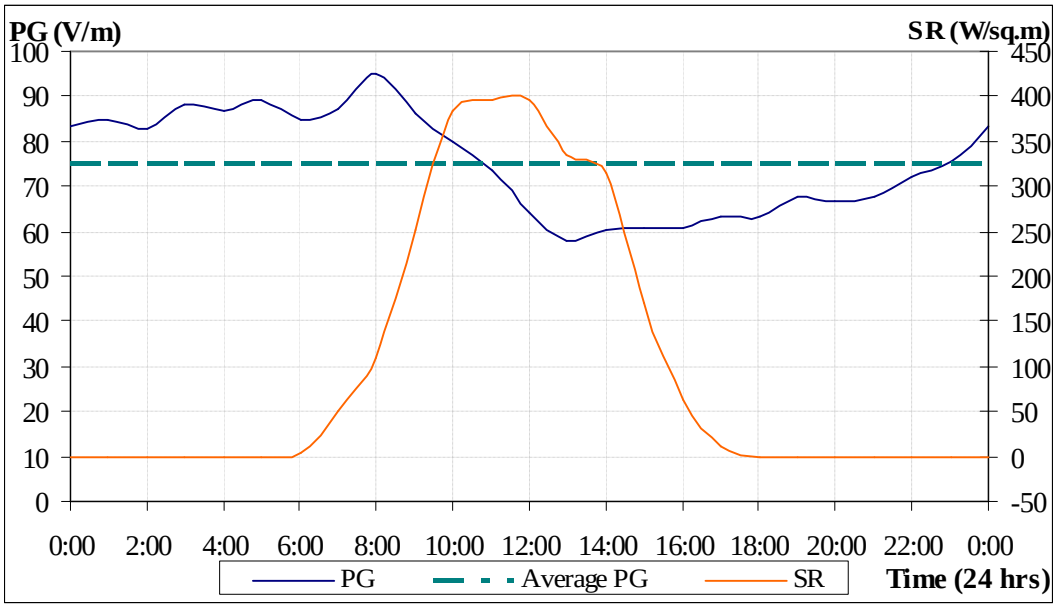

Figure 5.7: Diurnal variation in PG for Cloudy days using 1 hour averaged values.

The major criterion which was used to classify the days as fair-weather and cloudy days is the solar radiation which can be measured only during sunlight hours. The PG can be measured during the entire 24 hours of the day. When calculating the average PG, the cloud cover during the night was assumed to be similar to that of the daytime.

The sunrise effect on PG was noticeable even on cloudy days. The mean PG on cloudy days is 75.13 V/m. The morning peak of 95.23 V/m for cloudy days occurs around 8 am LT, which is a little delayed compared to the average fair-weather days' morning peak. The PG decreases gradually to the afternoon minimum of 58.04 V/m around 1 pm LT, and is maintained around 60 V/m till 4 pm LT, after which it starts to increase.

Though the late evening peak is not clearly visible here, it can be observed that the PG values are relatively high during the night when compared to daylight hours (except during the morning peak).

5.1.4 Comparison of Electric Field on Fair-weather and Cloudy days

This section investigates the effect of cloud cover on Earth's vertical electric field (PG). The PG of fair-weather days is compared with that of cloudy days. Figures 5.5 and 5.7 show the average diurnal variation of PG and solar radiation on fair-weather

days and cloudy days. For easy comparison they have been reproduced in Figures 5.8 and 5.9.

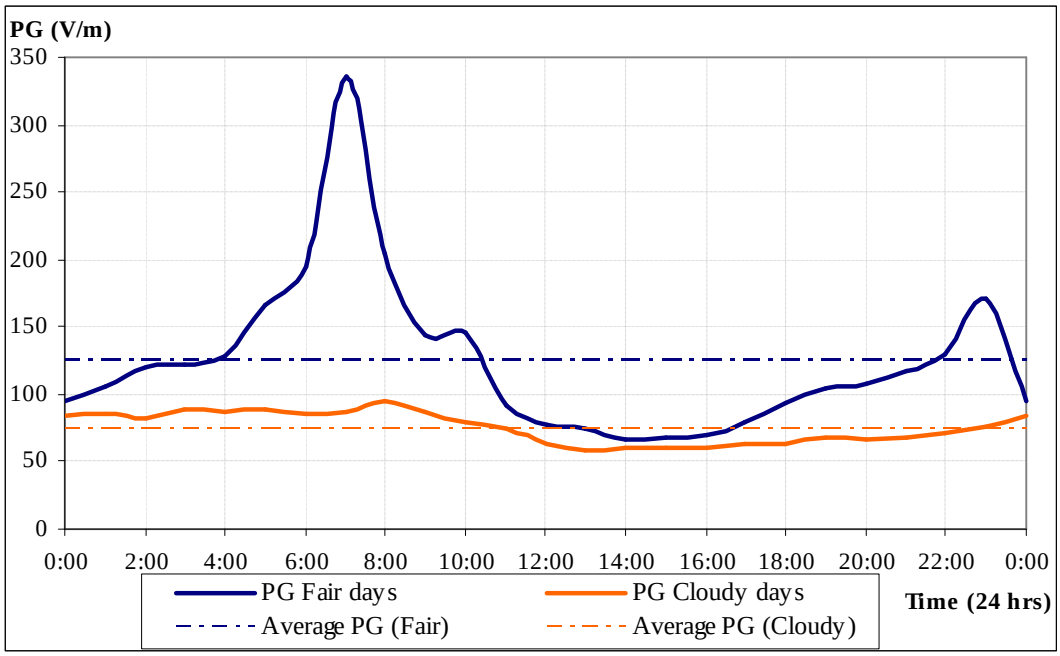

Figure 5.8: Variation of PG on Fair-weather days in contrast with Cloudy days.

Both the plots show the PG is high in the early morning hours. The morning peak (sunrise peak) is observed on fair-weather days but not so pronounced on the cloudy days. The evening peak is observed for fair-weather days but not for cloudy days. The general feature that can be seen in Figure 5.8 is that the PG on fair-weather days is always greater than that of cloudy days during the 24-hour period. If cloud cover is assumed to reduce PG, then the experimental observation confirms one assumption that on cloudy days, the non-sunshine hours are also cloudy.

Figure 5.9 shows the average insolation variation during the daytime on fair-weather days and cloudy days.

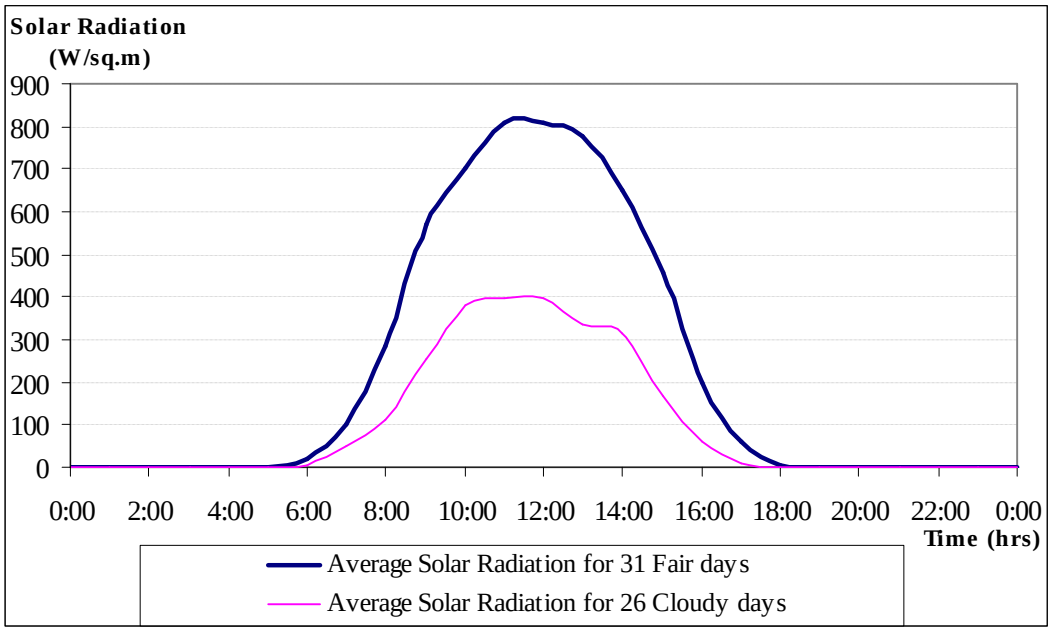

Figure 5.9: Average solar radiation patterns for Fair-weather days and Cloudy days.

Both groups of days exhibited a near bell shaped insolation variation and the insolation level of fair-weather days is always greater than that of cloudy days.

5.1.5 Variation of PG on the days with different levels of solar radiation

To understand the effect of cloud cover on PG, the cloudy days are further classified into 3 groups;

- Group 1 - containing 8 days with peak solar radiation values ranging from 200 to 400 W/m^2,
- Group 2 - containing 10 days with peak solar radiation values ranging from 400 to 600 W/m^2, and
- Group 3 – consisting of 8 days with peak solar radiation values ranging from 600 to 800 W/m^2.

This range of solar peak insolation was chosen so that a representative range of days could be selected from a total of 26 days. Figure 5.10 shows the hourly average PG pattern for the 3 groups of cloudy days.

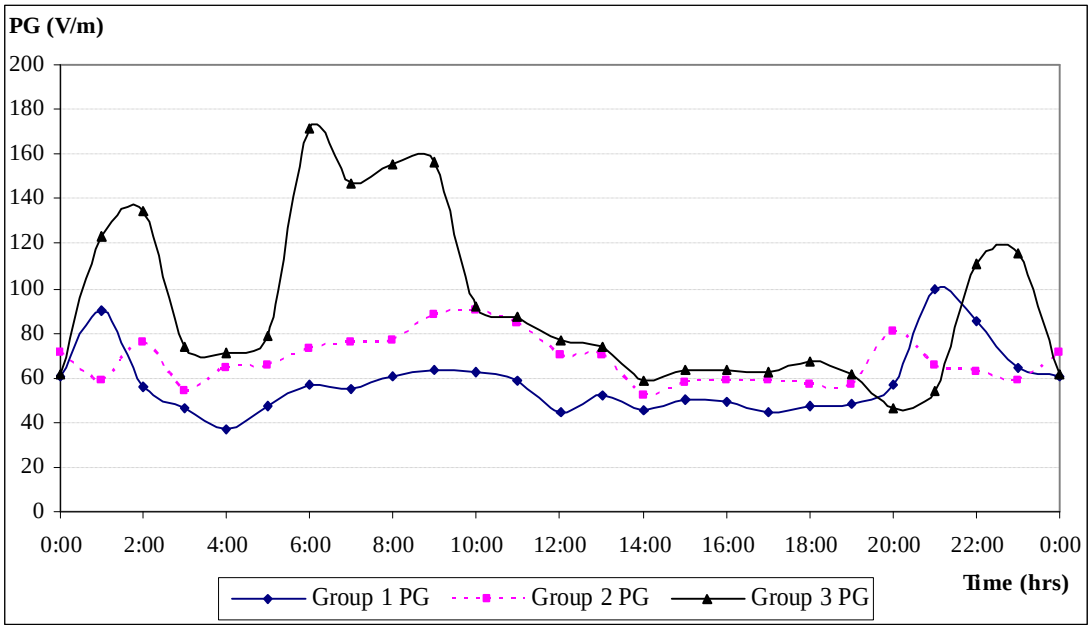

Figure 5.10: PG patterns of Groups 1, 2, and 3.

The 24-hour average PG for groups 1, 2, and 3 are 57.66 V/m, 67.62 V/m and 91.95 V/m respectively. Group 1 contains days with more dense cloud cover (lower solar radiation values) hence the 24-hour averaged PG for these days is lower than that of days in group 2. Similarly, the 24-hour averaged PG of group 2 is less than that of group 3.

Figure 5.11 shows the averaged solar radiation patterns for the three groups of days.

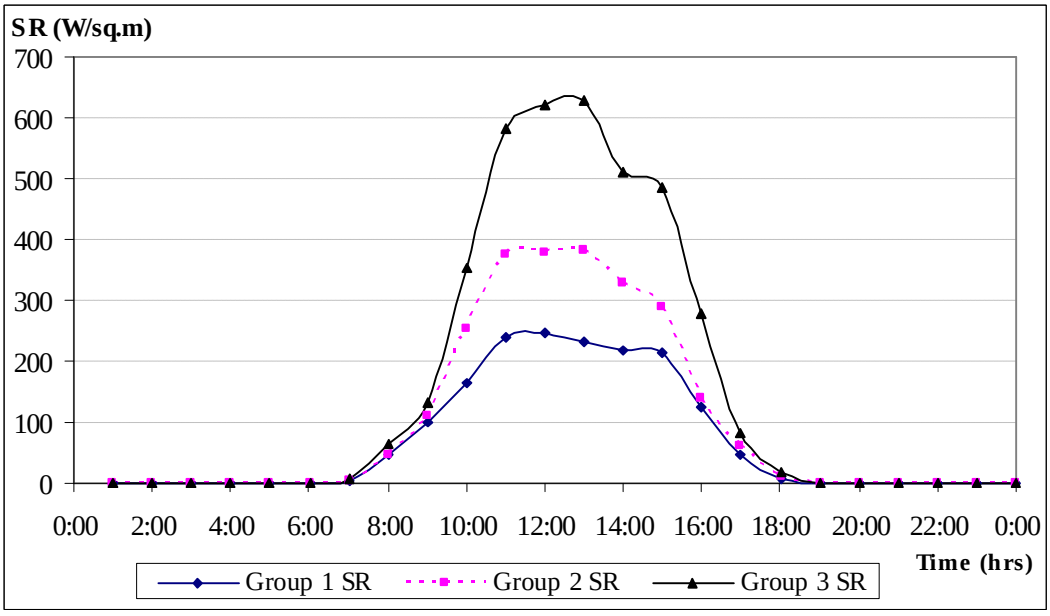

Figure 5.11: Average solar radiation patterns for Groups 1, 2, and 3

As seen in Figure 5.11, the group 2 days' solar radiation values are higher than that of group 1 but less than those of group 3 days. The peak solar radiation values for Groups 1, 2, and 3 are 245.19 W/m^2, 381.10 W/m^2, and 628.76 W/m^2 respectively. It is expected that if the cloud cover was uniform during the sunshine hours, the variation of solar radiation with time should resemble a bell-shape. The number of days in each group is relatively low. This may explain the irregularities in the shape of the solar radiation variation.

From Figure 5.10 it is evident that from 0700 hrs LT to 1900 hrs LT group 2 PG is greater than group 1 PG but less than that of group 3, implying there exists a directly proportional relationship between solar radiation and Earth's PG. More cloud cover is indicated by lower solar radiation values, for which the PG is lower when compared to higher solar radiation values, which is an indication of less cloud cover, for which the PG is higher.

The solarimeter measures the direct as well as diffused radiation from the surroundings of which the contribution by the former is dominant. During the time interval 10 am to 2 pm LT the radiation from the sun is nearly vertical. Thus a variation in the incoming radiation will be mainly due to cloud cover overhead. The variation in PG during 10 am to 2 pm will then be affected by the overhead cloud cover. Hence using the records of PG and solar radiation from 10 am to 2 pm LT, a possible correlation between cloud cover and the Earth's electric field could be established.

To correlate the observations on cloudy days to those on fair-weather days, another group is introduced. This group contains days with no cloud cover and solar radiation larger than 800 W/m^2 and will be termed as *'Group 4'* (fair-weather days).

The variation in PG for the 5 hourly intervals for the 4 groups is presented in Figure 5.12.

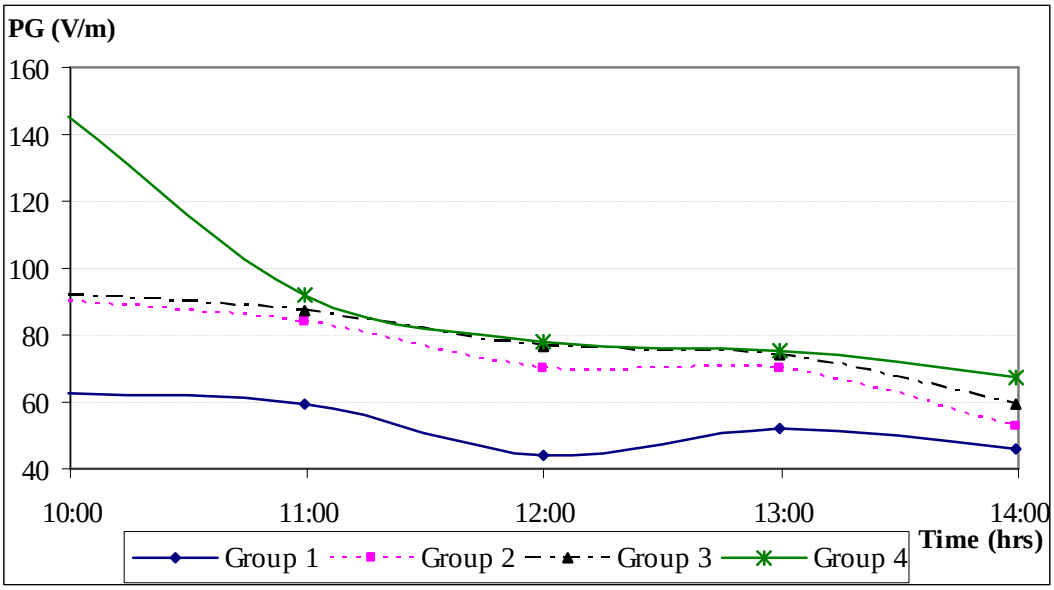

Figure 5.12: Variation of PG from 10 am to 2 pm LT for the 4 groups

It can be seen from the figure above that the PG at all times increases with increasing values of solar radiation.

Table 5.2 below shows the average solar radiation (SR) values at the 5 hourly intervals for the 4 groups of days.

Table 5.2: Average solar radiation (SR) in W/m^2 for the 4 groups at 5 hourly intervals

Group	SR at 10 am	SR at 11 am	SR at 12 noon	SR at 1 pm	SR at 2 pm
1	165.98	239.94	245.19	232.68	217.46
2	254.77	373.66	377.34	381.10	326.84
3	352.25	582.61	620.66	628.76	509.75
4	701.41	808.64	808.35	779.74	648.95

It should be noted that the PG and solar radiation values of fair-weather and cloudy days vary with time of observation. In order to establish a relationship between PG and cloud cover, the relationship between solar radiation and PG is illustrated first. This illustration utilizes the ratio form of solar radiation and PG. The ratio 'PG Cloudy/ PG Fair' at any time is plotted against 'SR Cloudy/ SR Fair' at the same time. Figure 5.13 shows the ratio plot at 10 am LT.

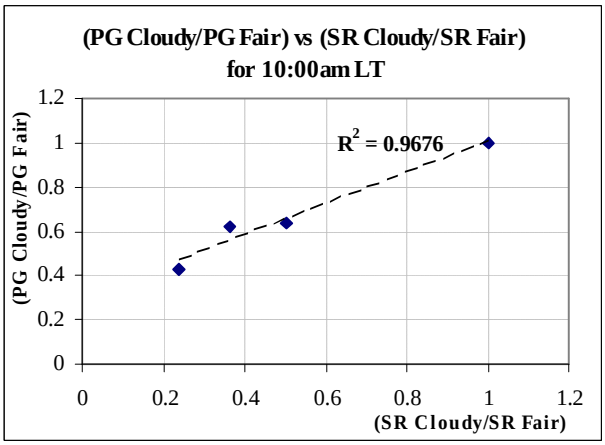

Figure 5.13: Relation between solar radiation and PG for the 4 Groups at 10 am LT.

It can be seen from the above figure that as the quantity 'SR Cloudy/SR Fair' increases 'PG Cloudy/PG Fair' also increases. This indicates there exists a direct proportionality between solar radiation and Earth's PG. The variation of the ratio at 10 am LT showed good correlation.

The difference in solar radiation on fair-weather days and cloudy days will be proportional to the cloud cover. Thus taking the ratio of this to fair-weather days' solar radiation will indicate the relative contribution by cloud cover. To illustrate the relationship between cloud cover and PG a new quantity is defined as:

$$\frac{SR\ Fair - SR\ Cloudy}{SR\ Fair} = 1 - \frac{SR\ Cloudy}{SR\ Fair} = SR' \qquad (5.1)$$

This quantity is denoted as **SR'**. The significance of this term is that it indicates the cloud cover intensity. The 'PG Cloudy/ PG Fair' was then plotted against SR'. The result is presented in Figure 5.14.

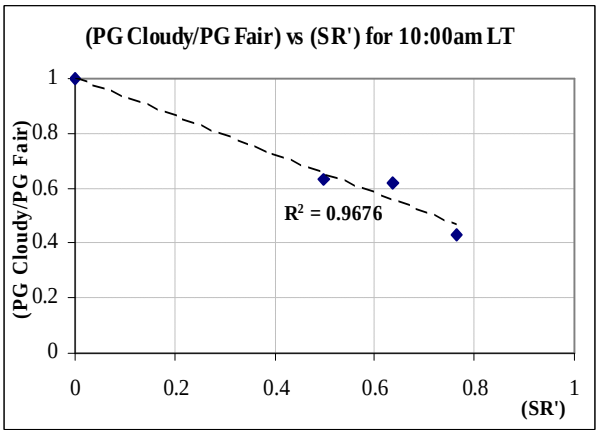

Figure 5.14: Relation between cloud cover and PG for the 4 Groups at 10 am LT.

The above figure reveals that as the quantity SR' increases (cloud cover increases) the quantity 'PG Cloudy/ PG Fair' decreases implying an inversely proportional relationship exists between cloud cover and Earth's PG. The results for 11 am, 12 noon, 1 pm, and 2 pm are presented in Figure 5.15.

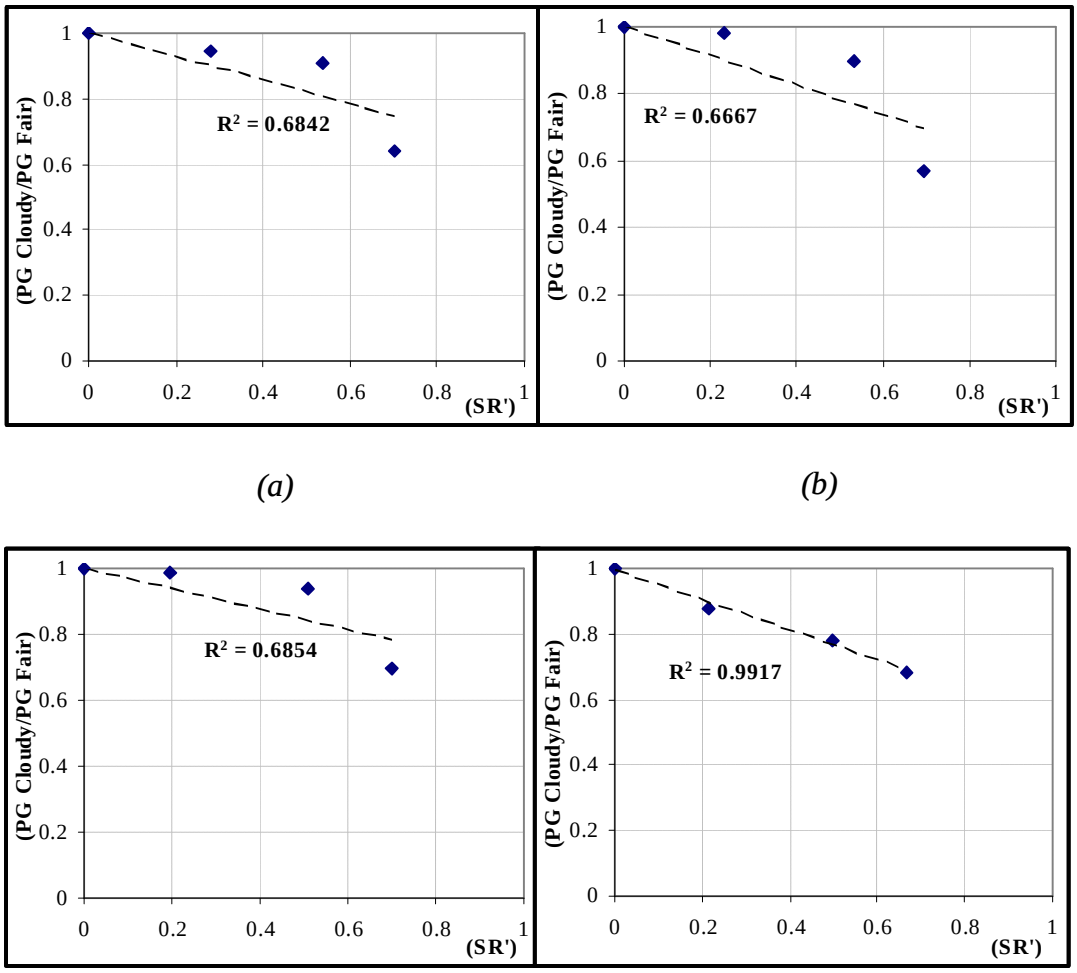

Figure 5.15: Relation between cloud cover and PG at (a) 11 am, (b) 12 noon, (c) 1 pm, and (d) 2 pm.

Figures 5.14 and 5.15 indicate that increasing cloud cover leads to a decrease in PG. The correlation at 10 am and 2 pm is good compared to the correlation for 11 am, 12 noon, and 1 pm. This may be due to the irregularities in the solar radiation pattern observed in Figure 5.11. Figure 5.16 gives a three dimensional change of the PG with times of day and solar radiation.

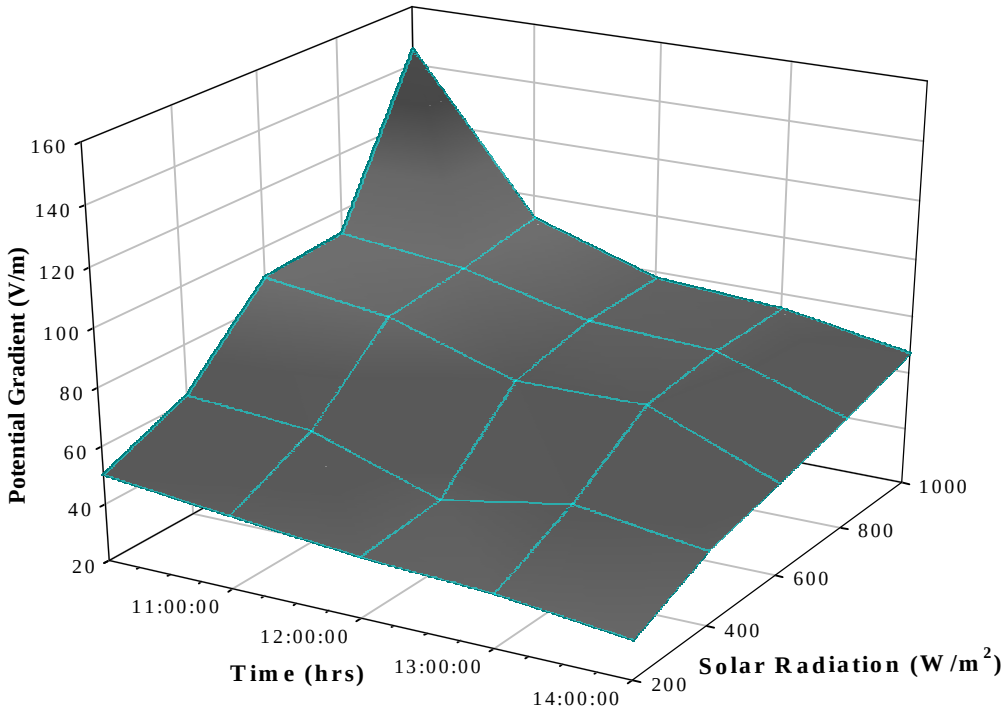

Figure 5.16: Variation in PG with changes in solar radiation from 1000 – 1400 hrs LT

If one observes the solar radiation pattern closely, it can be seen that one particular value of insolation occurs at two different times. This does not mean that at the two times corresponding to a same value of insolation the PG will be same. This can be viewed in Figures 5.5 and 5.7. The insolation level in Figure 5.5 at 10 am and 2 pm is ~ 680 W/m^2. But the PG for these two times is not the same; PG at 10 am is close to 150 V/m and at 2 pm is ~ 75 V/m. In Figure 5.7, the insolation level of 300 W/m^2 is common for times close to 9 am and 2 pm. The PG values for these two times are 85 V/m and 60 V/m respectively. It can then be concluded that there is no correlation between the PG values at two different times for one particular value of insolation. The PG possesses a diurnal variation in itself and, apart from insolation level, is dependent on factors such as aerosol concentration in atmosphere, ionization, wind speed, and occurrence of lightning and thunderstorm activities.

5.1.6 Possible reasoning for the reduction of solar radiation and Electric field on Cloudy days

In the case of solar radiation intercepted at the Earth's surface on a fair-weather day it can be said that there is no cloud cover present. Hence the insolation received does

not suffer absorption and scattering while travelling from the atmosphere to the surface of the Earth. In the case of cloudy days there exists significant cloud cover that affects the insolation received at the Earth's surface. If the cloud droplets are spherical in shape then the reduction in insolation can be explained by absorption and Rayleigh scattering. Being an EM wave, the solar radiation is absorbed by the cloud droplets plus significant scattering also occurs. The intensity of the scattered wave from the scattering particle to the point of observation is given by equation 2.17.

The general observation in this study of Earth's potential gradient was that the PG decreased on cloudy days. This decrease in PG can be explained by considering the charges within and outside cloud cover. According to Volland [1984, p 28] the cloud consists of opposite charges at the top and the bottom; the top is positively charged and the base is negatively charged.

Since the base of the clouds is negatively charged there is a transient electric field component directed from the surface of the Earth towards the cloud whilst the Earth's PG, which is directed downwards, is also present. The net PG observed on cloudy days is then a difference of the fair-weather electric field and the transient electric field induced by the cloud. Therefore the PG observed on cloudy days is less than that observed on fair-weather days.

According to Law [1963] the vertical electric field tends to drive positive ions towards the ground in fair-weather and negative ions away from the ground. On cloudy days, in the presence of atmospheric aerosols, the positive ions get attached to the neutrals and negatively charged ions within the cloud. Hence the positive ions are not able to reach the ground. To have a vertical conduction current of the order of 10^{-12} A/m^2 maintained, the magnitude of the electric field emerging out of the clouds decreases, thus the PG observed on cloudy days is lower than that on fair-weather days. The average cloud height for Suva, as estimated by the Fiji Meteorology Services, is 2.75 km. The reduction in PG during the morning hours can then be said to occur at a height of ~ 2.75 km.

5.2 Study of Pacific Broadcasting Services (PBS) Signal Strength

PBS is a joint venture between Citywest Broadcasting Services Ltd of Australia and Ba Provincial Holdings Ltd of Fiji. Shareholdings in PBS is split 41 percent to Ba Holdings and 59 percent to Citywest Broadcasting. PBS started providing service to Fiji in March 2005. With the delivery platform in Sydney, PBS receives the television signals through INTELSAT 701. Figure 5.17 below shows the footprint covered by INTELSAT 701.

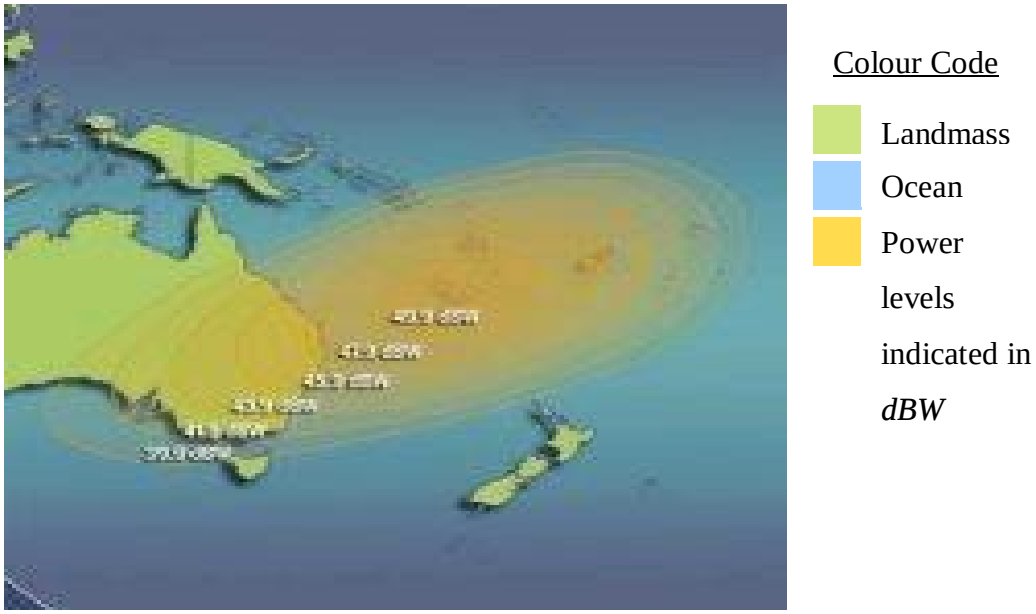

Figure 5.17: Showing the area covered by PBS footprint

The primary purpose of a *television receive only* operation (TVRO) is to receive analog/digital video channels transmitted by the Ku satellite transponders. Being a TVRO, PBS does not need to broadcast and uplink to their satellite transponder 22. The frequency of transmission from satellite is 12.648 GHz. As described earlier in section 4.2.2, the LNB downconverts this frequency to 1.348 GHz. The PBS signal is then observed at 1.348 GHz at this receiving station.

Figure 5.17 shows the signal strength in *dBW*. The signal strength is greatest at the center of the footprint (51.2 dBW) and decreases to 37.9 dBW as the radius of the footprint increases. This is due to the directivity of the transmitter antenna on the satellite.

Power is usually reported in decibel (dB). The *decibel* gives no indication of the input power. This problem is easily rectified by using a *reference value* to compare any other value. An often-used reference level in communications is 1 mW [Frenzel, 1998, p 49]. When a power value is compared to 1 mW, the result is a value called the *dBm*, given as:

$$dBm = 10 \log \frac{P_{OUT}}{0.001} \tag{5.2}$$

The PBS signal strength was measured with a spectrum analyzer (Brand: hp, Model # 8555A). The 'vertical output' terminal of the spectrum analyzer indicates the signal strength in Volts. This was recoded on a PC (Section 4.2.2.6). To obtain a conversion of the signal strength from Volts to *dBm*, a digital spectrum analyzer was used. This spectrum analyzer, Advantest R3131A, readily gives the signal strength in *dBm*. From the digital spectrum analyzer, the calibration shown below was obtained:

1 V = 124.0 dBm

The PBS signal was sampled every 10 seconds using LabVIEW. Six consecutive sampled readings were averaged in one minute and was recorded to a spreadsheet file. All the readings were in Volts. This was later converted to dBm. The data were recorded from 29th August to 26th October, 2007. The days during this period were later classified as 'Fair-Weather days' and 'Cloudy days' on the basis of solar radiation data and as 'Rainy days' by looking at the rainfall data.

To see the general feature of the PBS signal, the diurnal variation (*1-minute recording interval* and *averaged hourly intervals*) on a fair-weather day (8th October 2007) with no cloud cover and no rain is presented in Figure 5.18. This day is chosen because there are no sudden changes in insolation. The insolation gradually increases to a maximum of 998 W/m^2. The insolation data was sampled every 10 minutes and the averaged values were recorded at hourly intervals.

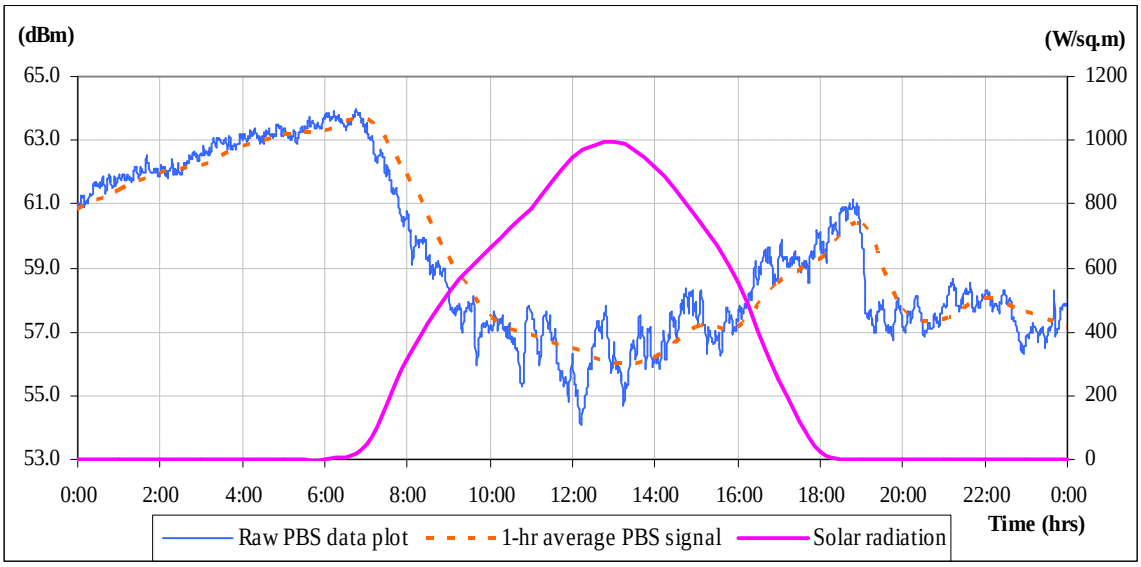

Figure 5.18: Diurnal variation of PBS signal strength on 8th October, 2007

Ideally the signal strength should remain a constant for a given transponder and a receiver. But the PBS signal showed variation in strength. From the diurnal variation in Figure 5.18, it can be seen that the signal has an early morning peak and an evening peak. It is evident from the above figure that the morning peak is observed around the sunrise hours and the evening peak is observed after sunset. The daily minimum is observed just around local noontime. It can be seen from the '*Raw PBS data plot*' (1-minute) that the signal fluctuates the most during daytime. This is further discussed in section 5.2.7 where the average signal strength variation is considered.

5.2.1 PBS Signal Strength on Fair-Weather days

Out of the 51 days for which the PBS data were recorded, 11 days were classified as Fair-Weather days. The PBS data for these days were collected together and averaged. Figure 5.19 shows the diurnal variation in PBS signal using 1 minute averaged values. The one minute averaged plot shows the very miniature fluctuations for the 11 days in consideration. The early morning peak and evening peak (*observed just around sunset hours*) are observed here. The 1-minute averaged data was further averaged over intervals of 30 minutes to present a smooth pattern and is plotted in Figure 5.19.

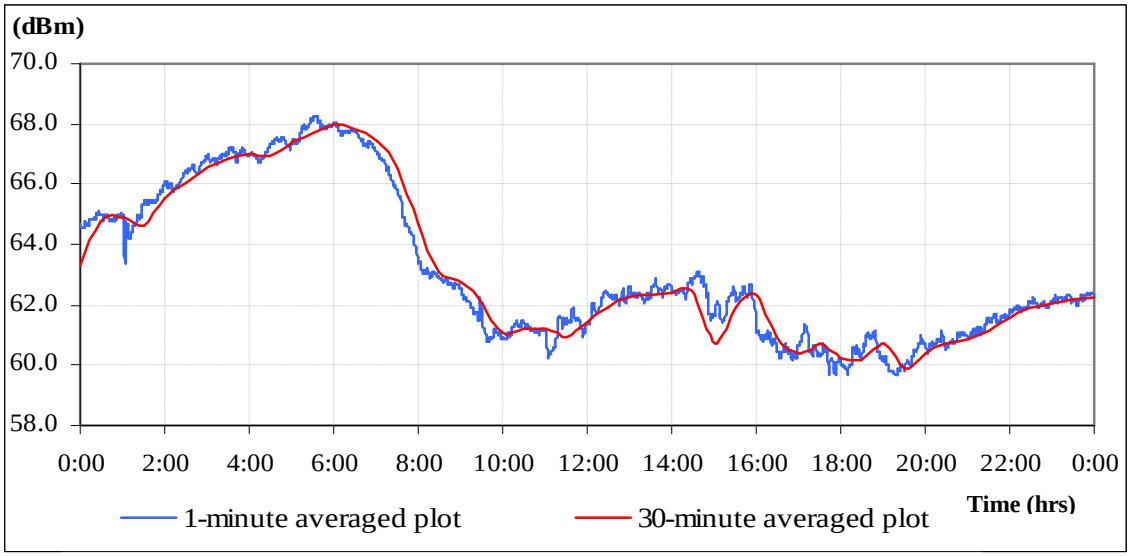

Figure 5.19: Fair-weather days PBS signal averaged at every minute

The PBS data was further averaged over the hour. This was done because the CR23X datalogger recorded the hourly average of the solar radiation data. The variation of PBS signal strength averaged at hourly intervals can then be compared well with the average

insolation pattern for the corresponding 11 days. The solar radiation data for the 11 days was also averaged, and is presented in Figure 5.20 together with the hourly average of the PBS signal strength.

Similar to the measurements in section 5.1, the solar radiation data is available only for the sunshine hours; the PBS signal strength data is recorded continuously. Therefore, analysis of cloud cover correlation with PBS signal strength will be valid only for the daytime hours. The night hours will be assumed to have a similar cloud cover.

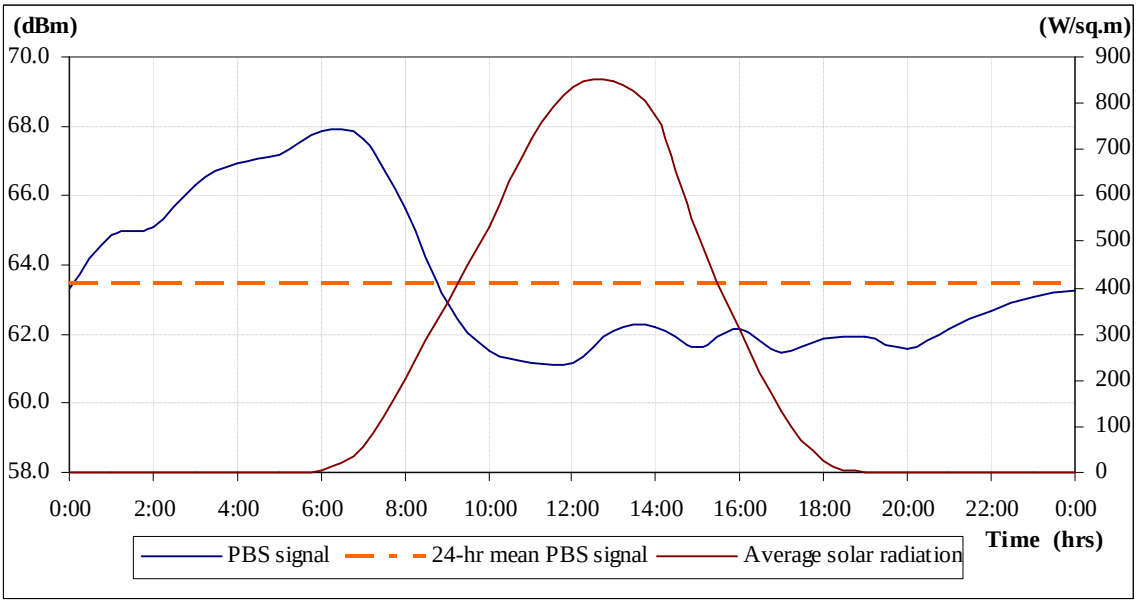

Figure 5.20: Fair-Weather days PBS signal averaged over the hour

It can be seen from Figure 5.20 that the PBS signal strength increases gradually from 64 dBm to the morning peak of 67.9 dBm, which occurs just around 7 am LT. After the morning peak, the signal strength reduces considerably. The signal level continues to decrease to a low of 61.2 dBm observed between 11 am and 12 pm, which is also the minimum in the 24-hour cycle. After 12 pm, the signal strength shows an increase but with a periodic type of variation. The signal strength varies between 61.6 dBm and 62.1 dBm up till 8 pm, after which it gradually begins to increase. The fair-weather days' mean PBS signal level is 63.5 dBm.

The fair-weather days' average signal strength ranges from 61.2 dBm to 67.9 dBm for the period of study. But the raw data shows the signal strength can go up to 92.71 dBm (observed on 20th October between 6 am and 7 am).

From equation 5.2, the fair-weather days mean output power (P_{OUT}) corresponding to the mean 63.5 dBm is 0.57 watts. The average maximum power (corresponding to 67.9 dBm) is 0.89 watts.

5.2.2 PBS Signal Strength on Cloudy days

During the period of study a total of 37 days were classified as Cloudy days, with solar radiation values ranging from 200 W/m^2 to 800 W/m^2. The cloudy days averaged solar radiation curve peaks around 397 W/m^2. Similar to the fair-weather days, the PBS data for cloudy days were collected together and averaged to get one set of 1-minute data. Figure 5.21 below shows the variation in PBS signal strength with 1-minute recording interval.

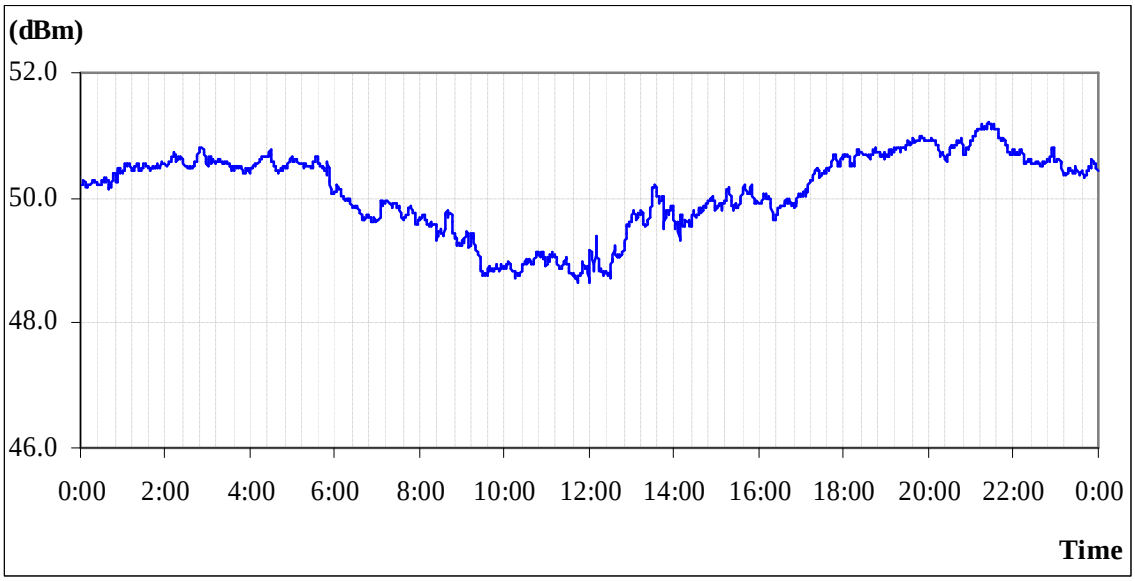

Figure 5.21: Cloudy days PBS signal averaged at every minute

From Figure 5.21 it can be seen that the signal strength retains high values in the early morning hours and late evening hours. The signal strength is lowest around noontime in the 24 hour period.

A point worth mentioning is that the signal strength recorded from 12th September to 18th September, between 11:43 am LT and 12:03 pm LT, showed unusual high values reaching up to a maximum of 97.7 dBm. This could be attributed to power fluctuation in the satellite together with *noise*. These high values were therefore neglected for this analysis.

Similar to the analysis of the fair-weather days PBS signal, the cloudy days signal strength is also averaged over the hour. The results are presented in Figure 5.22.

The Cloudy days' averaged PBS signal, to some extent, resembles the Fair-weather days PBS signal; high values in the very early morning and evening hours and the lowest values occurring around noon.

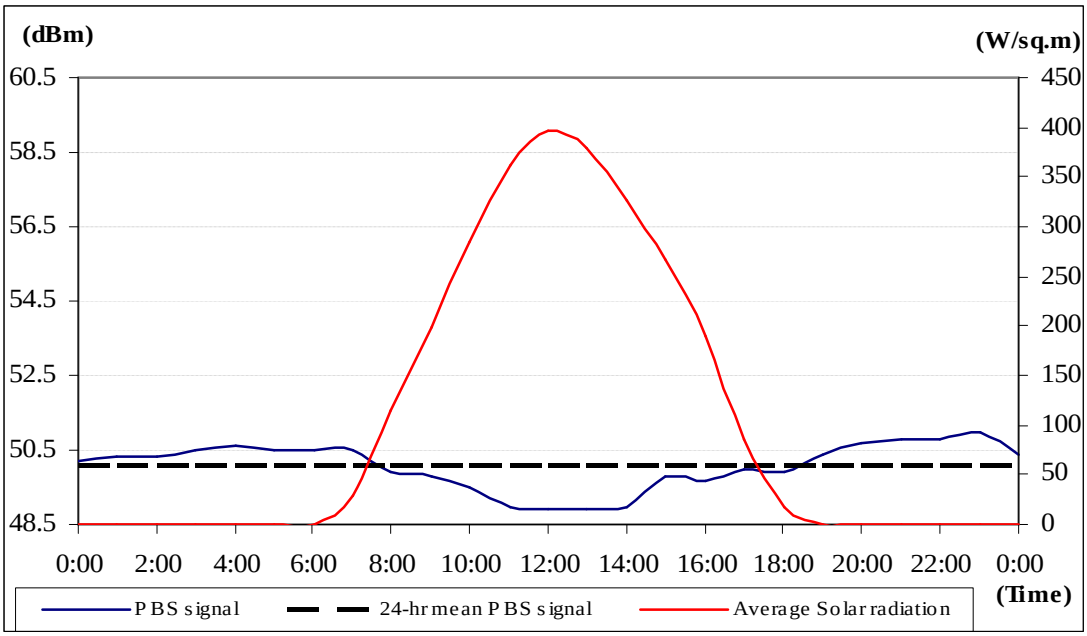

Figure 5.22: Diurnal variation of PBS signal strength on cloudy days using hourly values.

As can be seen from Figure 5.22, the signal level maintains the very early morning high values up till 0700 hrs LT, after which it begins to decrease significantly. Here, the morning maximum of ~ 50.6 dBm is observed around 0400 - 0600 hrs LT, which occurs earlier in comparison to the fair-weather days' morning peak (approximately 0700 hrs LT). After 0700 hrs LT, the signal continues to decrease till 1200 hrs LT, when the minimum of 48.9 dBm is observed. After 1400 hrs LT, the signal level increases gradually and fluctuates around 49.8 dBm till the sunset hours. After sunset the signal level increases significantly to a pre-midnight peak of 51.0 dBm, observed around 2300 hrs LT. This is also the maximum in the diurnal pattern. The cloudy days mean PBS signal level is 50.1 dBm.

The mean cloudy days signal strength varies between 48.9 dBm and 51.0 dBm. The averaged effect in Figure 5.22 shows the late night peak occurs close to 2300 hrs LT but

Figure 5.21 shows the discrepancy in time of the late evening peak, occurring around 2200 hrs LT. Using equation 5.1, the cloudy days mean output power (P_{OUT}) corresponding to 50.1 dBm is 0.15 watts. The average maximum power, corresponding to 51.0 dBm, is 0.16 watts.

5.2.3 Comparison of PBS Signal Strength on Fair-weather days and Cloudy days

From Sections 5.2.1 and 5.2.2 it can be seen that the 24-hr average PBS signal strength is higher on 11 fair-weather days than that on 37 cloudy days. The cloudy days mean PBS signal strength is 50.1 dBm, which is much less than the fair-weather days mean PBS signal of 63.5 dBm. This is illustrated clearly in Figure 5.23.

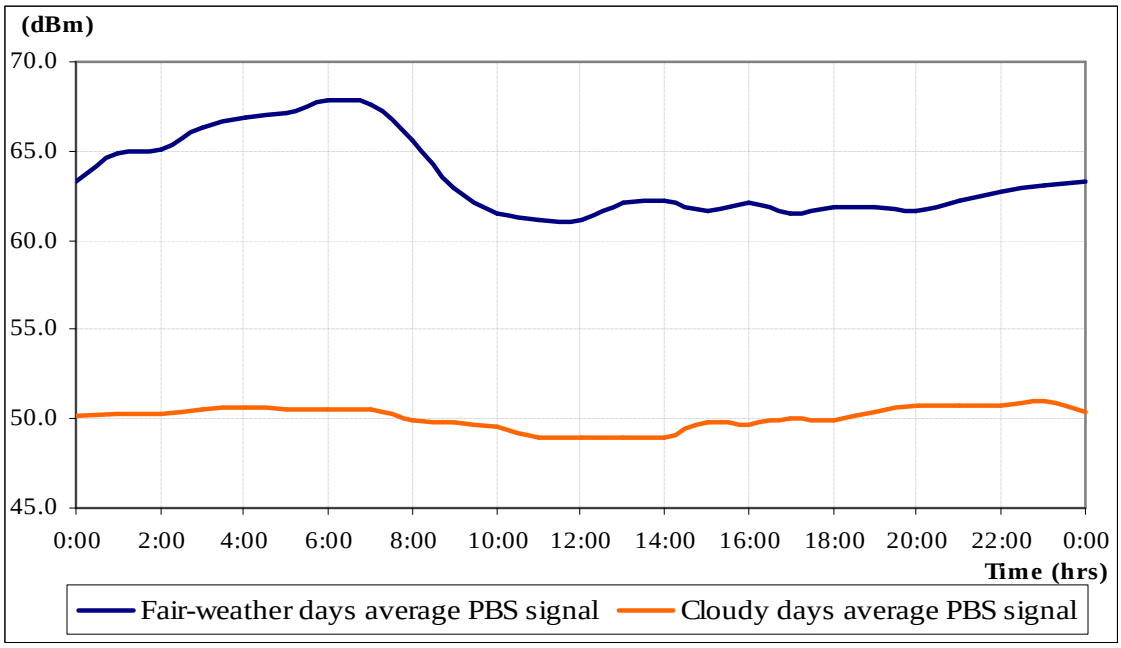

Figure 5.23: Average diurnal variation of PBS signal strength on Fair-weather and Cloudy days.

The plots indicate that cloud cover significantly affects the PBS signal strength. One notable feature from Figure 5.23 above is that morning peak in the cloudy days average signal pattern is not so pronounced when compared to the average fair-weather days signal pattern. The two curves shown in the above figure are separated by approximately 13 dBm on average.

The average insolation patterns for the 11 fair-weather days and 37 cloudy days are shown in Figure 5.24.

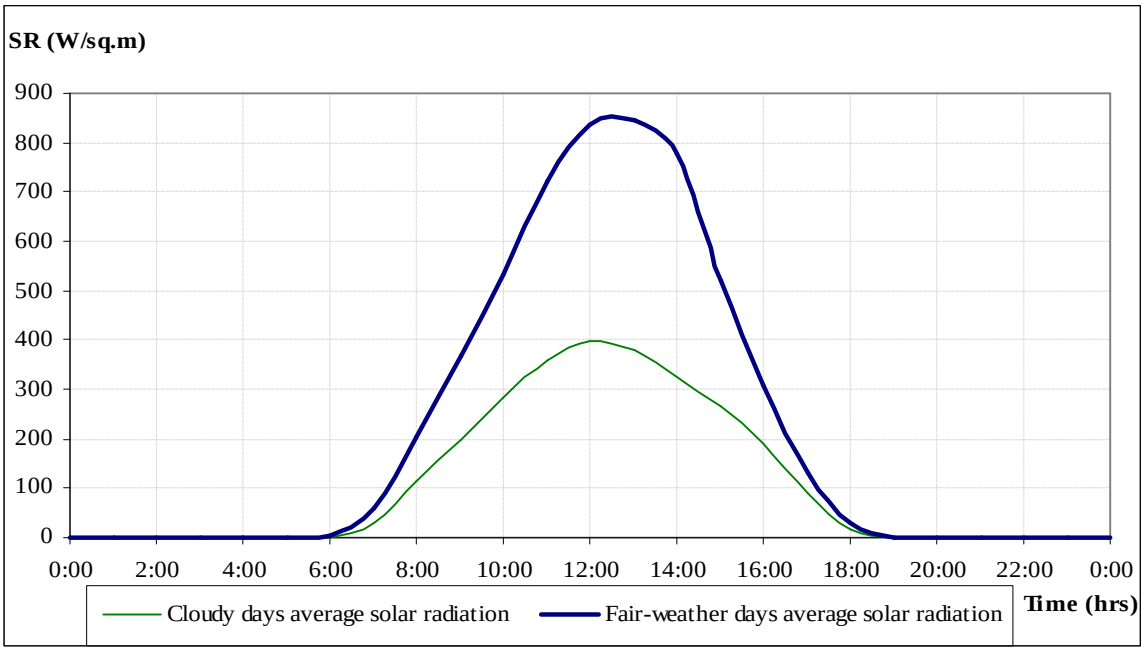

Figure 5.24: Average solar radiation pattern on Fair-weather days and Cloudy days.

5.2.4 Correlation of PBS signal strength on Fair-weather days to Cloudy days

To demonstrate the effect of cloud cover on PBS signal strength, the cloudy days are grouped, similar to the procedure adopted in Section 5.1.5. The list of these groups is tabulated below:

Table 5.3: Description of 3 subgroups of Cloudy days together with Group 4 (Fair-days)

Group	Range of peak insolation
1	(200 – 400) W/m^2
2	(400 – 600) W/m^2
3	(600 – 800) W/m^2
4	> 800 W/m^2

PBS signal strength data recorded from 29th August to 26th October, 2007 was grouped according to the range of peak solar radiation. This range of solar peak insolation was chosen so that a representative range of days could be selected from a total of 37 days. Group 1 consists of 5 days with the very low solar radiation values (200 – 400 W/m^2) thereby indicating the presence of dense cloud cover. Increase in solar radiation values from the upper limit of Group 1 indicates the presence of moderate cloud cover, which is classified as Group 2, which had 17 days. Group 3 consists of days with minimum cloud cover and 15 days were classified into this group. The PBS signal strength of the 3

groups of cloudy days is also compared with the fair-weather days signal strength (Group 4).

Figure 5.25 below shows the solar radiation curve for the 4 groups averaged over the hour. The peaks for Groups 1, 2, 3, and 4 are 242 W/m^2, 398 W/m^2, 552 W/m^2, and 850 W/m^2 respectively.

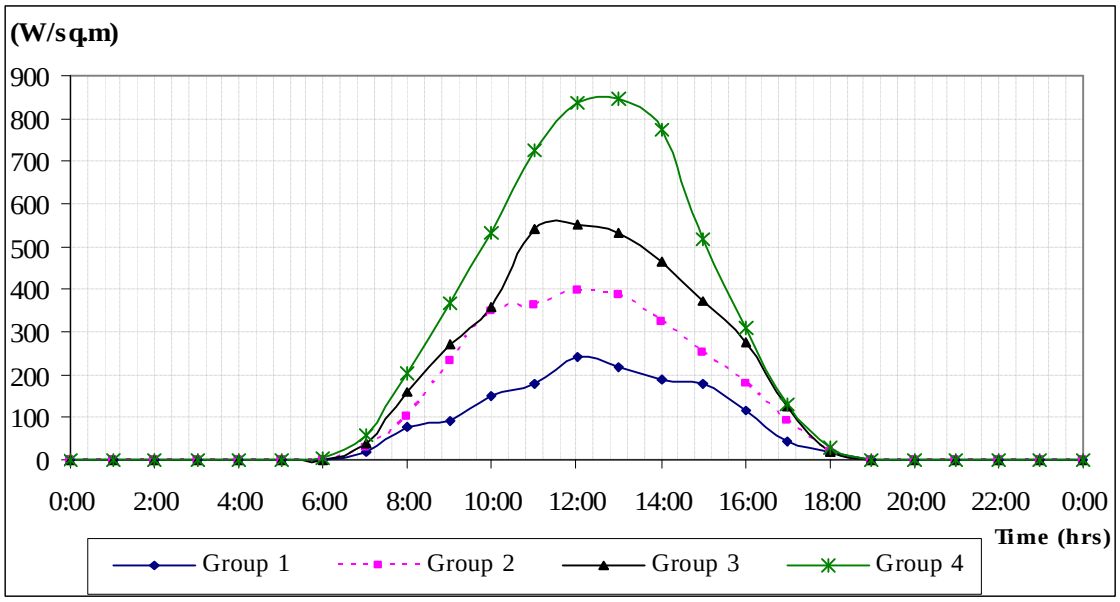

Figure 5.25: Solar radiation curves for Groups 1, 2, 3 and 4.

The diurnal variation of PBS signal strength for the 4 groups of days is presented in Figure 5.26.

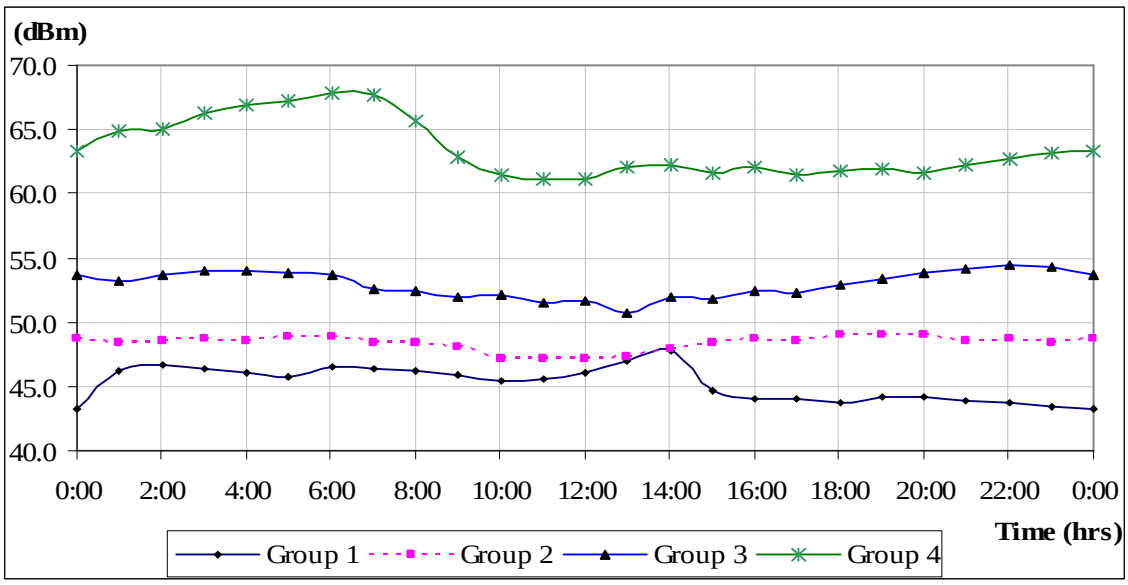

Figure 5.26: Diurnal variation of PBS signal strength for Groups 1, 2, 3, and 4 days.

It can be seen from Figure 5.26 that as the insolation increased the PBS signal strength also increased. The diurnal variation during cloudy days did not reveal anything substantial. The average PBS signal strengths for the three groups of cloudy days 1, 2, and 3 are 45.3, 48.4, and 52.9 dBm respectively.

5.2.5 Quantification of the effect of solar radiation on the satellite reception signal strength

The relationship between solar radiation and PBS signal strength is further studied. As seen earlier in section 5.2.1, the fair-weather days satellite signal strength varies with the time of observations. Therefore a comparison of the relative values was carried. The analysis performed here is similar to that in Section 5.1.4 where the ratio forms of solar radiation and PG are used. Here, the average solar radiation at any time for each group is divided by the average solar radiation of Group 4 at the same time. The results are termed as 'SR Cloudy/ SR Fair'. Similarly the average PBS signal strength for each group is divided by the average signal strength of Group 4. The results are termed as 'PBS Cloudy/ PBS Fair'. The quantity *SR'* is also utilized here (Section 5.1.5). For example, Table 5.4 shows the values of 'SR Cloudy/SR Fair', SR', and 'PBS Cloudy/PBS Fair' for the 4 Groups at 6 am LT.

Table 5.4: List of SR ratio, SR', and PG ratio at 0600 hrs LT for the 4 groups

Group	(SR Cloudy/ SR Fair)	SR'	(PBS Cloudy/ PBS Fair)
1	0.15	0.85	0.73
2	0.26	0.74	0.77
3	0.28	0.72	0.85
4	1	0	1

The ratio 'PBS Cloudy/PBS Fair' is plotted against SR'. Figure 5.27 shows the correlation between the two ratios.

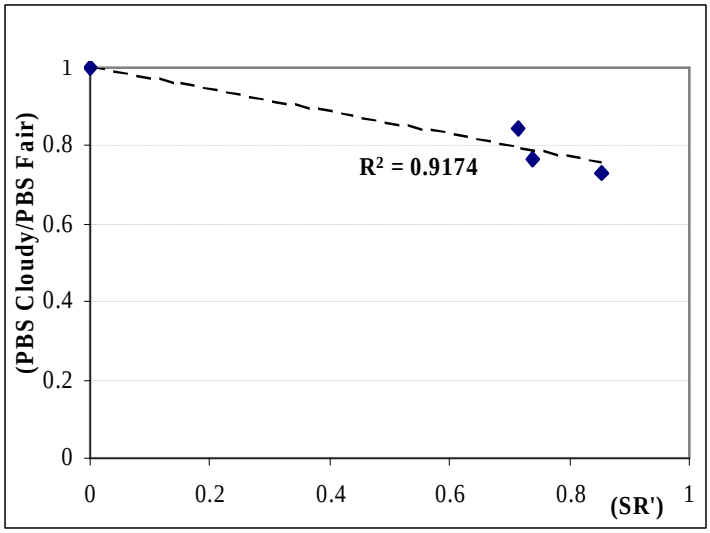

Figure 5.27: Relationship between increasing cloud cover and PBS signal strength at 0600 hrs LT.

The relative variation showed a near linear correlation. It can be seen from the above figure that as the quantity SR' increases the ratio 'PBS Cloudy/ PBS Fair' decreases implying an inversely proportional relationship exists between cloud cover and PBS signal strength. The R^2 value at 0600 hrs LT is ~ 0.92 indicating there is good correlation of PBS signal strength relative to cloud cover. The results for all the sunshine hours (from 7 am to 6 pm LT) are presented below together with the R^2 value.

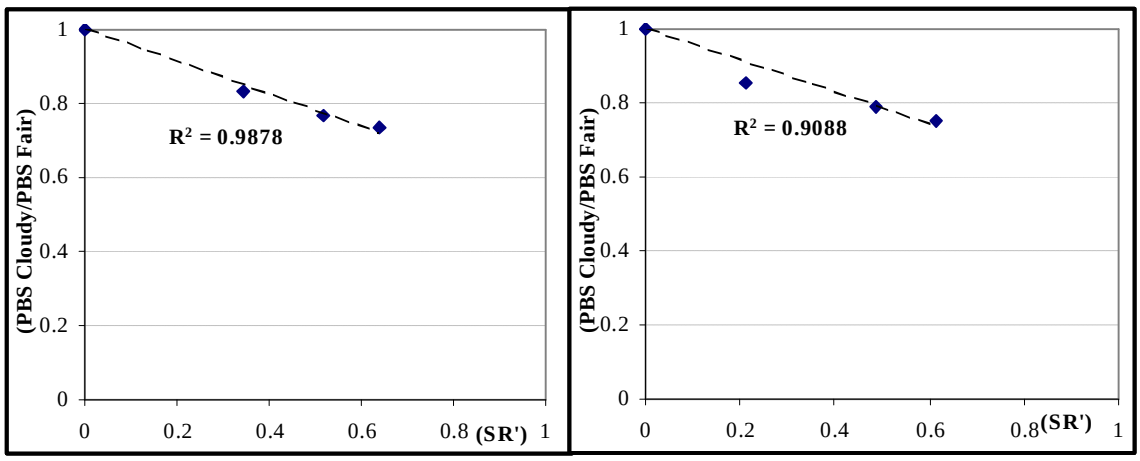

(a) *(b)*

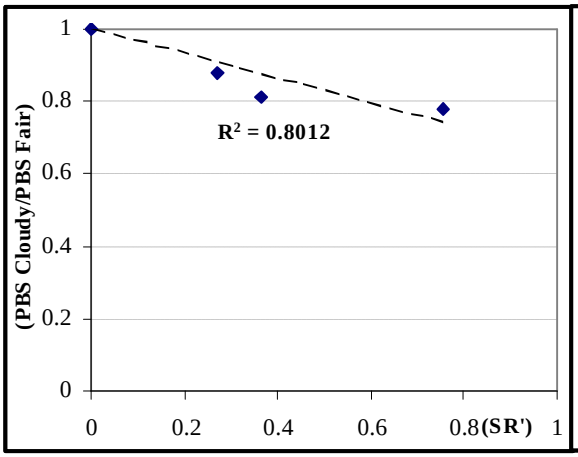
(PBS Cloudy/PBS Fair)
(SR')
R² = 0.8012
0
0.2
0.4
0.6
0.8
1

(c)

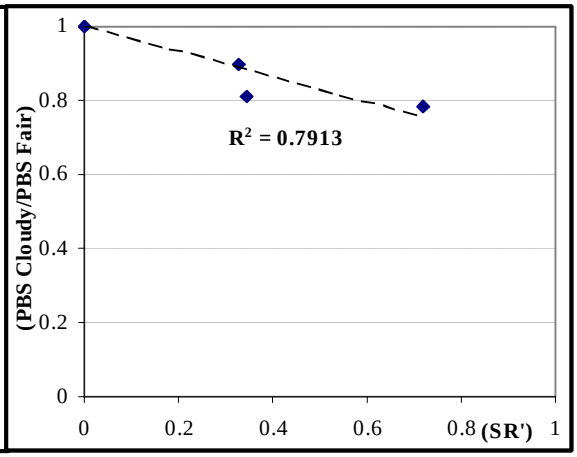
(PBS Cloudy/PBS Fair)
(SR')
R² = 0.7913
0
0.2
0.4
0.6
0.8
1

(d)

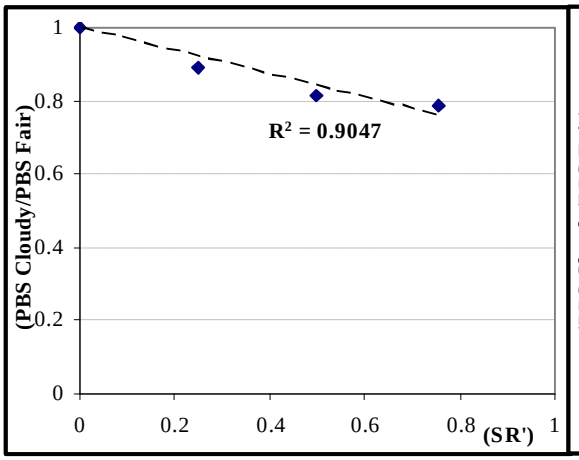
(PBS Cloudy/PBS Fair)
(SR')
R² = 0.9047
0
0.2
0.4
0.6
0.8
1

(e)

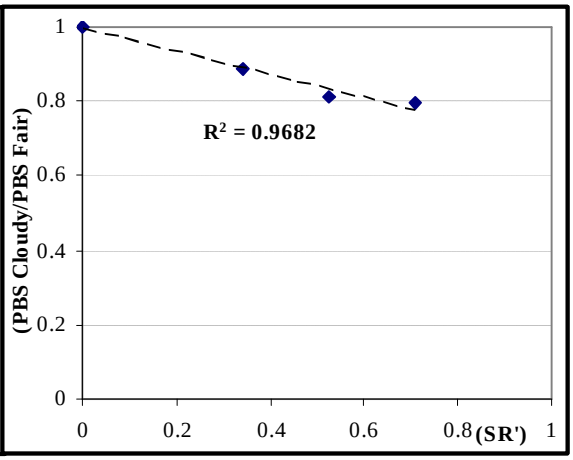
(PBS Cloudy/PBS Fair)
(SR')
R² = 0.9682
0
0.2
0.4
0.6
0.8
1

(f)

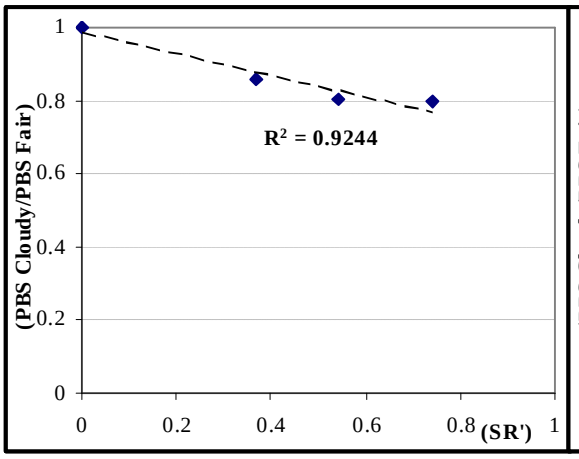
(PBS Cloudy/PBS Fair)
(SR')
R² = 0.9244
0
0.2
0.4
0.6
0.8
1

(g)

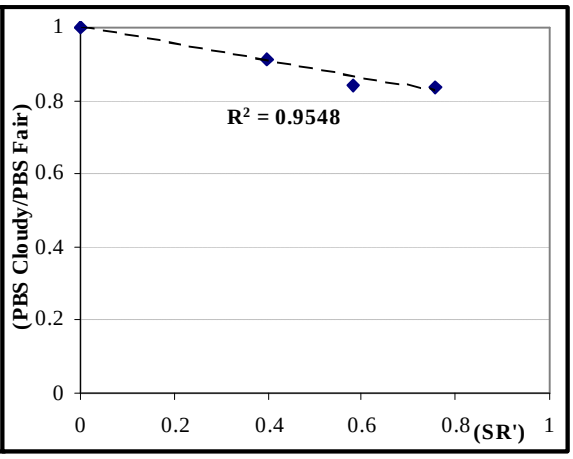
(PBS Cloudy/PBS Fair)
(SR')
R² = 0.9548
0
0.2
0.4
0.6
0.8
1

(h)

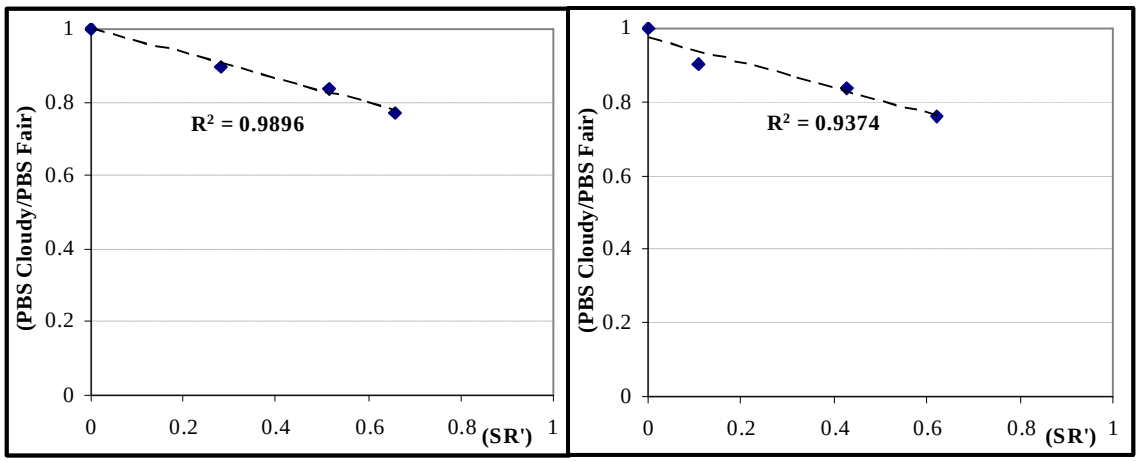

(j) *(k)*

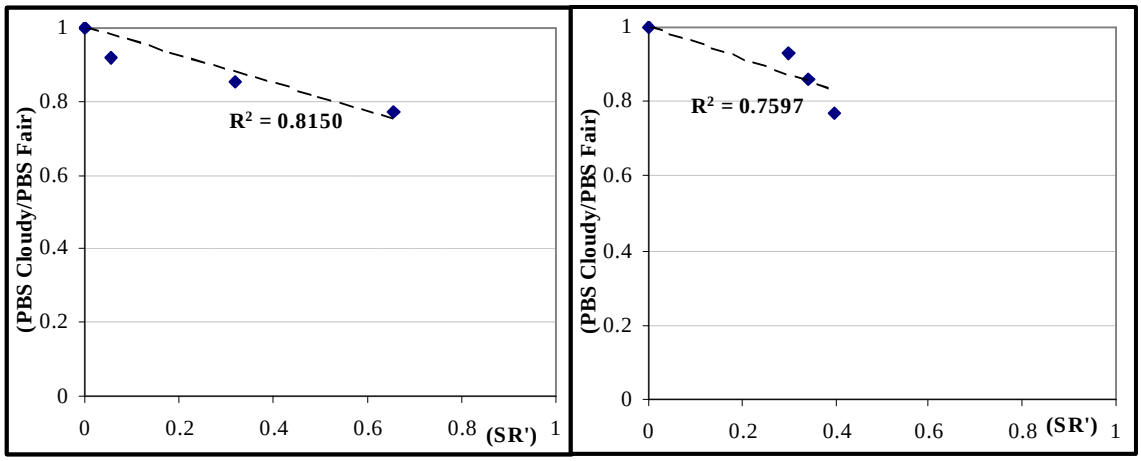

(l) *(m)*

Figure 5.28: Relation between cloud cover and PBS signal strength at (a) 0700, (b) 0800, (c) 0900, (d) 1000, (e) 1100, (f) 1200, (g) 1300, (h) 1400, (j) 1500, (k) 1600, (l) 1700, and (m) 1800 hrs LT.

It can be seen from Figure 5.28 that for all the solar radiation hours there exist an inverse proportionality between cloud cover and PBS signal strength. The R^2 value from 1100 to 1500 hrs LT is more than 0.9 thus indicating good correlation exists between cloud cover and PBS signal strength during these hours.

5.2.6 PBS Signal Strength on Rainy days

Attenuation by rain depends on the frequency of the radiowave and the rainfall intensity or rain-rate (mm/hr). Attenuation due to rainfall is reported in dB/mm of rainfall. The effect of attenuation on radiowave communication by rain has been of interest to many researchers and investigations in the tropics have been reported [Allnut and Haidara,

2000; Pan and Allnut, 2001]. Attenuation on 11.61 GHz signal downlink has been studied in detail at this station by Ramachandran and Kumar [2007]. A detailed study of attenuation effect by rain on PBS signal is beyond the scope of this research. However for comparison purposes, the PBS records on rainy days were analyzed.

3 out of 51 days from 29th August 2007 to 26th October 2007 were classified as rainy days. These days being 29th September, 30th September, and 13th October. Though these days were not continuously rainy for 24 hours significant signal attenuation was observed during the rain events. 13th October proved to be the rainiest out of the 3 days with a total of 116.5 mm of rainfall, most of which was received from 0400 hrs to 0900 hrs LT. Figure 5.29 shows the PBS signal level variation for 1-minute recording interval on 13th October. The maximum insolation on this day was 675.6 W/m^2.

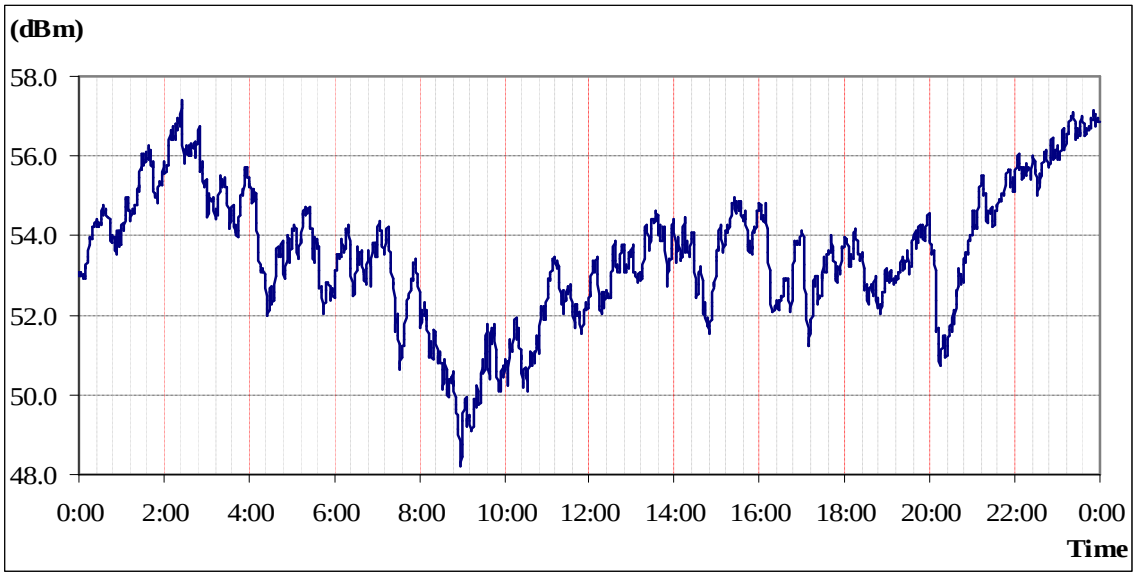

Figure 5.29: PBS signal level variation on 13th October 2007.

When Figure 5.29 is compared with Figure 5.18 (fair-weather day) a signal attenuation of ~ 6 dBm can be observed. PBS signal strength data for the 3 rainy days was collected and averaged over the hour similar to the fair-weather days and the cloudy days. The rainy days average PBS signal strength is shown in Figure 5.30 together with average solar radiation pattern for the 3 days. Also shown is the mean signal strength on fair-weather days.

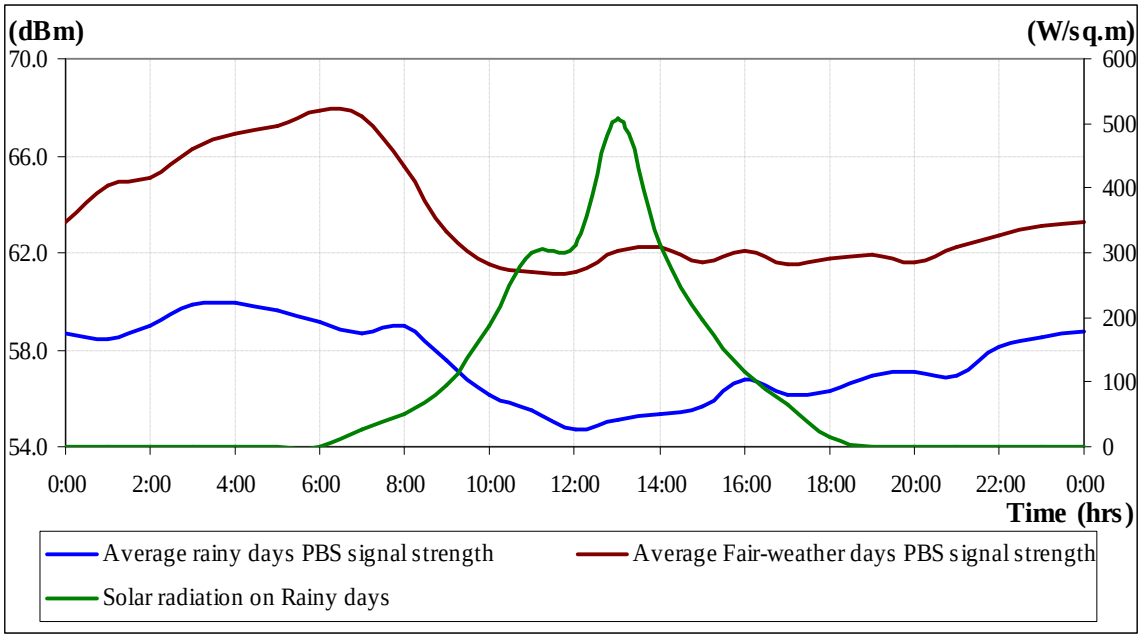

Figure 5.30: PBS signal strength averaged using hourly values on 3 rainy days together with signal strength on fair-weather days.

The general pattern observed in Figure 5.30 is very similar to fair-weather days pattern (Figure 5.20) with high PBS signal values in the very early morning and evening hours separated by the low values around noontime. This pattern is due to both rain and cloud cover. The mean strength of the rainy days signal is 57.5 dBm.

The early morning maximum signal strength is ~ 60 dBm. The 24-hr minimum is observed at ~ 1200 hrs LT. PBS signal strength at this hour is ~ 54.5 dBm. Also the variation in cloud cover is evident around 1200 hrs LT. The signal strength picks up after 1200 hrs LT and increases up till late evening.

The rainy days mean output power (P_{OUT}) corresponding to 57.5 dBm is 0.31 watts. The average maximum power corresponding to 60 dBm is 0.40 watts.

The average power output and average signal strength for the 3 types of days are shown in Table 5.5.

Table 5.5: Showing the average PBS signal strength and average power output for the different types of days

Day type	Peak Insolation Range	Average strength	Average Power output
Cloudy day	Group 1: (200-400) W/m^2	45.3 dBm	0.09 W
	Group 2: (400-600) W/m^2	48.4 dBm	0.13 W
	Group 3: (600-800) W/m^2	52.9 dBm	0.20 W
Rainy	Peak @ 500 W/m^2	57.5 dBm	0.31 W
Fair day	Greater than 800 W/m^2	63.5 dBm	0.57 W

The mean PBS signal strength is higher on rainy days when compared to cloudy days. This discrepancy can be due to the signal being boosted by the service providers during rainy days.

A 3-dimensional graph showing the effect of changing insolation level on PBS signal strength at different times of the day is presented in Figure 5.31.

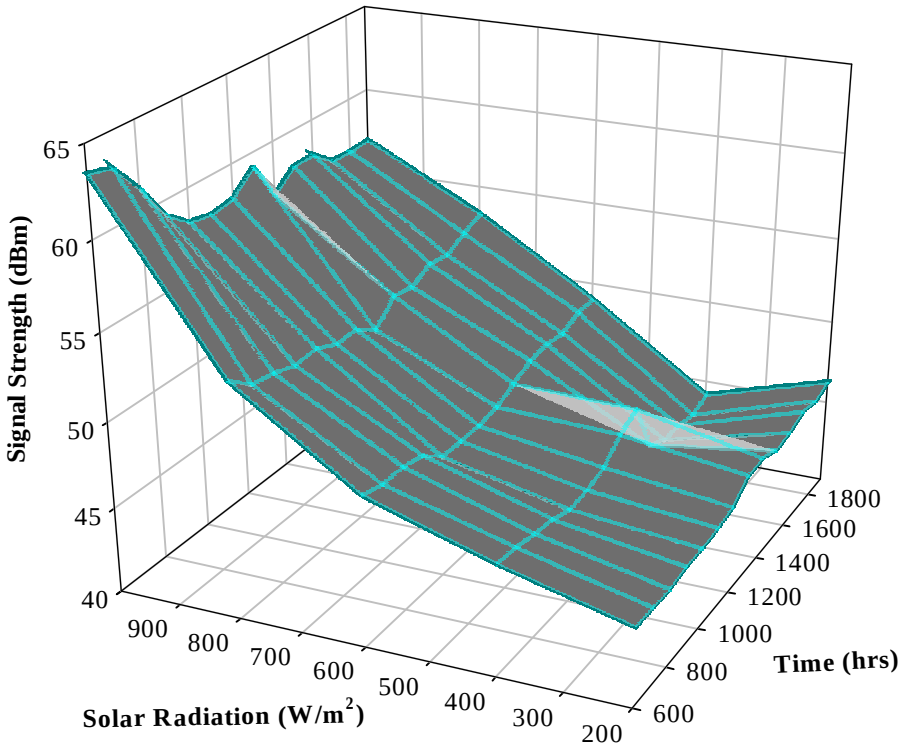

Figure 5.31: 3-dimensional view of PBS signal strength variation with respect to time for the sunshine hours

It can be seen that as the insolation level increases (*indication of decreasing cloud cover*) the PBS signal strength also increases. The characteristic of the PBS signal is also revealed; with increasing insolation levels the PBS signal strength retains high values during the morning and afternoon hours.

The *x-axis* (Time) shows the time span of the sunshine hours only. In this study a day is classified as cloudy based on the solar data for the sunshine hours. Cloud cover during the night is not known; hence the results are valid for the sunshine hours only.

5.2.7 Possible reason for the PBS signal strength variation

The satellite signal passes through the ionosphere to reach the ground station. The night time ionosphere electron content and thickness is small compared to that during daytime. The free electrons in the ionosphere may scatter the incoming signal. The lower ionosphere (D-region) which is dominated by neutrals may absorb the signal. Thus, this may contribute to the reduction of signal strength during daytime. During night (after 1800 hrs LT) the signal strength gradually starts increasing.

A possible explanation for the PBS signal pattern can be given based on the Fair-weather days signal variation where the effect of absorption and scattering due to clouds can be neglected. Figure 5.20, then represents the diurnal variation of average PBS signal strength.

On a fair-weather day the presence of aerosols and pollution from motor vehicles can be attributed as the main reason for the behavior of the PBS signal. In the morning hours before sunrise, the signal strength is maintained at a high level, and after early sunshine hours it begins to decrease gradually. The morning rush hour of traffic can act as a source of aerosol injection which, when enters the atmosphere, can cause significant scattering of the PBS signal. This can effectively reduce the intensity of the signal.

Another observation is that the daily minimum is observed around 1200 hrs LT (from Figure 5.20). This is also evident in Figure 5.22. Figure 5.30 also shows the occurrence of the daily minimum in conjunction with the maximum insolation hour. Thus, there is no contradiction that the daily minimum occurs sometime when the sun is expected to be overhead in Fiji.

The daily minimum can be due to the prevailing winds during this time of day. As seen earlier in Section 5.1.2 (Figure 5.6) the wind speed is greatest during the noontime. Significant winds can blow sand and dust particles off the ground surface up to considerable heights. These sand and dust particles can then affect signal propagation via scattering.

The high PBS signal strength values observed around late afternoon and in the evening can be due to the aerosol particles being cleared away by the afternoon winds. This helps the signal to propagate more effectively. The relatively low winds in the evening do not play a major role in signal attenuation hence the signal strength is higher.

The satellite signal strength variation during cloudy days is similar to that observed during fair-weather days except the magnitudes during the cloudy days are lower compared to the fair-weather days.

The relatively low values of PBS signal strength on cloudy days can be due to absorption and Rayleigh scattering of the signal from satellite. Lower insolation values indicate the presence of more cloud cover. The increased number of water drops within the cloud causes the signal to encounter more scattering sources than if it were propagating in free space or in the presence of minimum cloud cover. This causes the signal to attenuate considerably.

The general observation in the study of PBS signal strength was that on cloudy days the signal strength was relatively lower when compared to fair-weather days. This reduction in signal strength may be due to scattering of the signal within and outside cloud cover. From equation (2.25), for the scattering to be large, 'α' should be large. Since $a = 2p\,a / l$ where 'a' is the radius of the scattering sphere and 'λ' is the wavelength of PBS signal, which is fixed, for scattering to be large 'a' should be large. The wavelength of PBS signal (12.648 GHz) is ~ 0.02 m. The radius of the scattering cloud droplet, using the validity limit for equation (2.25), is then found as 1 mm. Since the mean radius of cloud droplets is large, the reduction in PBS signal strength can be attributed to attenuation by scattering.

Chapter 6

Conclusions

6.0 Conclusions

For the analyses of the Earth's potential gradient at the site, 31 days were classified as fair-weather days and another 31 days were classified as cloudy days during the period study (1st June 2005 to 30th June 2006). For the fair-weather days selected, the variation of insolation showed a gradual variation peaking at ~ 800 W/m^2. The diurnal variation of the PG closely followed the globally accepted Carnegie curve, showing a bimodal oscillation. However, the magnitude of the primary (morning) and the secondary (evening) maxima deviated. The mean PG for the fair-weather days was ~125 V/m, which is less than that reported by other researchers. The PG values increase with atmospheric contamination, thus the low PG value at the site indicates that on fair-weather days, the atmosphere is relatively "clean" at the site.

On cloudy days, the peak insolation dropped to ~ 200 W/m^2. Analyses showed that the PG values close to the Earth's surface also reduced on all the cloudy days. The magnitudes of the Earth's vertical PG and insolation vary with the time of measurement during the day. To understand the relationship between these two measurable quantities, their relative values as compared to the fair-weather day values were carried out at times when the insolation is approximately normal to the surface of the Earth (10:00 am – 2:00 pm LT). The analysis clearly showed that the percentage reduction in PG is nearly proportional to the intensity of the cloud cover. A possible reason for this dependence is that when a cloud is present overhead, the negative charges at the base of the cloud will induce a *dc* field directed upwards from the Earth's surface. The magnitude of this field will depend on the amount of negative charges at the cloud base, which in turn depends on the electrical activity in the cloud. In thick strato-nimbus and cumulo-nimbus clouds, the electrical activity is relatively more. Such clouds also inhibit the insolation, by scattering (Rayleigh) and absorption caused by cloud droplets, hence the reduced variation and the peak values.

The effect of cloud cover on satellite downlink was investigated using the commercial television transmission signal. INTELSAT 701 provides a signal centered at 12.648 GHz for television transmission to Fiji. This signal and the insolation were monitored from August to October 2007. Adopting the criterion described earlier, 11 days were classified as clear days with peak insolation

> 800 W/m^2. Ideally, the carrier strength for a given transponder and a receiver should remain a constant. However, observations on the clear days showed, in addition to the rapid fluctuation of the signal strength, it exhibited a diurnal variation (~ 61 dBm – ~ 68 dBm). The signal strength was relatively higher during the night hours compared to the values during the daytime hours. The *RF* signal traverses through the ionosphere. A detailed analysis of the effect of the ionosphere on electromagnetic waves traversing through them is beyond the scope of this research. However, a qualitative explanation is given here to support the experimental observation. The ionosphere, which is composed of equal numbers of positive and negative charges, is always electrically neutral. Irregularities may occur within this region, which may then cause diffraction and scattering of trans-ionospheric radio signals. When received at a station, these signals may present random temporal fluctuations in intensity. Thus, this could be a possible reason for the minor fluctuations observed on the TV signal. The lowermost *D* region of the ionosphere, which is produced by photo-ionization, is present only during daylight hours – the ionization density being maximum at noon [Chatterjee, 1963 pp 73-78]. Due to high rate of recombination at this low region, ionization dies down as the ionizing solar radiation is absent. It follows that ionospheric absorption would be greatly reduced after dark. This may be a plausible reason for the observed diurnal variation of the *RF* signal.

During the period of study, 37 days were classified as cloudy days, records on these days again showed a diurnal variation with a mean signal strength of ~ 50 dBm which is lower than the mean fair-weather days signal strength (~63.5 dBm). Further analysis of the cloudy days' records showed a nearly linear dependence of the percentage reduction in *RF* signal strength to the intensity of the cloud cover. One of the parameters that adversely affect tropospheric propagation of electromagnetic waves is scattering. When the dimensions of the scattering particles are small, Rayleigh scattering is dominant. Cloud particles thus contribute to the reduction in signal strength of *RF* signals in the troposphere, and the number density of the scattering particles increase with the increase in cloud cover. To understand the relationship between cloud cover and *RF* signal strength, their relative values as compared to the fair weather day values were calculated for the sunshine hours. The analysis clearly showed that the percentage reduction in signal strength is nearly

proportional to the intensity of the cloud cover. The cumulative effect of scattering by cloud droplets thus decreases the *RF* signal proportionally.

6.1 Suggestion for further work

In the detailed analysis to find the correlation between cloud cover (assumed to be proportional to insolation) with PG and *RF* signal strength, only four insolation values were considered. This was because of the limited number of days considered to obtain the average values for the three parameters. The study should be extended for a longer period so that more representative values for insolation and corresponding PG and signal strength values could be obtained. This can further improve the near-linear relationship between insolation and corresponding PG and signal strength values found in this research. In the analysis of the diurnal variation of the satellite downlink signal, the effect of the cloud cover during night was ignored. Weather data during night time should be analyzed to eliminate the effects due to cloud cover.

References

Adlerman, E.J., Williams, E.R., (1996), “Seasonal variation of the global electric circuit”, J. Geophys. Res. 101, pp 29679–29688.

Allen, K. C., (1983), “Attenuation of Millimeter Waves on Earth-Space Paths by Rain Clouds”, NTIA report, 83-132.

Allnut, J.E. and Haidara, F., (2001), “Ku-band diurnal fade characteristics and fade event duration data from three, two-year earth-space radiometric experiments in equatorial Africa”, Int. J Satellite Commun., 18, pp 161-182.

Alexander, R. M., (1999), “Energy for Animal Life”, Kindle Edn., Oxford University Press, America [Online] Available from - Animal-Life/dp/B000SIX7CC [Accessed 20 May 2008].

Anisimov, S. V., (2003), “Global Electric Circuit and Lower Atmospheric Electricity”, Borok Geophysical Observatory, 152742 RF.

Balanis, C. A., (2005), “Antenna Theory Analysis and Design”, 3rd Edn. John Wiley & Sons, Inc., New Jersey, pp 27-74, 94-96, 893-926.

Bansal, R., (2006), “Fundamentals of Engineering Electromagnetics”, CRC Press, Taylor and Francis Group., Boca Raton, pp 12-16, 57, 67, 163-182.

Bering, E. A. III., Few, A. A., Benbrook, J. R., (1998) “The global electric circuit”, Physics Today, pp 24-30.

Blake, R., (2002), “Electronic Communication Systems”, 2nd Edn., Thomson Learning, Inc., America, pp 30-33.

Brown, C. J., (1935), “The local variation of the earth’s electric field”, *Terrestrial Magnetism and Atmospheric Electricity,* 40, pp 413–424.

Chalmers J.A., (1967), “Atmospheric electricity”, 2nd Edn., Pergamon, New York, p 515.

Chatterjee, B., (1963), “Propagation of Radio Waves”, Asia Publishing House, New York.

Cho, M., Rycroft, M.J., (1998), “Computer simulation of electric field structure and optical emission from cloud top to ionosphere”, J. Atmos. Sol.-Terr. Phys. 60, pp 871–888.

Christian H. J., (2003), “Global lightning activity”, Proceedings of the 12th Atmospheric Electricity, Versailles, France, June 9-13, 673-676.

Cobb, W.E., Wells, H.J., (1970), “The electrical conductivity of oceanic air and its correlation to global atmospheric pollution”, J. Atmos. Sci. 27, pp 814–819.

Davydenko, S. S., Mareev, E. A., Marshall, T. C., Stolzenburg, M., (2004), “On the calculation of electric fields and currents of mesoscale convective systems”, Journal of Geophysical Research, Vol. 109.

Delgado, M. L., Garcia, D. E., De Pablo, D. F., Rivas, S. L., (2003), “Relationship between the atmospheric electric field and air pollution in the lower levels of the atmosphere”, Proceedings of 12th ICAE, p 365.

Dhanorkar, S., Kamra, A. K., (1994), “Diurnal variation of ionization rate close to ground”, J. Geophys. Res., 99 (D9), 18523–18526.

Dickinson, R.E., (1975), “Solar Variability and the Lower Atmosphere”, Bull. Atm. Meteorol. Soc., 56, pp 1240–1248.

Fleagle, R. G., Businger, J. A., (1963), “An Introduction to Atmospheric Physics”, Academic Press Inc., New York, pp 21-22, 84-87, 114-124.

Franke, M., (1949), “The double periodic diurnal variation of the atmospheric electric potential or gradient as a consequence of exchange”, *Geophysica pura e applicata,* 14, pp 1–12.

Frenzel, .L., (1994), “Communication Electronics”, 2nd Edn. McGraw-Hill Book Co., New York, pp 283-301.

Frenzel, .L., (1998), “Electronic Communication Systems”, 3rd Edn. McGraw-Hill Book Co., New York, pp 49, 608, 631-635, 667-668, 670-673.

Garimella, S., Deo, R. N., (2007), “Neutron Activation Analysis of Atmospheric Aerosols from a small Pacific Island Country: A Case study of Suva, Fiji Islands”, Aerosol and Air Quality Research, Vol. 7, No. 4, pp 500-517.

Gibson J. D., (1997), “The Communications Handbook”, Boca raton, Fla., CRC Press, New York, pp 58.

Harrison, R.G., (2003), “Reply to Comment by E.R. Williams of 'Twentieth century secular decrease in the atmospheric gradient”, Geophysical Research Letters, Vol. 30, p 1804.

Harrison, R. G., (2005), “The global atmospheric electric circuit and climate”, Surveys in Geophysics, Volume 25, Numbers 5-6, November 2004, pp 441-484.

Harrison, R. G., Aplin, K. L., (2002), “Mid-nineteenth century smoke concentrations near London”, Pergamon, Atmopheric Environment, 36, pp 4037-4043.

Hays, P.B., Roble, R.G., (1979), “A quasi-static model of global atmospheric electricity In The lower atmosphere”, J. Geophys. Res. 84, pp 3291–3305.

Ippolito Jr. L. J., (1986), “Radiowave Propagation in Satellite Communication”, Van Nostrand Reinhold Company, New York, America, pp 56-60.

Israel, H., (1948), “The diurnal variation of atmospheric electric potential gradient”, Meteor. Rdsch, 1, pp 200–204.

Israel, H., (1973), “Atmospheric Electricity”, Israel program for scientific translation, Jerusalem, Vol II, p 350.

Jayaratne, E. R., Verma, T. S., (2003), “Environmental aerosols and their effect on the Earth’s local fair-weather electric field”, J. Meteorol. Atmos. Phys. 86, 275-280.

Jones, D.L., (1999), “ELF sferics and lightning effects on the middle and upper atmosphere”, Modern Radio Sci. pp 171–189.

Junge, C., (1955), “The size distribution and aging of natural aerosols as determined from electrical and optical data on the atmosphere”.

Kerker, M., (1969), “The Scattering of Light and other electromagnetic radiation”, Academic Press, New York, pp 12-38.

Kumar, V. V., (2003), “Effects of Atmospheric parameters on Ku band satellite link”, Fiji.

Latha, R., (2003), “Diurnal variation of surface electric field at a tropical station in different seasons: a study of plausible influences”, Earth Planets Space, 55, 677-685.

Law, J., (1963), “Ionization of the atmosphere near the ground in fair weather”, Quarterly Journal of Royal Meteorological Society, 89, 107-121.

Lorrain, P., Corson, D. R., (1970), “Electromagnetic Fields and Waves”, 2nd Edn, W. H. freeman and Company, America, pp 97-102.

Lyons, W., (1996), “Sprites observations above the US high plains in relation to their parent thunderstorms systems”, J. Geophys. Res. 101, pp 29641–29652.

Makino, M., Ogawa, T., (1984), “Response of atmospheric electric field and air–earth current to variations of conductivity profiles”, J.Atmos. Terr. Phys. 46, pp 431–445.

Manwell, J.F., McGowan, J.G., Rogers, A.L. (2002), “Wind Energy Explained; Theory, Design and Application”, John Wiley & Sons Limited, Chichester, England, pp 26-38.

Markson, R., (1978), “Solar modulation of atmospheric electrification and possible implications for the sun–weather relationship”, Nature 273, pp 103–109.

Markson, R., (1981), “Modulation of the earth's electric field by cosmic radiation”, Nature 291, pp 304–308.

Marsh, N., Svensmark, H., (2000), “Cosmic rays, cloud, and climate”, Space Sci. Rev. 94, pp 215–230.

Marshal, T.C., (2001), “Voltages inside and just above thunderstorms”, J. Geophys. Res., Vol. 106, D5, pp 4757-4768.

Marshall, C. T., Rust, W. D., Stolzenburg, M., Roeder, P. W., Krebheil, R. P., (1999), “A study of enhanced fair weather electric fields occuring soon after sunrise”, J. Geophys. Res., 104 (D20), pp 24455-24469.

Milikh, G., Valdivia, J.A., (1999), “Model of gamma rays flashes fractal lightning”, Geophys. Res. Lett. 26, p 525.

Monteith, J. L., Unsworth, M. H., (1990), “Principles of Environmental Physics”, 2nd Edn. Chapman and Hall, Inc., New York, pp 36-50.

Muhleisen, R., (1977), “The global circuit and its parameters”, Steinkopff, Darmstadt, pp 467 – 476.

Ogawa, T., (1985), “Fair-weather electricity”, J. Geophys. Res. 90, pp 5951–5960.

Oke, T. R., (1987), “Boundary layer climates”, 2nd Edn., Methuen Press, New York, pp 51-52

Pan, Q.W., Allnut, J.E., (2001), “Some second-order Ku-Band site diversity results on a high elevation angle path in a rainy tropical region” 11th Int. Conf. on Antennas and Propagation, Manchester, pp 551-555.

Pan, Q.W., Allnut, J.E., Haidara, F., (2000), “12 GHz diurnal fade variations in the tropics”, Electron. Lett., 30, (10), pp 891-892.

Pan, Q.W., Bryyant, G.H., McMahon., J., Allnut, J.E., Haidara, F., (2001), “High elevation angle satellite-to-earth 12 GHz propagation measurements in the tropics”, Int. J Satellite Commun., 19, pp 363-384.

Panneerselvam, C., Nair, K. U., Jeeva, K., Selvaraj, C., Gurubaran, S., Rajaram, R., (2003), “ A comparative study of atmospheric Maxwell current and electric field from a low latitude station, Tirunelveli”, Earth Planets Space, 55, 697-703.

Raj, E. P., Devara, P. C. S., Maheshkumar, R. S., Pandithurai, G., Dani, K. K., (1997), “Lidar measurements of aerosol column content in an urban nocturnal boundary layer”, Atmospheric Research, 45, 201–216.

Ramachandran, V. and Kumar, V., (2004), “Rain attenuation measurement on Ku-band satellite TV downlink in small island countries”, Electron. Lett., 40, pp 49-50.

Ramachandran, V., Kumar, V., Prakash. J.N., Kumar, S., (2007), “Preliminary Findings of surface fair-weather electric field trends over small tropical island station, Suva, Fiji”, The South Pacific Journal of Natural Science, 12, pp 70-72.

Reiter, R., (1984), “Under which conditions can recordings of atmospheric electric conductivity be regarded as indicator of particulate air pollution?”, Res. Lett. Atmos. Electr. Japan, 4, pp 35-48

Reiter, R., (1992), “Phenomena in atmospheric and environmental electricity”, The Netherlands: Elsevier.

Ruhnke, L.H., (1969), “Area averaging of atmospheric current”, J.Geomagn. Geoelectr. 21, pp 453 – 462.

Russell, C.T., Fleishman, M., (2002), “Joint control of region-2 field aligned current by the east-west component of the interplanetary electric field and polar cap illumination”, J. Atmos. Sol.-Terr. Phys. 64, pp 1803–1808.

Saha, S. K., Ananthakrishnan, R., (1976), “Diurnal and seasonal variation of thermal stability close to the surface at Poona in relation to air pollution”, Indian Journal of Meteorology Hydrology and Geophysics, 27, 333–334.

Sapkota, B.K., Varshneya, N.C., (1990), “On the global atmospheric electric circuit”, J. Atmos. Terr. Phys. 52, pp 1–20.

Sentman, D.D., Fraser, B.J., (1999), “Simultaneous observations at Schumann resonance in California and Australia: Evidence for intensitymodulation by the local height of the D-region”, J. Geophys. Res. 96, 15973–15984.

Siingh, D., Gopalakrishnan, V., Singh, R P., Kamra, A. K., Singh, S., Pant, V., Singh, R., Singh, A. K. (2006), “The atmospheric global circuit: An overview”, J. Atmos. Res. 84, 94-110.

Stephens, G. L., (1994), “Remote sensing of the Lower Atmosphere *An Introduction*”, Oxford University Press, Inc., New York, pp 11-24, 115-121.

Stephenson, D. J., (1994), “Newness Guide to Satellite TV”, 3rd Edn, Butterworth-Heinemann Ltd., Oxford, pp 10-23.

Svensmark, H., and Friis-Christensen, E., (1997), “Variation of cosmic ray flux and global coverage - a missing link in solar-climate relationships”, J. Atmospheric and Solar-Terrest. Physics, 59, 11, pp 1225-1232.

Tinsley, B.A., (2000), “Influence of the Solar Wind on the Global Electric Circuit and Inferred Effects on Cloud Microphysics, Temperature and Dynamics in the Troposphere”, Space Sci. Rev., 94, 231–258.

Turco, R.P., Zhao, L.X., Yu, F., (1998), “A new source of tropospheric aerosol: Ion–ion recombination”, Geophys. Res. Lett. 25, pp 635–638.

Unsworth, M. H., McCartney, H. A., (1973), “Effects of Atmospheric Aerosols on Solar Radiation”, Atmospheric Environment, Vol. 7, Issue 12, pp 1173-1185.

Volland, H., (1984), “Atmospheric Electrodynamics”, 11th edn. Springer-Verlag Berlin Heidelberg, Germany, pp 1-28.

Whipple, F.J.W., (1929), “On the association of the diurnal variation of electric potential in fine weather with the distribution of thunderstorms over the globe”, Quart. J. Roy. Meteor. Soc. 55**,** 1–17.

Wilson, C.T.R., (1920), “Investigation of lightning discharges and on the electric field of thunderstorms”, Philosophical Transactions of the Royal Society of London, 221**,** 73-115.

Williams, E.R., (1992), “The Schumann Resonance: a global thermometer”, Science 256, pp 1184–1187.

Williams, E.R., (2005), “Lightning and climate: a review”, Atmos. Res. 76, pp 272–287.

Williams, E.R., Heckman, S.J., (1993), “The local diurnal variation of cloud electrification and the global diurnal variation of negative charge on the Earth”, J. Geophys. Res. 98, pp 5221–5234.

Appendix

Appendix A

This section contains the front panel and the block diagrams used to acquire and record Earth's electric field data.

Front Panel:

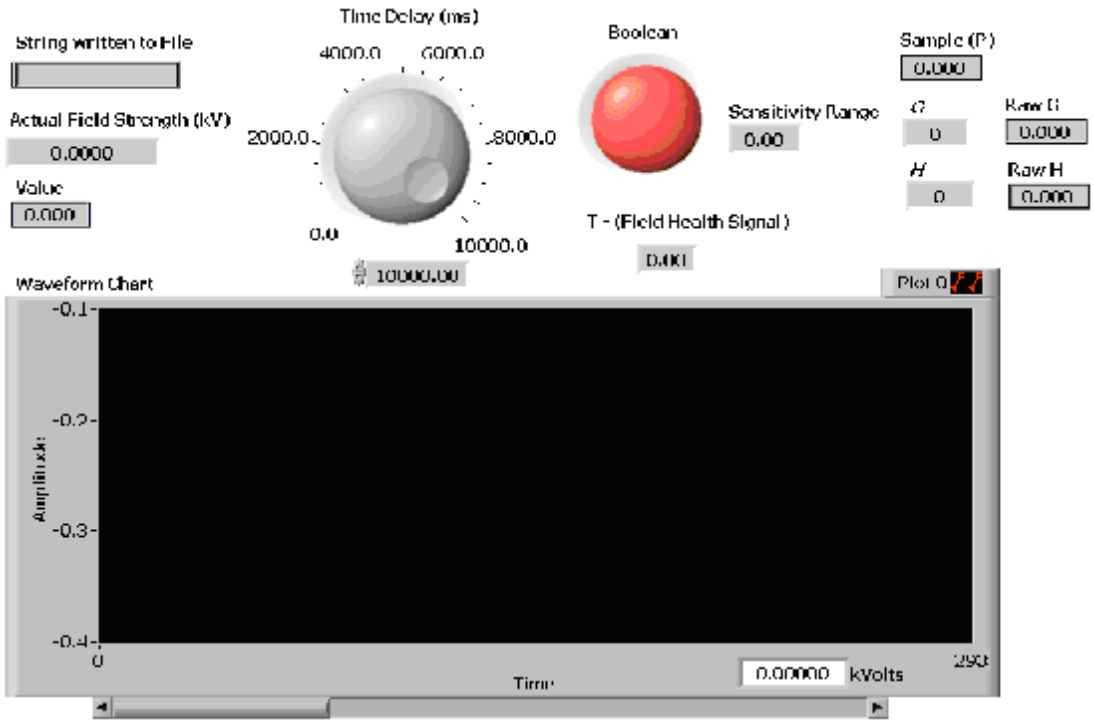

The following are the block diagrams.

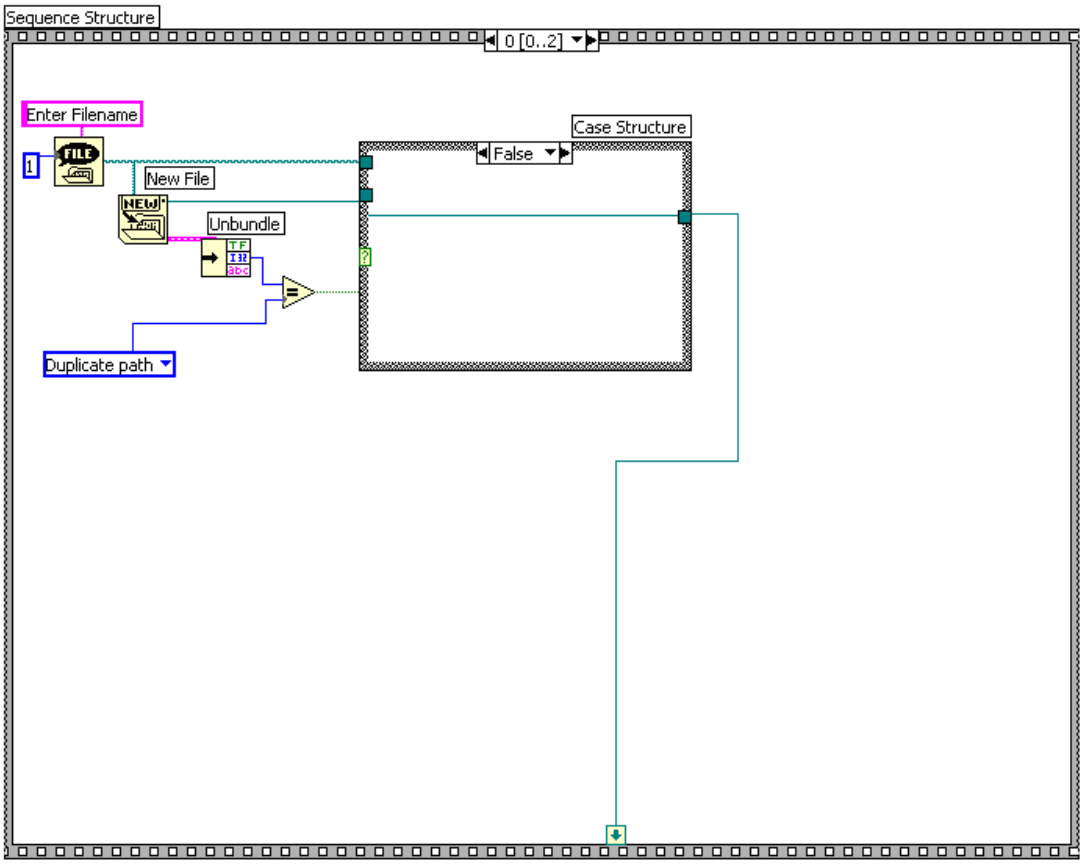

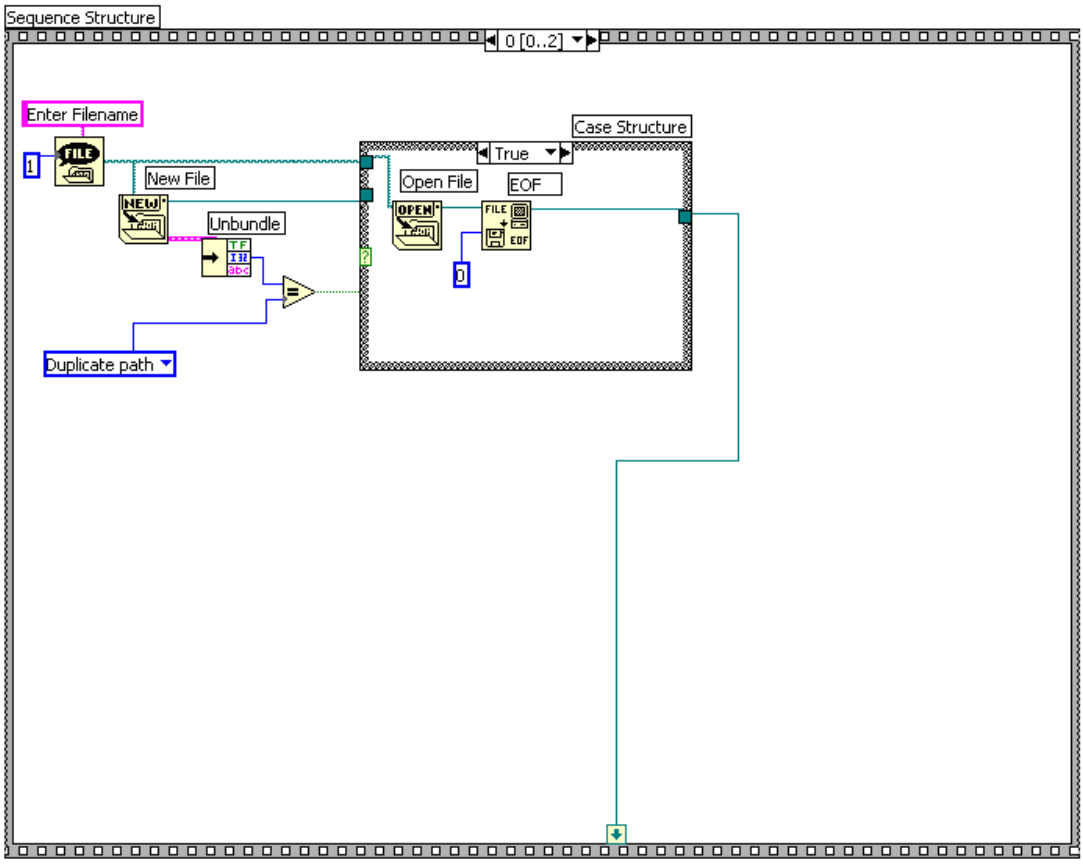

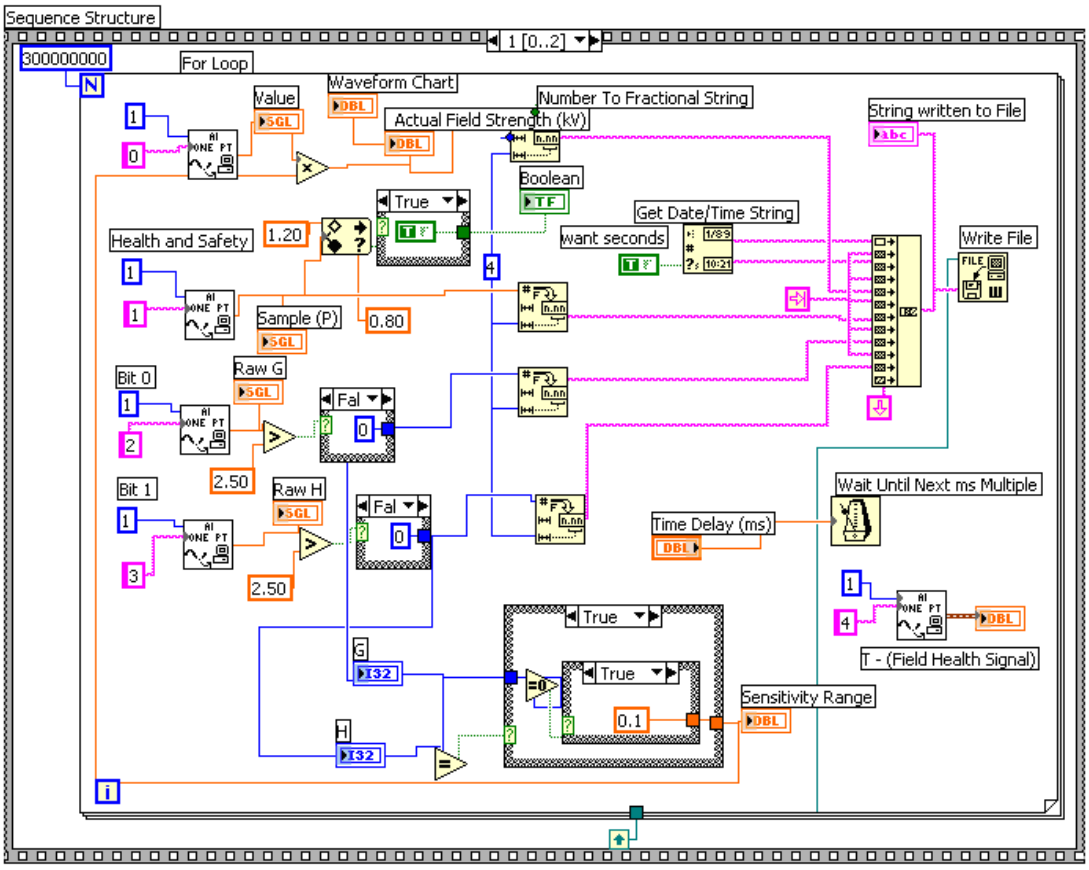
Sequence Structure
1 [0..2]
300000000
For Loop
Value
Waveform Chart
Number To Fractional String
Actual Field Strength (kV)
String written to File
Boolean
Get Date/Time String
want seconds
Write File
Health and Safety
1.20
True
Sample (P)
0.80
Raw G
Bit 0
Fal
2.50
Raw H
Bit 1
Wait Until Next ms Multiple
Time Delay (ms)
T - (Field Health Signal)
G
H
I32
Sensitivity Range
0.1

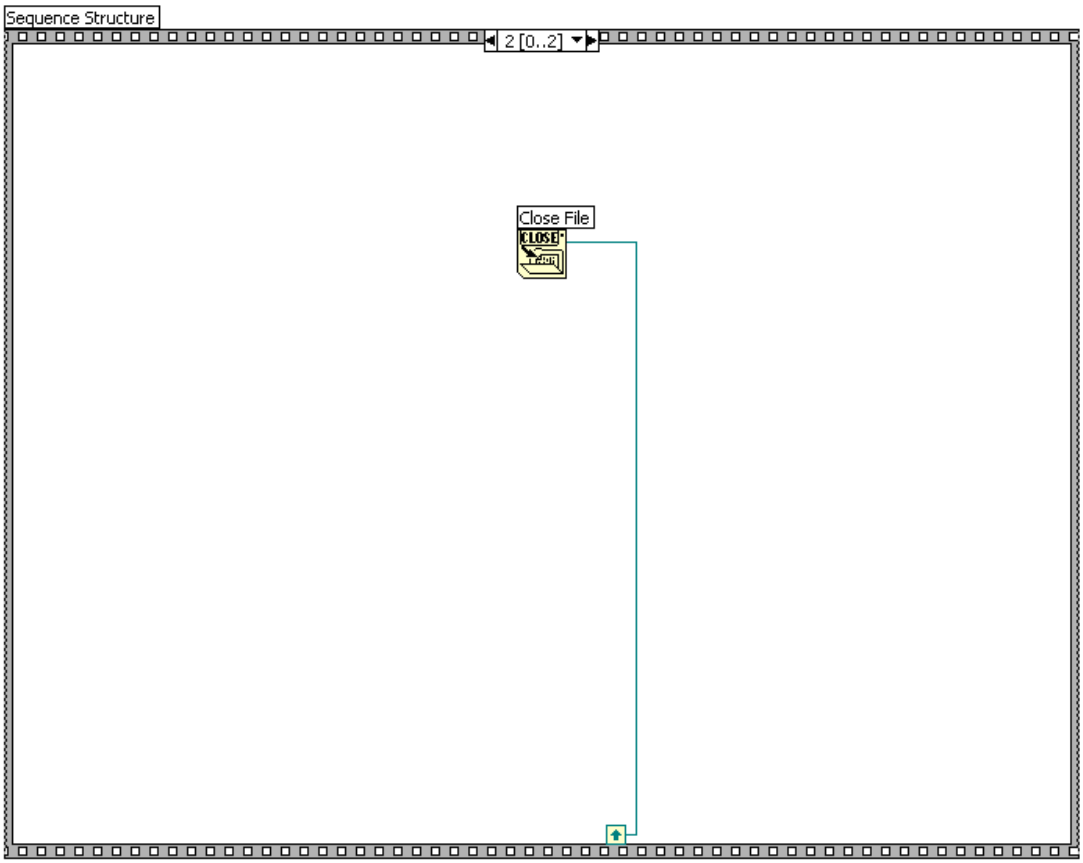
Sequence Structure
2 [0..2]
Close File
CLOSE

Appendix B

This section contains the front panel and the block diagrams used to acquire and record the PBS signal strength data.

Front Panel:

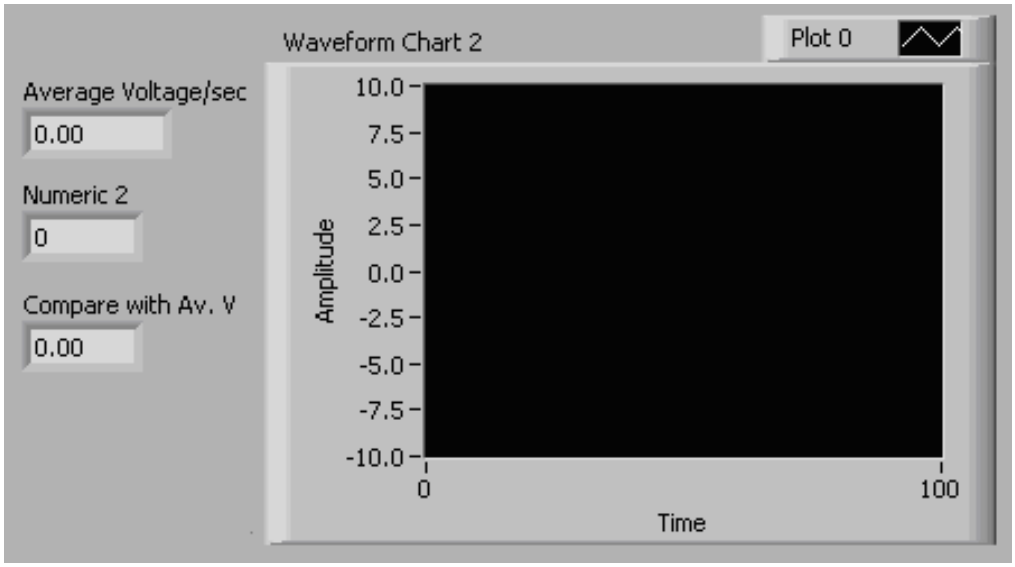

The following are the block diagrams.

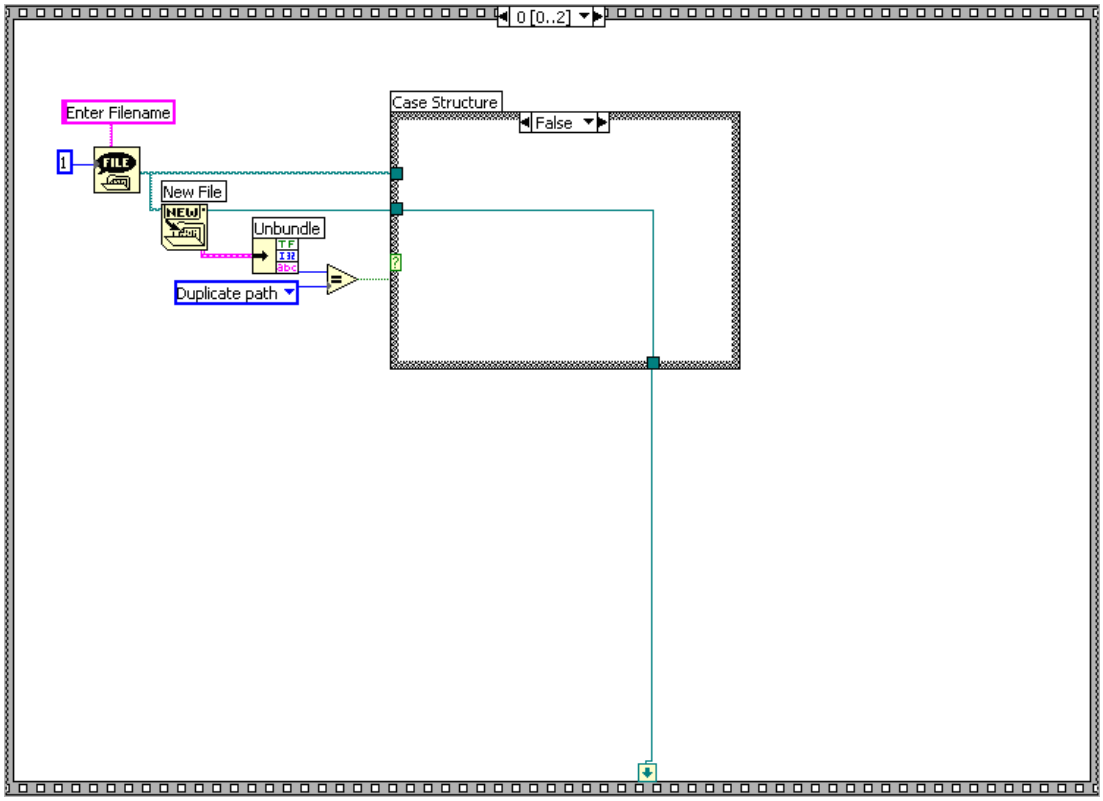

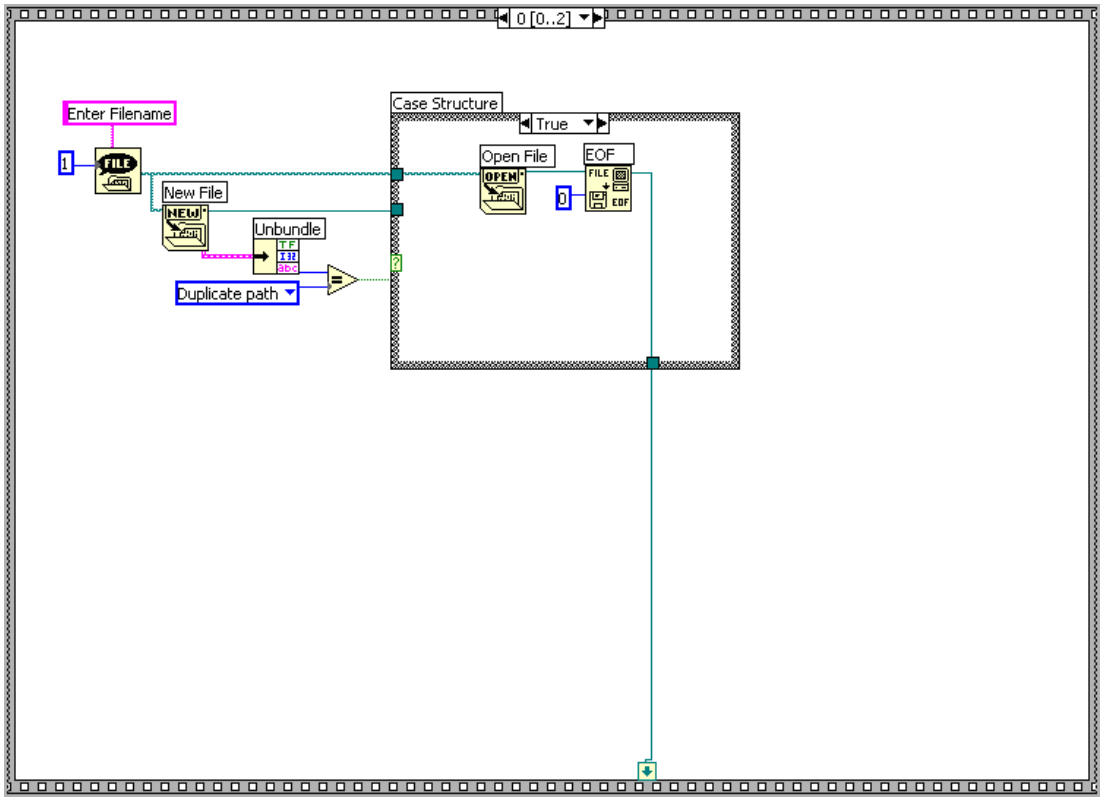

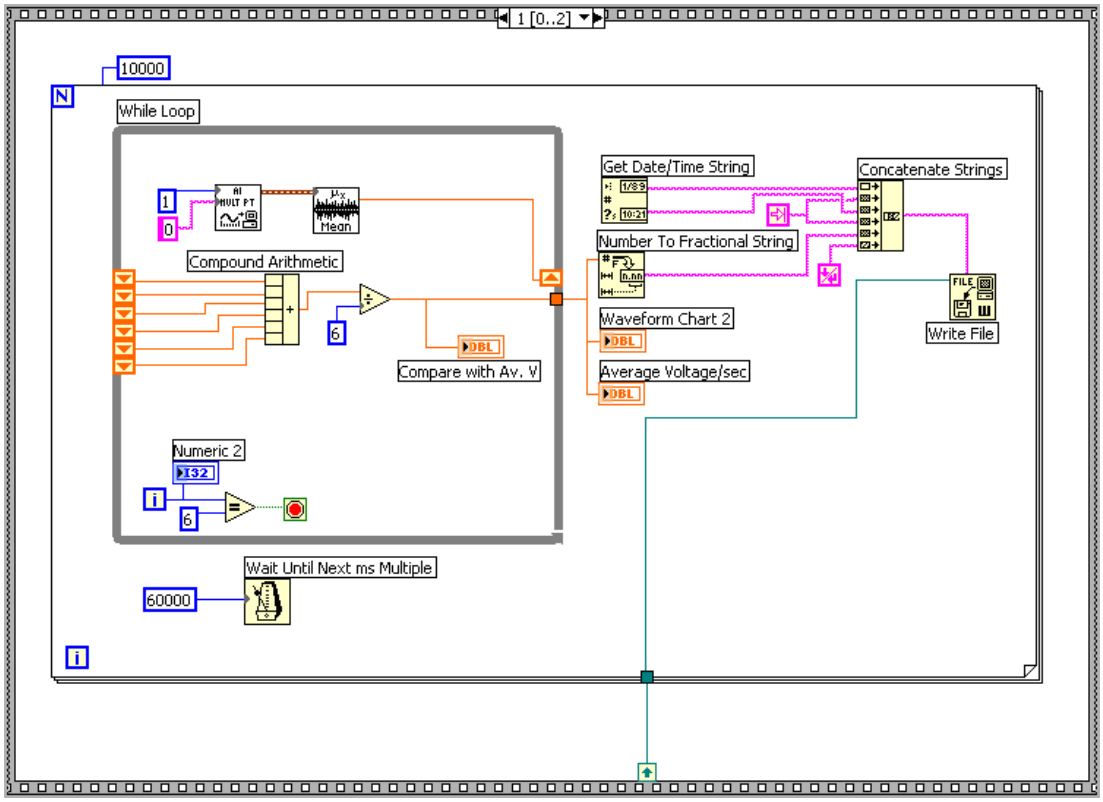
1 [0..2]
10000
N
While Loop
1
0
Mean
Compound Arithmetic
6
Compare with Av. V
Get Date/Time String
Concatenate Strings
Number To Fractional String
Waveform Chart 2
Average Voltage/sec
Write File
Numeric 2
6
Wait Until Next ms Multiple
60000
i

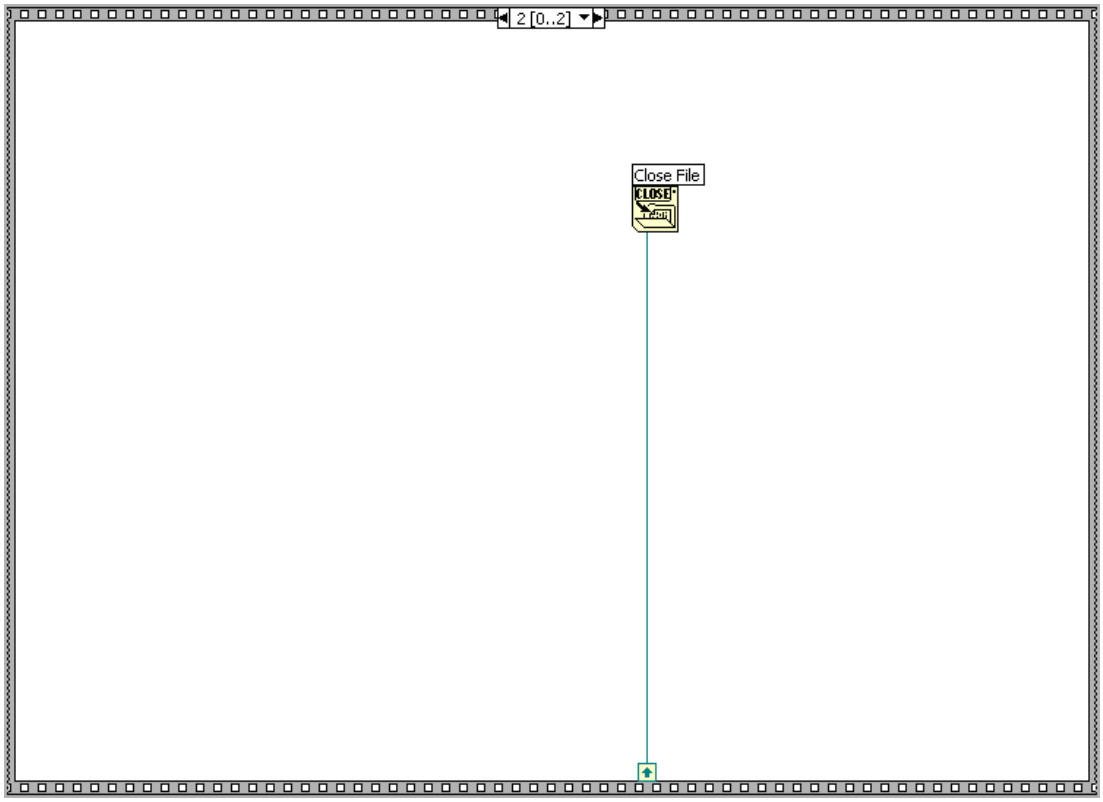
2 [0..2]
Close File